COMPUTATIONAL FLUID DYNAMICS

FOR

PERSONALIZED AIRWAY STENTS

S.M.J. van Beelen

Master Thesis
Technical Medicine

14/09/2022

University of Twente & NKI-AVL

Computational Fluid Dynamics for Personalized Airway Stents

Master Thesis Technical Medicine

Master Track Medical Imaging & Interventions

14/09/2022

S.M.J. van Beelen

S1788981

ACKNOWLEDGMENTS

THESIS COMMITTEE

Chair	Prof.dr.ir. C.H. Slump
Medical supervisor	Dr. J.A. Burgers
Technical supervisor	Dr. F.J. Siepel
Technical supervisor institution	Dr. R.L.P. van Veen
Process supervisor	Drs. P.A. van Katwijk
External committee member	Dr. L. Alic

SUMMARY

Lung cancer is one of the most commonly diagnosed cancers within the Netherlands with 14.336 new cases in 2019. Of these patients, 30% develops a central airway obstruction (CAO), an obstruction of >50% of the airway lumen. These patients suffer from symptoms as dyspnea, stridor, and hemoptysis. Treatments such as debulking, coagulation, or stent placement can be performed. Placement of an conventional airway stent is a palliative treatment for malignant cases. Unfortunately, mucus plugging and stent migration are present in some cases, which may require stent removal. Personalized airway stents may overcome these complications, since these are based on the patients' CT-data, and are therefore more congruent to the airway. This improved congruence, compared to conventional airway stents, is expected to decrease the chance of complications and to relieve symptoms. However, quantitative evidence of the underlying processes that cause conventional airway stent related complications remain unknown. Hence, evidence-based improvement in personalized stent designs cannot yet be performed. To gain quantitative insight into the causes of clinical effects of stent implantation, computational fluid dynamics (CFD) can be used. CFD enables simulation of fluid behavior, which can also be performed to stents and airways. This thesis therefore aims to obtain quantitative evidence for the use of personalized airway stents, by using computational fluid dynamics (CFD) and performing an analysis of airways, stents, or these two combined.

Results of CFD analysis of conventional airway stents show that an increased diameter goes with decreased pressure drop (PD), wall shear stress (WSS) and turbulence intensity (TI). These parameters can be related to less work of breathing, chance of stent migration and mucus plugging respectively. Additionally, simulations of tracheas show that a more complex geometry, relatively to a conventional airway stent, affects the PD, WSS and TI. In short, the best design of an airway stent based on these results is the largest possible stent diameter with a smooth lumen.

Moreover, pre-obstructed, obstructed and post-obstruction airways with conventional airway stents were simulated. The PD, WSS, TI, static pressure to the wall, velocity path lines and mass flow rate ratios were compared. Simulations showed that visually present anatomic variation has effect on these parameters, which does not allow determining a range of healthy values for pre-obstructed airways. For the evaluated case, simulations showed a decrease of the PD and static pressure to the wall after stent placement, hence decreasing the work of breathing and airway wall damage. However, poor congruence and sub-optimal use of the conventional airway stent was demonstrated quantitatively by increased WSS proximal to the stent, TI, and velocity path lines, and qualitatively by a visualization.

In short, CFD quantitatively evaluated clinical effects of stent placement for one case. Conventional airway stents decrease the work of breathing and airway wall damage, compared to the obstructed situation. However, poor congruence to the airway wall, sub-optimal use and still increased chance of complications compared to the pre-obstructed situation presented. Therefore, CFD prove that conventional airway stents have room for improvement so also has the clinical outcome of airway stent placement. Personalized airway stents can be designed, with a smooth lumen, great diameter and congruent to the airway, which virtual designs can be simulated with CFD to predict the clinical outcome.

CONTENTS

TABLE OF FIGURES

LIST OF ABBREVIATIONS

CAO	Central Airway Obstruction
CFD	Computational Fluid Dynamics
LMB	Left Main Bronchus
MFR	Mass Flow Rate
PD	Pressure Drop
RMB	Right Main Bronchus
TI	Turbulence Intensity
WSS	Wall Shear Stress

Chapter 1: Clinical Background

"The good physician treats the disease; the great physician treats the patient who has the disease."

In the Netherlands, nearly 14.000 people are diagnosed with lung cancer every year. It is the leading cause of death among all cancer patients, with a mortality rate of 22%. [1] The Netherlands Cancer Institute treats, among others, this group of patients. Almost 30% of these lung cancer patients develop a central airway obstruction (CAO). [2] The obstruction develops due to the growth of the carcinoma, which often results in complex anatomy of the airway. [3] If this obstruction is significant, i.e., <50% left of the endoluminal diameter, symptoms such as stridor, wheezing, and shortness of breath become present. [4, 5] A treatment option for CAO is the implantation of an airway stent to ensure immediate patency of the airway and to improve the quality of life. Unfortunately, the complication rate is as high as 69% within the first six months. [6] Personalized airway stents decrease this rate since the design of these stents is more congruent to the airway. [7-9] However, guidelines for their design (e.g., diameter, length, thickness) are undefined and the clinical outcome remains unknown. Computational fluid dynamics (CFD) can help understand the airflow within the airways quantitatively. [10] Parameters such as pressure, wall shear stress, turbulence, and velocity can be simulated. Comparing results from different stages of the disease (pre-obstruction, obstruction, post-obstruction with stent) will give insight into differences in airflow and corresponding symptoms. These quantitative data will be useful for design of a personalized airway stent.

This chapter starts with the anatomy and physiology of the lung. The pathophysiology of CAO will be explained, followed by treatment options, airway stents in particular. Lastly, the goal, objectives, and outline of this thesis are included.

1.1. ANATOMY

One of our vital organs in the body is the lungs, located in the thorax. [12] Its main function is to provide blood with oxygen (O_2) and release carbon dioxide (CO_2). The gas exchange takes place in the most distal part of the airways, the alveoli. [13] To reach the alveoli, air starts by following the pathway from the upper airway, made up of the nose, pharynx, and larynx. The lower airway starts inferior to the larynx with the trachea. The tracheal walls consist of horseshoe-shaped rings of cartilage. The flat part of the horse-shoe shape is located distally to allow food to pass the esophagus.
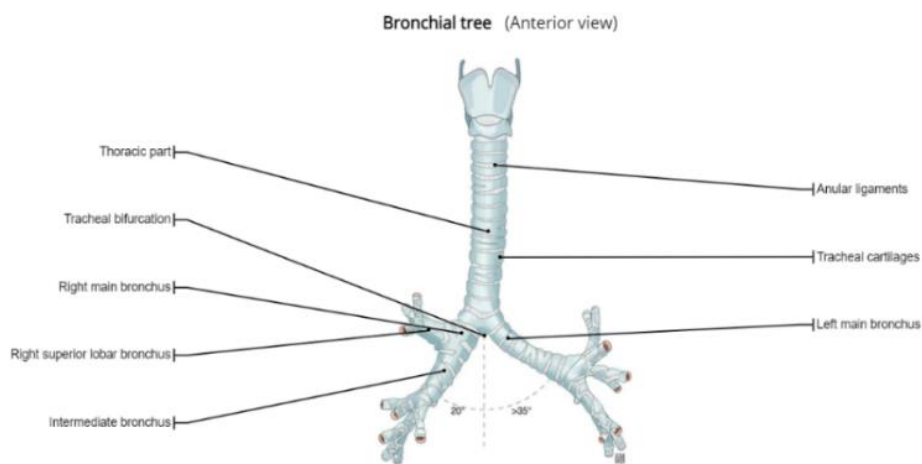
Figure 1-1 Schematic visualizations of the inferior part of the trachea, left and right main bronchi, and secondary bronchi for each lung segment. From IMAIOS [11]

The cartilage rings are connected with fibrous structures, called annular ligaments. At the distal end of the trachea, the first bifurcation is located, called the main carina. It divides the airway into the left main bronchi (LMB) and the right main bronchi (RMB). Lobar and segmental bronchi follow from the bifurcation of both main bronchi which are depicted in Figure 1-1. [12, 14] The trachea, both main bronchi, bronchus intermedius, and lobar bronchi make up the central airways. [15]

The architecture of the airway can be described by generation numbers which increase with each bifurcation, as depicted in Figure 1-2. The first 16 generations make up the conducting zone, where warming and filtration of air take place. [16] The remaining eight generations make up the respiration zone, where the oxygen and carbon dioxide exchange takes place. [16, 17]
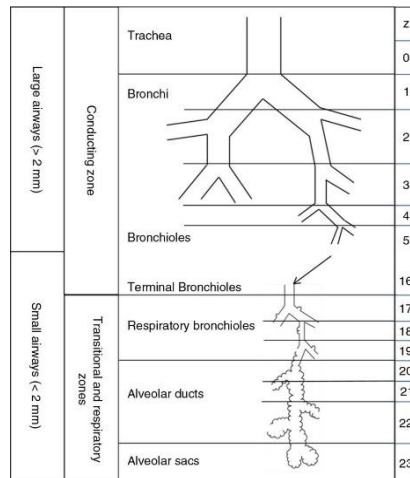
Figure 1-2 Schematic image of the airway generations from the trachea (z=0) to the last generation, the alveoli (z=23). From McNulty and Usmani [17]

Air has to reach the most distal parts of the airways to enable gas exchange. Thorax muscles expand the thorax in the sagittal and transversal planes. [18] This induces a negative pressure in the thorax, extending over the intrapleural cavity, to the alveoli. On the contrary, expiration can occur passively. The breathing mechanism is further explained in section 1.2 Physiology. [19]

1.2. PHYSIOLOGY

Pressure differences between the lungs and the external environment are the driving force for breathing. During tidal inspiration, a relative under intrapleural pressure of -8 cmH_2O is required for air to flow into the lungs. This is mainly achieved by thorax expansion due to the musculature. [18] Air subsequently flows into the lungs that increase in volume. [20, 21] During tidal expiration the thorax muscles relax, and intrapleural pressure increases towards -5 cmH_2O. Deflation of the lungs is mainly caused by compliance that prevents a collapsed lung by preserving the remaining lung volume after expiration. [16]

Compliance describes the change in volume per unit of change in pressure. It is a characteristic of both the lungs and chest wall, that interact with each other. The presence of elastic fibers and surfactant on the surface of the alveoli reduces surface tension thus compliance. [16, 22] Compliance of the lungs works inwards while the chest wall goes in the opposite direction. Consequently, together they indicate the expandability of both the lungs and chest wall. It is therefore a passive mechanism that is a key component of breathing physiology. [18, 19, 22]

1.2.1. Breathing mechanism

The pressure difference between the lungs and the external environment enables airflow to reach the alveoli. An increased pressure difference goes with a higher airflow $\dot{V}$ in liters per second [L/s], expressed as

$$\dot{V} = \frac{\Delta P}{R_{aw}} = \frac{P_A - P_B}{R_{aw}}$$

Eq. 1.1

with ΔP [cm·H$_2$O] describing the pressure difference between the alveolar P_A and barometric pressure P_B and total airway resistance R_{aw} [cm·H$_2$O/(L/s)]. [23] R_{aw} is described using Hagen-Poiseuille's law for laminar flow, which is not valid everywhere in the airway system:

$$R_{aw} = \frac{8\mu l}{\pi r^4}$$

Eq. 1.2

with μ being the dynamic viscosity [Pa·s], l the length of the tube [m], and r the radius [m]. Note the importance of the radius; doubling the radius decreases the resistance by a factor of 16. [24] Accordingly, the lowest resistance is located at the terminal bronchioles since the total radius is the greatest due to all bifurcations. [23]

Three types of airflow are present in the airways. Laminar airflow presents at relatively low velocities and describes layers of particles. Towards the center in the radial direction, the speed of the particles increases which is called a parabolic velocity profile. [24] Turbulent flow is present at high velocities of fluid and causes the particles to behave randomly. [20] Transient flow is the third type and is an intermediate between laminar and turbulent flow. The Reynolds number can be used to predict whether the flow is laminar or turbulent. It can be calculated with equation 1.3.

$$Re = \frac{vL\rho}{\mu}$$

Eq. 1.3

where v is the velocity [m/s], μ the dynamic viscosity [Pa·s] and ρ the density [kg/m^3] of the fluid, and L the characteristic length (in a circular pipe it is the diameter) [m]. Reynolds numbers <2000 indicate laminar flow; turbulent flow is dominantly present >3000. Between these values, the airflow is unstable called transient airflow. [25] Schematic visualizations of these three types of flow are depicted in Figure 1-3. In the trachea, the Reynolds number is on average 2084 for a flow rate of 0.5 L/s. More distally the Reynolds number drops to 1.3 and 0.01 in the transitional bronchioles and alveolar sacs, respectively, due to the increased cross-sectional area. [26]
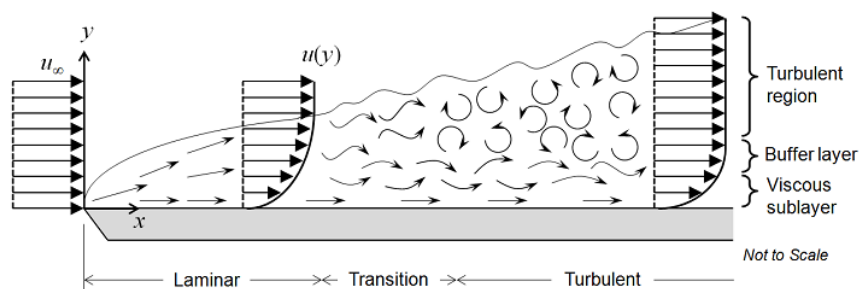
Figure 1-3 A schematic overview of the flow patterns for the three different kinds of flows: laminar, transient, and turbulent, indicated horizontally. In the turbulent region, the flow consists of three different layers: the viscous sub-layer, the buffer layer, and the turbulent region indicated vertically. The viscous-sublayer is the layer closest to the wall where the interaction of the fluid with the geometry takes place. The buffer layer has the greatest increase in velocity throughout the layer towards the center. Lastly, the turbulent region is the fully developed turbulent flow. From Frei [27]

1.2.2.   Airway clearance

Mucus is present in the airways where it provides a barrier for external pathogens. It is produced by mucus-secreting cells, more present in the peripheral than the central airways. [28] The mucus is cleared from the airways by ciliary movement and breathing flow. Consequently, it is removed by coughing or swallowing. [29]

Mucus is present at the airway wall, and as indicated in Figure 1-3, airflow is shearing against it. This shear is called wall shear stress (WSS) and indicates mucus clearance. Easy transportation of the mucus requires an airflow >1 m/s. Easier clearance can be achieved with higher shear stresses, generated with forced expirations. [28] WSS can additionally be used to indicate injury to the airway wall. [30]

1.3.   CENTRAL AIRWAY OBSTRUCTION

Obstruction of the airway located in the trachea, main bronchi, bronchi intermedius, or lobar bronchus that occludes more dan 50% is called a central airway obstruction (CAO). [15, 31, 32] It can be caused either by the growth of intrinsic carcinomas, extrinsic tumor compression, or a combination of both as illustrated in Figure 1-4. [2, 15, 31, 33] The degree of obstruction determines the symptoms and the number of work patients perform. The clinical presentation of benign and malignant origin is commonly indistinguishable, both causing dyspnea, hemoptysis, wheezing, stridor, and diminished sputum clearance. [2, 5, 31, 34, 35]

Figure 1-4 Three examples of central airway obstruction (FLTR): an intrinsic carcinoma, extrinsic tumor compression onto the airway, or a combination of both. From D'Andrilli, et al. [36]

1.3.1.   Benign causes

The most common cause of airway stenosis is post-intubation trauma, but systemic diseases, infections, and weakness of the cartilage in the airway can also contribute to the development of benign stenosis. [36, 37] Next, a specific group remains that suffers from stenosis with unknown etiology. [38] This is called idiopathic subglottic stenosis (ISGS) and is characterized by inflammation with localized fibrosis with an unknown cause. [38, 39] It is defined as an obstruction in the lower airway between the epiglottis and the second tracheal ring. [38] It occurs mostly in adult women between 30-50 years and has an incidence of 1:400.000. [39, 40] Next to symptoms related to a CAO, it is in advanced stages and also associated with hoarseness and swallowing problems. [37, 40]

1.3.2. Malignant causes

The most frequent cause of CAO is lung cancer. Lung cancer is the leading cause of cancer-related deaths worldwide with an estimation of 2.20 million new cases and 1.79 million deaths per year. [41] In the Netherlands, the incidence is increasing with 14.336 new diagnosed cases in 2019. [1] Within this diagnosis, two types can be distinguished: small cell and non-small cell lung carcinoma (NSCLC). NSCLC is the most common type and occurs in 85% of total diagnoses. [35, 41] Lung cancer can be classified into different stages. The stage of the disease is determined with the TNM classification and depends on tumor size (T, range 0-4), spread to lymph nodes (N, range 0-3), and metastasis to other organs (M, 0, or 1). Table 1-1 shows a summary of the stages for NSCLC. Unfortunately, lung cancer is in 50% of all cases diagnosed in the last, fourth, stage of the disease. [42] The 5-year survival rate for patients diagnosed with stage IV NSCLC is only 0% to 10%. [43]

Table 1-1 The four diagnostic TNM stages of NSCLC with suggested treatment. [1] TNM classification according to Rosen and Sapra [44]

	Stage 1	Stage 2		Stage 3				Stage 4
T	1-2	1-2	3	1-2	3	1-4	4	1-4
N	0	1	0	2	1	3	1-2	1-3
M	0	0	0	0	0	0	0	1
Location	Primary tumor	Spread to nearby lymph nodes		Metastasis to other lung or lymph nodes				Metastasis to other organs
Most common treatment	Resection of (a part of) the lung; otherwise, RT	Resection and/or RT; adjuvant treatment considered.		Chemoradiation				Palliative therapy; chemo- and/or immunotherapy

T = tumor, N = nodes, M = metastases, RT = radiotherapy

CAO can occur in all stages with different etiology. Small stage I tumors might develop in the central airways, large T4 tumors might grow into the central airways, as might mediastinal lymph nodes metastasis (N2 or N3 disease). In the fourth stage of the disease, carcinomas have grown and metastasized which makes the disease more complex. As a result, more than 30% of these patients develop a CAO. [2, 5, 15, 31] Immediate recognition and intervention of malignant CAO are required since it may lead to respiratory failure. [33] Without treatment, the prognosis of these patients is approximately 1-2 months. [31] Malignant CAO presents with symptoms such as dyspnea, hemoptysis, wheezing, and stridor, severely impeding the patients' quality of life. [5, 31, 45] Restoring patency of the airway can palliate the CAO and thereby improve the patients' quality of life. [5, 15, 37]

1.3.3. Treatments

Treatment of a CAO is commonly performed by a bronchoscopic intervention. Options are debulking, thermotherapy (laser, cauterization, cryotherapy), dilation of the airway, or stent placement. [15, 31, 37, 46] Dependent on the skills of the physician and the location and nature of the obstruction the right treatment is chosen. [47] Afterward, patients experience almost immediate relief from their symptoms. [9] Especially for benign causes, surgical intervention is the gold standard. [34]

Malignant cases have a palliative approach in which an interventional bronchoscopy is considered to relieve dyspnea. [34] Insertion of an airway stent has proven to provide palliative relief in symptoms of extraluminal malignant CAO in large airways. [2, 9, 31, 34, 38, 47, 48] Whether the placement of the stent is possible depends on the anatomic features of the obstructed airway. It is required that the stent covers the whole area of obstruction and it recovers the airflow when it is fully expanded. In

short, stent characteristics must fit the airway and obstruction. In malignant cases, the approach is palliative and has proven to be effective. [9]

1.4. AIRWAY STENTS

An airway stent is an endobronchial prosthesis used in the management of airway obstruction. [47, 48] It has the unique ability to overcome the extrinsic forces exerted on the airway or compress endoluminal tissue. [2, 7] Patients are eligible for stent placement if it is possible to place one, it can prevent occlusion of the airway and if viable lung tissue is present behind the obstruction. [2, 48, 49] Airway stents are manufactured in silicone, nickel-titanium, or a combination of these and vary in length, size, diameter, and shape. [2, 7, 9, 45, 49] These characteristics determine the biomechanical properties of the airway stents which relate directly to the postoperative outcomes. Silicone stents are most commonly used worldwide. [9] Well-known examples are Y-shaped, Dumon, or Hood stents. [2, 31, 48] Benefits of silicone stents are minimal elicit of tissue reactivity, a varying degree of firmness and flexibility, relatively inexpensive, and well-tolerated. Additionally, they can be customized by the physician on-site to achieve better congruence to the airway. [9, 33] However, their internal-to-external ratio is relatively small which narrows the lumen and can result in mucus plugging. [2] This complication is also caused by the tight fit of silicone to the airway which inhibits the cilia to push mucus upwards. [7]

Figure 1-5 Examples of different airway stents: (A) Hood stent, (B) Nova-Stent, (C) Polyflex, (D) Dumon bronchial stent, (E) Dumon hourglass tracheal stent, (F) Silmet stent, (G) Dynamic Freitag stent and (H, I) patient-specific airway stents. From Guibert, et al. [9]

Since only limited dimensions of conventional stent geometries are manufactured, complex airways remain difficult to treat properly. [45] Despite the immediate relief of symptoms following placement of a conventional airway stent their success rate is moderate; within 6 months of insertion 20-69% of all airway stents fail. [45] Bad congruence of an airway stent is related to a higher complication rate. Improved congruence of an airway stent can be achieved by on-site customization of silicone stents by the physician. [9] However, limited adjustments can be performed, and the outcome of the stent remains undefined. Performing computer-aided design enables a patient-specific virtual model of the airways on which an airway stent can be designed. The airway can be segmented from CT data and a 3D model can be developed. [7, 8] This mold can be 3D printed and filled with biocompatible silicone, which creates the final airway stent. [8] A such personalized workflow may lead to improved tolerance of the airway stent and decreases the complication rate. [7] One limitation is the turnaround

time (design, fabrication, sterilization) of an airway stent which approximately takes 1-3 months. Acute cases are therefore unsuitable for such workflow. [9]

1.5. PROBLEM

The current arsenal of conventional airway stents does cover the majority of the obstructions resulting from CAO. However, they are prone to complications of which the underlying cause is yet quantitatively undefined. Hence, the effect of both the obstruction and the inserted stent on the airway and the work of breathing must be investigated before an improved design of a personalized airway stent. Therefore, Computational Fluid Dynamics (CFD) software can be used. It is capable of simulating airflow and pressure during respiration and provides quantitative data. [10, 30] Investigating multiple cases with and without obstruction will give insight into the problems to address. Additionally, an airway with a conventional airway stent will prove whether these are not sufficient and how to improve the design.

1.6. GOAL

The aim of this thesis is:

To generate quantitative evidence to support the use of personalized airway stents using computational fluid dynamics (CFD) and performing airflow analysis of airways, stents, and a combination of the latter

Reach this goal, it is divided into different objectives:

1. How to perform a CFD analysis for a stable, reliable, and accurate simulation, for parameters of interest with assumptions required for an airway simulation?
2. Which quantitative differences are present between different stent sizes and tracheas?
   a. What are the clinical effects of different stent sizes and tracheal shapes?
3. How does an obstructed airway influence airflow?
4. What are the current problems of conventional airway stents considering numerical data and parameters?

Chapter 2 provides both theoretical and practical background information about computational fluid dynamics (CFD). The three main stages of a CFD simulation will be discussed in further detail, with the boundary conditions and input parameters that must be considered. Next, parameters that are of interest during airway simulations will be introduced. Lastly, proof-of-concept tests will be performed for the mesh and inlet, and outlet boundary conditions. These are necessary to create reliable results for airway simulations.

Chapter 3 starts with assumptions that are incorporated in this and the following chapter 4. Secondly, simulations of different airway stents will be simulated. It provides a guide for the physician to use when choosing the stent dimensions. Lastly, tracheas will be simulated to compare with similar stent sizes. The impact of the stent on the tracheal geometry can be evaluated. In the discussion are the assumptions and their effect on the simulation described.

Chapter 4 provides simulations of pre-obstructed airways, obstructed airways, and a post-obstructed airway with a conventional airway stent. One case will be discussed in which all three situations are simulated. A comparison shows differences and remarks about the placed stent.

Chapter 5 is the general discussion of this thesis with the outcome and future perspectives.

REFERENCES

[1]   N. Integraal kankercentrum, "Incidentie longkanker Nederland," ed, 2021.

[2]   J. Xu, H. X. Ong, D. Traini, M. Byrom, J. Williamson, and P. M. Young, "The utility of 3D-printed airway stents to improve treatment strategies for central airway obstructions," *Drug Development and Industrial Pharmacy,* vol. 45, no. 1, pp. 1-10, 2019/1// 2019, doi: 10.1080/03639045.2018.1522325.

[3]   H. Saji *et al.*, "Outcomes of airway stenting for advanced lung cancer with central airway obstruction," *Interactive cardiovascular and thoracic surgery,* vol. 11 4, pp. 425-428, 2010.

[4]   A. Ernst, D. Feller-Kopman, H. D. Becker, and A. C. Mehta, "Central airway obstruction," (in eng), *Am J Respir Crit Care Med,* vol. 169, no. 12, pp. 1278-97, Jun 15 2004, doi: 10.1164/rccm.200210-1181SO.

[5]   L. Mudambi, R. Miller, and G. A. Eapen, "Malignant central airway obstruction," *Journal of Thoracic Disease; Vol 9, Supplement 10 (September 2017): Journal of Thoracic Disease (Interventional Pulmonology),* 2017. [Online]. Available: https://jtd.amegroups.com/article/view/15458.

[6]   A. Rosell and G. Stratakos, "Therapeutic bronchoscopy for central airway diseases," (in eng), *Eur Respir Rev,* vol. 29, no. 158, Dec 31 2020, doi: 10.1183/16000617.0178-2019.

[7]   N. Guibert *et al.*, "Treatment of complex airway stenoses using patient-specific 3D-engineered stents: a proof-of-concept study," *Thorax,* vol. 74, no. 8, pp. 810-813, 2019/8// 2019, doi: 10.1136/thoraxjnl-2018-212732.

[8]   N. Guibert *et al.*, "Integration of 3D printing and additive manufacturing in the interventional pulmonologist's toolbox," *Respiratory Medicine,* vol. 134, pp. 139-142, 2018/1// 2018, doi: 10.1016/j.rmed.2017.11.019.

[9]   N. Guibert, H. Saka, and H. Dutau, "Airway stenting: Technological advancements and its role in interventional pulmonology," *Respirology,* vol. 25, no. 9, pp. 953-962, 2020/9// 2020, doi: https://doi.org/10.1111/resp.13801.

[10]   T. Zobaer and A. Sutradhar, "Modeling the effect of tumor compression on airflow dynamics in trachea using contact simulation and CFD analysis," *Computers in Biology and Medicine,* vol. 135, pp. 104574-104574, 2021, doi: https://doi.org/10.1016/j.compbiomed.2021.104574.

[11]   M. A. IMAIOS, Hoa D,. "e-Anatomy." www.imaios.com (accessed.

[12]   K. L. Moore, A. F. Dalley, and A. M. R. Agur, *Clinically oriented anatomy*. 2014, pp. Chapter 1 and 10-Chapter 1 and 10.

[13]   A. M. R. Agur and A. F. Dalley, *Grant's Atlas of Anatomy*, 13th ed. Philadelphia: Lippincott Williams & Wilkins, 2013, pp. 38-38.

[14]   K. P. Strohl, J. P. Butler, and A. Malhotra, "Mechanical properties of the upper airway," *Comprehensive Physiology,* vol. 2, no. 3, pp. 1853-1872, 2012/7// 2012, doi: 10.1002/cphy.c110053.

[15]   S. D. Murgu, K. Egressy, B. Laxmanan, G. Doblare, R. Ortiz-Comino, and D. K. Hogarth, "Central Airway Obstruction: Benign Strictures, Tracheobronchomalacia, and Malignancy-related Obstruction," *Chest,* vol. 150, no. 2, pp. 426-441, 2016, doi: https://doi.org/10.1016/j.chest.2016.02.001.

[16]   Z. Edwards and P. Annamaraju, "Physiology, Lung Compliance," in *StatPearls*. Treasure Island (FL): StatPearls Publishing

[17] W. McNulty and O. Usmani, "Techniques of assessing small airways dysfunction," *European Clinical Respiratory Journal,* vol. 1, 10/17 2014, doi: 10.3402/ecrj.v1.25898.

[18] M. F. Lutfi, "The physiological basis and clinical significance of lung volume measurements," *Multidisciplinary Respiratory Medicine,* vol. 12, no. 1, pp. 3-3, 2017, doi: 10.1186/s40248-017-0084-5.

[19] E. R. Donley and M. R. Holme. "Anatomy, Thorax, Wall Movements." StatPearls Publishing. https://www.ncbi.nlm.nih.gov/books/NBK526023/ (accessed.

[20] W. F. Boron and E. L. Boulpaep, "Medical Physiology: A cellular and molecular approach," 2nd ed. Philadelphia: Saunders/Elsevier, 2012.

[21] M. Haddad and S. Sharma, "Physiology, Lung," in *StatPearls [Internet]*, ed, 2021.

[22] J. P. Desai and F. Moustarah, "Pulmonary Compliance," in *StatPearls*. Treasure Island (FL): StatPearls Publishing

Copyright © 2022, StatPearls Publishing LLC., 2022.

[23] J. Hurley and J. Hensley. "Physiology, Airway Resistance." StatPearls Publishing. https://www.ncbi.nlm.nih.gov/books/NBK542183/ (accessed 2022).

[24] A. v. Oosterom and T. F. Oostendorp, *Medische Fysica*, 4 ed. Amsterdam: Bohn Stafleu van Loghum, 2008, pp. 198-198.

[25] A. Davies and C. Moores, "Airflow in the Respiratory System," *The Respiratory System,* pp. 41-59, 2010, doi: 10.1016/b978-0-7020-3370-4.00004-9.

[26] B. Sul, A. Wallqvist, M. Morris, J. Reifman, and V. Rakesh, "A computational study of the respiratory airflow Characteristics in normal and obstructed Human airways," *Computers in Biology and Medicine,* vol. 52, 2014/9// 2014, doi: 10.1016/j.compbiomed.2014.06.008.

[27] W. Frei, "Which Turbulence Model Should I Choose for My CFD Application? | COMSOL Blog," ed, 2017.

[28] C. P. van der Schans, "Bronchial Mucus Transport," *Respiratory Care,* vol. 52, no. 9, p. 1150, 2007. [Online]. Available: http://rc.rcjournal.com/content/52/9/1150.abstract.

[29] J. Stéphano and B. Mauroy, "Wall shear stress distribution in a compliant airway tree," *Physics of Fluids,* vol. 33, no. 3, pp. 031907-031907, 2021/3// 2021, doi: 10.1063/5.0038706.

[30] W. M. Faizal *et al.*, "Computational fluid dynamics modelling of human upper airway: A review," *Computer Methods and Programs in Biomedicine,* vol. 196, pp. 105627-105627, 2020, doi: 10.1016/j.cmpb.2020.105627.

[31] A. Mohan *et al.*, "A Prospective Outcome Assessment After Bronchoscopic Interventions for Malignant Central Airway Obstruction," *Journal of Bronchology & Interventional Pulmonology,* vol. 27, no. 2, 2020. [Online]. Available: https://journals.lww.com/bronchology/Fulltext/2020/04000/A_Prospective_Outcome_Assessment_After.5.aspx.

[32] S. Miyawaki, E. A. Hoffman, and C.-L. Lin, "Numerical simulations of aerosol delivery to the human lung with an idealized laryngeal model, image-based airway model, and automatic meshing algorithm," *Computers & fluids,* vol. 148, pp. 1-9, 2017/4// 2017, doi: 10.1016/j.compfluid.2017.02.008.

[33] C. Oberg, E. Folch, and J. F. Santacruz, "Management of malignant airway obstruction," *AME Medical Journal; Vol 3 (December 2018): AME Medical Journal,* 2018. [Online]. Available: https://amj.amegroups.com/article/view/4747.

[34] F. Guedes, M. V. Branquinho, A. C. Sousa, R. D. Alvites, A. Bugalho, and A. C. Maurício, "Central airway obstruction: is it time to move forward?," *BMC Pulmonary Medicine,* vol. 22, no. 1, p. 68, 2022/02/19 2022, doi: 10.1186/s12890-022-01862-x.

[35] N. Integraal kankercentrum, "Sterfte Longkanker Nederland," ed, 2019.

[36]   A. D'Andrilli, F. Venuta, and E. A. Rendina, "Subglottic tracheal stenosis," *Journal of thoracic disease,* vol. 8, no. Suppl 2, pp. S140-S147, 2016/3// 2016, doi: 10.3978/j.issn.2072-1439.2016.02.03.

[37]   V. K. Holden and C. L. Channick, "Management of benign central airway obstruction," *AME Medical Journal,* vol. 3, pp. 76-76, 2018/7// 2018, doi: 10.21037/AMJ.2018.07.04.

[38]   C. Aravena *et al.*, "Idiopathic subglottic stenosis: a review," *Journal of thoracic disease,* vol. 12, no. 3, pp. 1100-1111, 2020/3 2020, doi: 10.21037/jtd.2019.11.43.

[39]   A. Gelbard *et al.*, "Treatment options in idiopathic subglottic stenosis: protocol for a prospective international multicentre pragmatic trial," *BMJ open,* vol. 8, no. 4, pp. e022243-e022243, 2018/4// 2018, doi: 10.1136/bmjopen-2018-022243.

[40]   F. Maldonado *et al.*, "Idiopathic subglottic stenosis: An evolving therapeutic algorithm," *The Laryngoscope,* vol. 124, no. 2, pp. 498-503, 2014/2// 2014, doi: https://doi.org/10.1002/lary.24287.

[41]   A. A. Thai, B. J. Solomon, L. V. Sequist, J. F. Gainor, and R. S. Heist, "Lung cancer," *The Lancet,* vol. 398, no. 10299, pp. 535-554, 2021/08/07/ 2021, doi: https://doi.org/10.1016/S0140-6736(21)00312-3.

[42]   T. Miyazawa *et al.*, "Stenting at the Flow-limiting Segment in Tracheobronchial Stenosis due to Lung Cancer," *American Journal of Respiratory and Critical Care Medicine,* vol. 169, no. 10, pp. 1096-1102, 2004/5// 2004, doi: 10.1164/rccm.200312-1784OC.

[43]   N. Duma, R. Santana-Davila, and J. R. Molina, "Non–Small Cell Lung Cancer: Epidemiology, Screening, Diagnosis, and Treatment," *Mayo Clinic Proceedings,* vol. 94, no. 8, pp. 1623-1640, 2019/08/01/ 2019, doi: https://doi.org/10.1016/j.mayocp.2019.01.013.

[44]   R. D. Rosen and A. Sapra, "TNM Classification," *StatPearls NCBI,* 2021/2// 2021. [Online]. Available: https://www.ncbi.nlm.nih.gov/books/NBK553187/.

[45]   J. Xu *et al.*, "Using individualized three-dimensional printed airway models to guide airway stent implantation," *Interactive CardioVascular and Thoracic Surgery,* vol. 31, no. 6, pp. 900-903, 2020/12// 2020, doi: 10.1093/icvts/ivaa206.

[46]   B. Shin, B. Chang, H. Kim, and B.-H. Jeong, "Interventional bronchoscopy in malignant central airway obstruction by extra-pulmonary malignancy," *BMC Pulmonary Medicine,* vol. 18, no. 1, pp. 46-46, 2018, doi: 10.1186/s12890-018-0608-6.

[47]   E. M. Walser, B. Robinson, S. A. Raza, O. S. Ozkan, E. Ustuner, and J. Zwischenberger, "Clinical Outcomes with Airway Stents for Proximal versus Distal Malignant Tracheobronchial Obstructions," *Journal of Vascular and Interventional Radiology,* vol. 15, no. 5, pp. 471-477, 2004/5// 2004, doi: 10.1097/01.RVI.0000124944.58200.D9.

[48]   E. Folch and C. Keyes, "Airway stents," *Annals of Cardiothoracic Surgery; Vol 7, No 2 (March 2018): Tracheal Surgery,* 2018. [Online]. Available: https://www.annalscts.com/article/view/16462.

[49]   S. D. Murgu and B. Laxmanan, "Biomechanical Properties of Airway Stents," *Journal of Bronchology & Interventional Pulmonology,* vol. 23, no. 2, pp. 89-91, 2016/4// 2016, doi: 10.1097/LBR.0000000000000267.
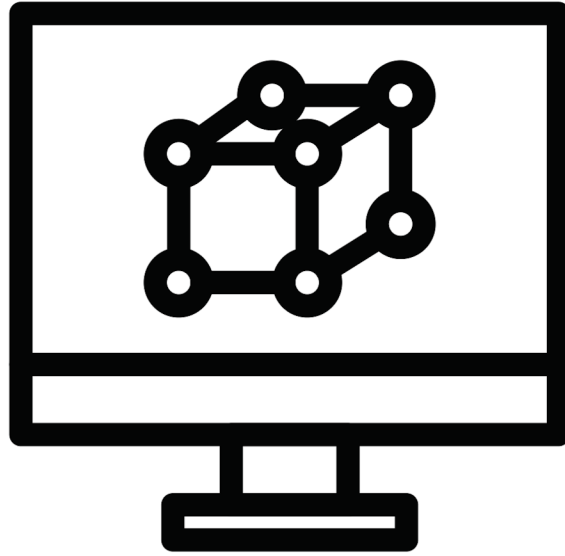
Chapter 2: Computational Fluid Dynamics Simulations

"I see music as fluid architecture."

JONI MITCHELL

Computational Fluid Dynamics (CFD) uses equations to numerically solve the behavior of fluids: xliquids and gases. [1] It is used by engineers e.g. the design of vehicles since CFD enables simulations of both the flow around the vehicle and inside the engine. [2] Governing equations that provide this purpose of fluid behavior are coupled differential equations, called Navier-Stokes. Together they describe the pressure, velocity, density, and temperature of a moving fluid, which is the heart of CFD. [3, 4] Different software programs are available to practice CFD with, such as COMSOL, ANSYS, or Autodesk CFD. Since ANSYS is widely used for (upper) airway simulations [5-13], it is also used within this thesis.

ANSYS consists of three software packages with different contributions to the simulation. ANSYS Workbench acts as the dashboard where the main components of the simulation will be defined. ANSYS SpaceClaim enables the design and optimization of the concerning geometry. Lastly, the three stages of a CFD simulation are performed within ANSYS FLUENT: pre-processing, processing, and post-processing, which processes will be explained further in this chapter. [7, 14]

All three stages of CFD contain input, both boundary conditions, and input parameters, for the simulations. Reliable results of the simulation are based on choosing the right input and knowing its effect on the outcome. Therefore, two proof-of-concepts studies will be conducted. Two boundary conditions will be tested, namely the fineness of the mesh and inlet and outlet conditions of the geometry. The mesh is the main component of the simulation where calculations are performed to. Especially when working on airways with relatively small obstructions, the mesh must be accurate. Studying the effect of the mesh fineness evaluates the influence on results within an acceptable computational time. Secondly, different conditions for the inlet and outlet will be tested. Since multiple options are present and assumptions for the airway can be made differently, the effect of different conditions on the results will be assessed.

2.1. SETTING UP THE MODEL

A CFD simulation consists of three main stages containing the input for a simulation. Towards reliable results relevant to the clinical situation, and understanding the simulation, this chapter elaborates on the theoretical side of CFD. Boundary conditions, input parameters, and the influence on the simulation will be described. Concerning airway simulations, this chapter can be used to further understand the simulations and suggest improvements.

2.1.1. Pre-Processing

The first stage of a CFD simulation is pre-processing, consisting of the geometry and detailed definition of all elements. Elements of the pre-processing stage and their parameters are explained in this section.

2.1.1.1.   Meshing

The simulation starts with a geometry of interest, a 3D shape, which is virtually described by a 2D surface. Such a virtual surface is called a surface mesh and is made up of smaller surfaces: mesh elements. Mesh elements are made up of edges, vertices, and faces and create shapes such as triangles or prisms. Examples are indicated in Figure 2-1 and a generated surface mesh is indicated in Figure 2-2. Smaller surfaces can provide higher accuracy of the geometry thus better approach the actual geometry. Regarding CFD simulations, the number of elements also describes the accuracy of the calculations. Since the calculation is performed at every face, more faces mean more results,

increasing the accuracy. At a certain point, the result does not change with a more refined mesh. The point where the result remains constant is where the mesh resolution is high enough. Increasing refinement of the mesh, hence the number of faces, only results in an increased calculation time.
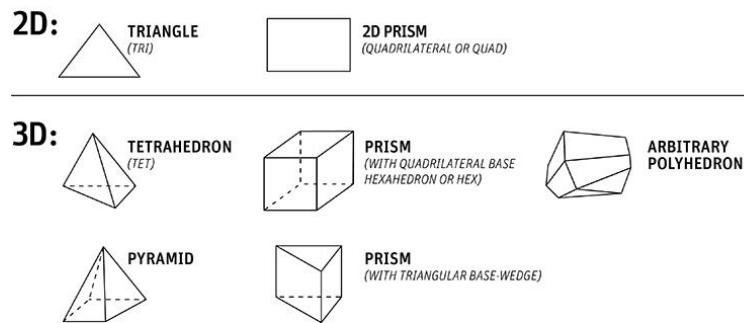
Figure 2-1 Different examples of shapes that a mesh can consist of. Both examples for a 2D and 3D mesh are given. From Codes [15]

Next to a description of the outer surface of the geometry, the interior is required to mesh for fluid flow calculation through the model. The interior mesh is built up of 3D elements instead of 2D. Considering these 3D elements, tetrahedral and polyhedral elements are commonly chosen. Tetrahedral elements are sufficient for simulations with low Reynolds numbers (<1000). Higher Reynolds numbers require more detailed meshes since flow is more challenging. Polyhedral elements have superior performance and are relatively less sensitive to stretching. [10, 16] Additionally, they discretize a complex geometry. [13] These elements are used in the mesh of Figure 2-2. An increased number of elements hence provides more thus enhanced results. But again, this also goes with increased computational time.

The last element in meshing is the transition from the interior mesh to the surface mesh. Interaction of the fluid with the wall is the main cause of turbulence and takes place in the boundary layer (Figure 1-3). In airway modeling, turbulence and wall interaction are the main results to evaluate. Therefore, an accurate mesh of the boundary layer is required which is elaborated on in the following sections.

2.1.1.1.1.   Near wall modeling

Modeling fluid flow near the wall is an important aspect while this is the region of interest in evaluating the flow effect on airways. In CFD, fluid enters the geometry with a laminar or uniform flow profile and induces zero velocity at the wall in the x-direction (no-slip boundary condition, see 2.1.1.2.4 Wall). In the direction orthogonal to the wall, the fluid reaches its bulk velocity. This flow transition from the wall toward the center is called the boundary layer. It has a non-uniform velocity profile, dependent on shape and interaction with the geometry and Reynolds number. The transition of horizontal layers within a turbulent flow is depicted in Figure 1-3.

Interaction of the fluid with the geometry takes place at the layer closest to the wall, called the viscous sub-layer. (Figure 1-3). Interaction causes movement in the fluid, thus increased velocity induces more movement in the flow and requires refined meshing to capture this behavior. [5, 17] Within the meshing process, the cell sequence orthogonal to the wall that captures the near-wall behavior of fluid is called inflation layers. These layers are indicated in Figure 2-2 and describe the transition from the wall to the bulk. The y+ value indicates the fineness of the inflation layers. It is a dimensionless measure for the orthogonal distance from the wall to the center of the first cell of the inflation layer. A y+ < 1 ensures the center of the first cell is in the viscous sub-layer, thus a high spatial resolution of the inflation layers for capturing near-wall fluid behavior. [5, 18, 19] The y+ is influenced by the transition ratio (TR) among others. It describes the ratio between cell areas: the last cell of the inflation

layer and the first cell out of the inflation layer. A low TR means that the first cells out of the inflation layers are relatively small hence more near-wall modeling is performed. [20]

Out of the inflation layers, the ratio between finer and coarser areas is the growth rate (GR). It describes the maximum growth of the connected cells. Tweaking these parameters changes the mesh and will show the best setting. [21]
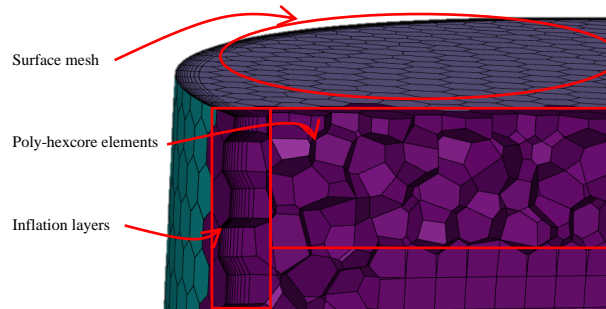
Figure 2-2 Screenshot of a generated mesh within Ansys Fluent. It shows the surface mesh, inflation layers, and poly-hexcore elements that enable near-wall modeling.

2.1.1.1.2.   Mesh Quality

After meshing the geometry, it is necessary to determine whether the quality is sufficient. First, skewness indicates the deformation of the elements in the mesh. Ideally, none of the elements are skewed thus the value is 0. In practice, this is not achievable and a maximum skewness below 0.95 is aimed. Above, it decreases the accuracy and destabilizes the simulation. As a consequence, ANSYS may experience difficulties converging. [19]. Another measure of quality is the orthogonal quality. It describes how close the angles are between adjacent element faces to the optimal determined angle. The optimal angle depends on the topology of the mesh. [22] A value of 1 is best but aimed at a minimum value above 0.1. [19] It becomes of interest when the simulation does not converge (fast enough). [23] ANSYS has set up a range for both metrics to identify your mesh quality, depicted in Figure 2-3.

Skewness mesh metrics spectrum

Excellent	Very good	Good	Acceptable	Bad	Unacceptable
0-0.25	0.25-0.50	0.50-0.80	0.80-0.94	0.95-0.97	0.98-1.00

Orthogonal Quality mesh metrics spectrum

Unacceptable	Bad	Acceptable	Good	Very good	Excellent
0-0.001	0.001-0.14	0.15-0.20	0.20-0.69	0.70-0.95	0.95-1.00

14   © 2015 ANSYS, Inc.   February 12, 2015
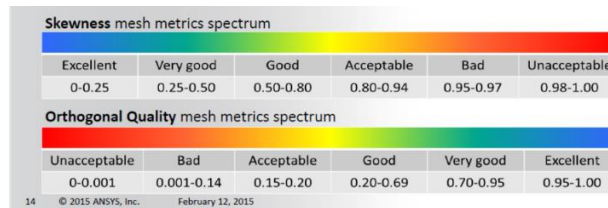
Figure 2-3 Mesh quality values for ANSYS meshing. Adapted from Ansys [19]

2.1.1.2.   Boundary conditions

Simulations are based on governing equations that describe fluid behavior. These equations result in a general solution to the problem. Generating a unique solution requires input to the model to use these as endpoints. Both boundary conditions and parameters are therefore required. Boundary conditions are characteristics that help a unique simulation, such as assuming a rigid wall. Parameters are input values, such as velocity. [14]

2.1.1.2.3.   Inlet, outlet, and wall

Regarding the geometry of the airways, air enters the model and subsequently leaves. This implies the presence of an inlet, outlet, and other structures of the geometry. In ANSYS, all regions must be defined before meshing using *Named Selections*. A boundary condition can, but also is required to

assign to each named selection. Hence, the inlet, outlet, and wall must be defined in the case of an outlet. Results for each named selection can also be evaluated separately. If required, the obstruction can therefore be selected and defined separately as a wall to see more specific results. Furthermore, it is important to set the right boundary conditions for each named selection. Especially choosing appropriate boundary conditions for the inlet and outlet determines the input values, based on initial available information or assumptions, by which the results are calculated. [24, 25]
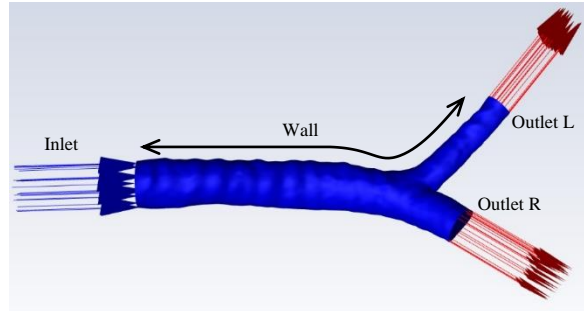
Figure 2-4 A screenshot of a segmented airway with the inlet (blue arrows), both outlets (red arrows), and airway wall (blue) defined as named selections. Boundary conditions for each named selection are defined within ANSYS.

Different boundary conditions are available for the inlet and outlet. Regarding airways, the inflow can be assumed to be velocity or mass flow rate. The mass flow rate is expressed in kg/s and describes the amount of fluid mass going through the model per period. The velocity boundary condition can only be applied in the use of incompressible flows. Both conditions are related to Eq. 2.1.

$$v = \frac{Q}{A}$$

<div align="right">*Eq. 2.1*</div>

with v the velocity in [m/s], Q the flow rate in [m³/s], and A the area of the inlet [m²]. The flow rate can be used to calculate the mass flow using the density of the substance. For the outlet, an open outflow or assumption of 0 Pa gauge pressure can be made. An outflow outlet is an open boundary and does extrapolate results towards the boundary. However, accurate placement of this outflow plane is required for reliable results without reversed flow (see Figure 2-5). [25] A pressure outlet with the assumption of 0 Pa decreases computational time since extrapolation of the interior is unnecessary and is also commonly performed for airway simulations. [8, 13, 24, 26]
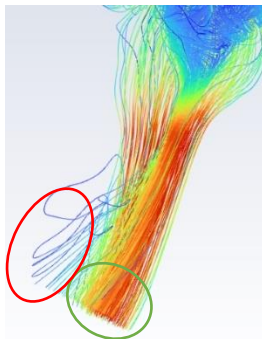
Figure 2-5 A screenshot of a simulation of a part of the airway. Visualized is the outlet of the right main bronchi of an airway. The green circle indicates flow that leaves the geometry, the red circle highlights the reversed flow going back into the geometry.

2.1.1.2.4.   Wall

Fluid flows through the geometry, and experiences friction with the wall. Two assumptions about the wall can be made:

- Non-slip: a velocity of zero in the x-direction relative to the wall. This is the default case for solid boundaries. The wall shear stress is computed by the viscous law or wall functions. [8, 13, 25]
- Slip: the velocity normal to the wall vanishes. This setting is used if solving the boundary layer is not required. [25]

Considering the airways, a non-slip boundary wall can be assumed. Trachea walls can be considered rigid due to the relatively high percentage of cartilage above the central airways. [12]

2.1.1.2.5.   Solver

The laminar flow consists of a stable velocity field whereas the velocity profile of turbulent flow is not consistent. These fluctuations can be too computationally expensive, but they are relatively small, therefore a simplification can be made. This is performed with the governing equations, which give a more averaged answer and are therefore quicker to solve. [27] Different models with other turbulence approximations are available which are shortly explained.

Simulation of turbulence effects can be performed with three different models, all having different turbulence approximations: direct numerical simulation (DNS), large-eddy simulation (LES), and Reynolds-averaged Navier-Stokes (RANS) models. Fluid swirls develop at low Reynolds that DNS resolves at all levels. DNS is therefore the most accurate model but is only suitable for low Reynolds numbers and computationally the most expensive. LES resolves fluid swirls only at large scales but is still accurate. [28] Airways do contain higher Reynolds numbers and require solving swirls at all levels; thus, the remaining model is RANS. RANS does not solve fluid swirls but predicts their dynamics. Two types of RANS models exist, κ-ε and κ-ω. [29] The κ-ε is suitable for low-Reynolds numbers and calculates the free stream dynamics, but has been found not accurate enough for the oropharynx. [29, 30] The κ-ω is capable of resolving the viscous sub-layer and hence suitable for near-wall dynamics [17, 30]

Combining the RANS κ-ω model with the shear stress transport (SST) model uses properties of both the κ-ω and κ-ε models. Thus, the SST κ-ω model can simulate laminar and turbulent streams. [13, 30] Moreover, it has shown useful results in clinical applications for the respiratory airway. The model accurately predicts the turbulence at transitions in the airway, such as bifurcations or obstructions. [10, 28] Concluding, the κ-ω SST model is considered the most suitable solver for flow in the respiratory system. [12]

2.1.1.2.6.   Entrance length

The inlet flow velocity profile in ANSYS is uniform. Due to the shape of the geometry and Reynolds number, it may become turbulent. the geometry As Figure 1-3 and Figure 2-6 indicate it takes a certain time to fully develop into such a velocity profile. An entrance length can therefore be added before the geometry that provides time, thus length, for the flow to develop.
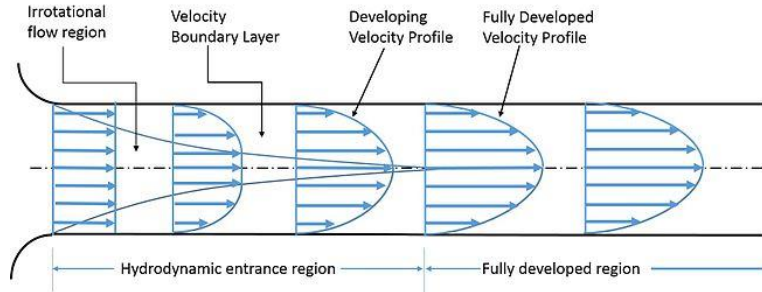
Figure 2-6 A schematic overview of the developing flow. On the left side, the flow enters the model. Towards the right side, it becomes more developed.

Upper airways make the airflow turbulent when entering the trachea. [31] Different methods for extruding the geometry are stated. For example, Zobaer and Sutradhar [13] extruded their geometry five times the hydraulic diameter in its normal direction. In contrast, Davies and Moores [32] extruded 0.03 x diameter x Reynolds number. Based on experience, ANSYS suggests a length of $80 *$ $internal\ diameter$ of the pipe. [23] Hence, no final assumption can be made about the entrance length of the model. Additionally, another method was proposed by Miyawaki, et al. [31] who designed a geometric laryngeal model visualized in Figure 2-7. Next to adding extra length to the current geometry, it also simulates turbulent flow from the upper airways. However, this geometry must be designed for every individual geometry.

$$L_g = 8.64 D_{h,t}$$
$$D_{h,g} = 0.677 D_{h,t}$$
$$D_{h,gu} = 1.24 D_{h,t}$$
$$l_{gu} = 1.3 D_{h,t}$$
$$l_{gl} = 1.3 D_{h,t}$$
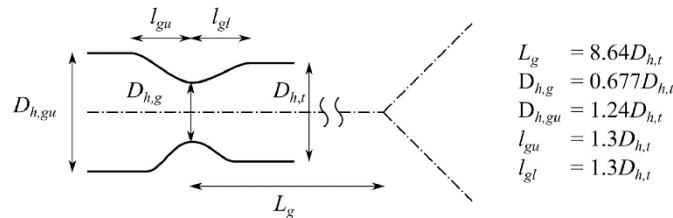
Figure 2-7 Definitions to design the geometrical laryngeal model by Miyawaki, et al. [31]. The hydraulic diameter of the trachea $D_{h,t}$, the location of the glottis L_g, the diameter at the glottis $D_{h,g}$, the diameter proximal to the glottis $D_{h,gu}$, the length of the upper part of the glottis l_{gu}, and the length of the lower part of the glottis l_{gl}.

To summarize, multiple methods can be applied to ensure entrance length, but standardization remains absent. This thesis does not implement any entrance length because of multiple reasons. First of all, it requires more meshing thus complicating the simulation and increasing computational time. Next, the post-processing phase becomes more complex. Different planes must be defined to calculate values across only the lower airway and exclude the upper airway. Lastly, the translation of simulated results to experiments becomes more complicated. However, it is considered the main concern in further research to investigate an enhanced clinical representation of the simulation.

2.1.1.2.7.   Convergence

Convergence is the process of the simulation where the error of the results is minimized. The definition takes place in the pre-processing stage, but the convergence process occurs during the processing stage. The final result of a CFD analysis is reached if either the residual level or the maximum number of iterations has been reached. In other words, convergence has been accomplished before reaching the maximum number of iterations. Otherwise, it quits at the maximum number of iterations but is not converged. Fast convergence, ±100 iterations, indicates a good quality of the mesh with stable in and outflow. If it takes a relatively longer time, ±300 iterations, either the mesh quality is poor or the balance of the in- and outflow is disturbed. ANSYS recommends 300-500 iterations to ensure enough time to converge, especially with a complex mesh but quit in time if the simulation does not converge at all.

The remaining error is defined as the residuals, that quantify the error in the run-through equations. A residual level of 10^{-4} is considered to be loosely converged; 10^{-6} is highly accurate. However, it is not always possible in complex situations to achieve residual levels lower than 10^{-5}. [33] Among others, this can be due to the location of the outlet boundary. If this plane is not placed adequately or the outlet area is relatively small, the reversed flow may present that inhibits convergence. Subsequently, the results are not valid. [25] Since airways are relatively complex geometries, a convergence of 10^{-4} is chosen together with Vandervelpen [23], assumed to be satisfactory.

2.1.2.   Processing

The second stage of a CFD analysis is called processing. During processing, the convergence of the final results takes place to reach the defined level of residuals. Hence, processing tries to minimize the error by the convergence of the results. Figure 2-8 gives a schematic overview of ANSYS, the software that is used in this thesis to simulate, and the software components that it uses (SpaceClaim for the geometry, Fluent for the mesh, boundary conditions, and input parameters).
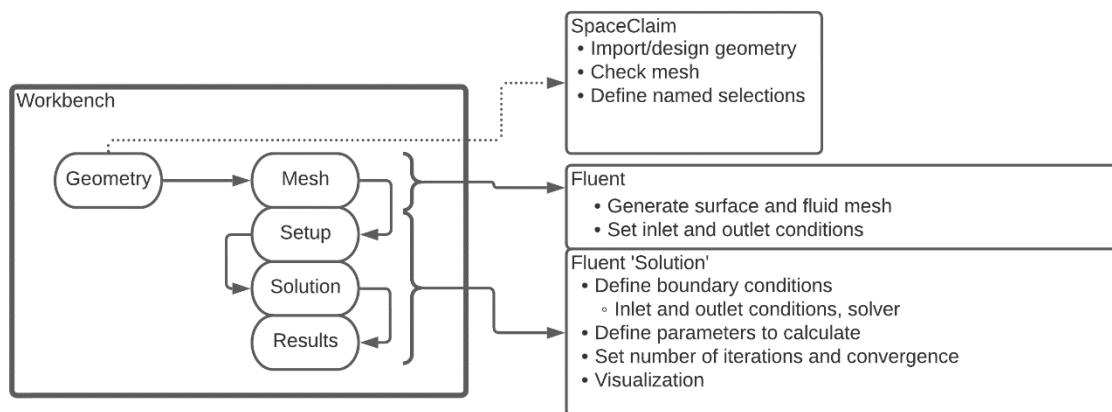
Figure 2-8 Schematic overview of the ANSYS software with the components Workbench, SpaceClaim and Fluent.

2.1.3.   Post-processing

After simulating, the results can be visualized in graphs, contour plots, videos, path lines, vectors, or in different planes. Hence, multiple ways are available, but the kind of visualization depends on the results. For example, pressure can be plotted onto the model as a contour plot whereas velocity can be visualized using path lines through the geometry.

2.2. <u>PARAMETERS OF INTEREST</u>

The physiology of breathing is based on the pressure difference between the environment and intrapleural space. The resistance of the airways indicates the amount of work required to achieve sufficient air flow, as Hagen-Poiseuille's law states in section 1.2.1 Breathing mechanism. Another applicable principle is Bernoulli, which states that the total energy of the fluid remains constant. In other words, a narrow airway has a higher velocity but lower pressure. [34] Hence, Bernoulli's principle is summarized as:

$$P_{in} + \frac{1}{2}\rho v_{in}^2 = P_{out} + \frac{1}{2}\rho v_{out}^2 \qquad \text{Eq. 2.2}$$

where P is static pressure [Pa], ρ the density [kg/m³] and v the velocity of the fluid [m/s]. The input is defined at the inlet and the outlet of the airway. In this thesis, the absolute pressure drop (PD, [Pa]) will be studied, which is the difference in pressure between the inlet and outlet. It is a parameter to study the severity of the obstruction as well as the shape of the geometry. A moderate obstruction of 50-70% of the cross-sectional area already contributes to variable symptoms and a significant pressure drop at higher flow rates. [35] For laminar flow, the pressure drop doubles with a doubled flow rate, whereas for turbulent flow the pressure drop quadruples. [36]

Interaction of fluid with the wall (also see 1.2.2 Airway clearance) is called wall shear stress (WSS). It is defined as the force per unit area exerted by the airflow on the wall at the tangent plane. [37, 38] Higher velocity results in increased WSS, since WSS is the first derivative of velocity. Additionally, the turbulent flow has a lower velocity gradient relative to the wall than the laminar. As a consequence, turbulent flow results in an increased WSS value since the area of shear is increased. [38]

WSS plays a role in mucociliary clearance in the airways. The mucus must be moved upwards for elimination, which process is most convenient if the mucus is in a fluid-like form provided by a sufficiently high WSS. [11] An airway stent will inhibit the possibility of the upwards moving of the mucus since cilia are not present within an airway stent. Additionally, mucus is stuck between the stent and the airway. These two factors explain the complication of mucus plugging and clinically plead for a short stent. Healthy WSS ranges from 0.03 – 0.49 Pa during inspiration (Figure 2-9, left), dependent on the pressure difference between the in- and outlet. [35] Another application of WSS is the indication of injury executed onto the airway wall where endothelial cells are at risk. [7, 12] Not only the airway wall suffers from increased WSS, but stent migration is expected to be also caused by this parameter. Higher shear stresses than radial forces will cause the stent to migrate, a well-known complication. [39] In short, WSS influences mucus elimination in the airways, stent migration, and airway wall damage and will therefore be evaluated within this thesis.
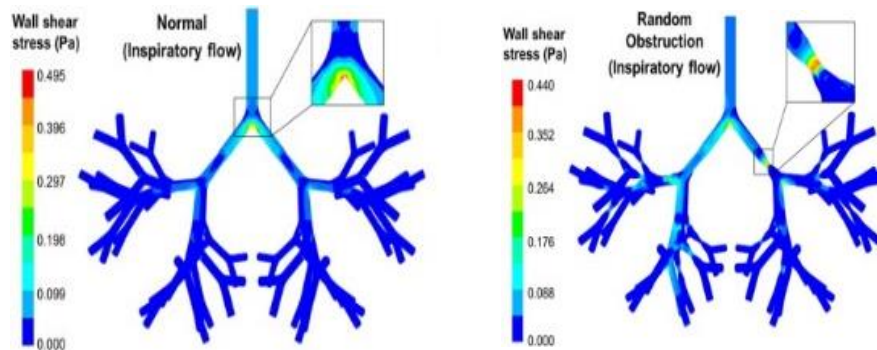
Figure 2-9 Wall shear stresses in the bronchial tree resulting from a Computational Fluid Dynamics simulation of the airway. Results from a normal inspiratory (left) and additional random obstruction in the airway (right) is depicted. From Sul, et al. [11]

Next, turbulence intensity (TI) is of interest in the airway. It is defined as the ratio between the standard deviation of the fluctuating velocity and the mean velocity of the fluid. The presence of turbulence intensity can help in understanding the result of the pressure drop and WSS. The range of turbulence intensity in the trachea is between 5-20%. [29]

Lastly, the mass flow rate (MFR) will be evaluated. It is the amount of mass in kilograms per unit of time that flows through the inlet or outlet. Therefore, it indicates the balance between the inlet and outlet. Since these have to be in balance for a stable simulation, this parameter also implies to which extent the simulation is stable. Moreover, the ventilation of each lung can be derived from the MFR. In healthy subjects, the MFR of the left and right side relative to the inlet is 46.83:53.28% [40] and 43.43:56.57% [8], respectively.

2.3. EFFECT OF MESHING

As described in chapter 2.1, one of the first steps toward a CFD analysis is generating a surface and interior mesh of the geometry. An agreement between the fineness of the mesh, and the computational time and its effect on the results is required for the optimization of the simulations. A proof-of-concept study is therefore conducted to understand meshing parameters. The influence of two parameters on the mesh quality, skewness, and orthogonal quality, is evaluated: the size of the mesh elements and inflation layers. For both parameters is expected that an increased number prolongs the computational time but improves results. Not only mesh quality but also the effect of the pressure drop (PD) will be evaluated. The best results depend on the agreement between mesh quality and PD.

2.3.1. Methods

ANSYS Academic Research CFD (Ansys Inc. v. 2021R2) Workbench was used to define the steps of the simulation. A step-by-step guide is included in Appendix A: Manual for setting up airway simulations within ANSYS. SpaceClaim was used to design the stent geometry, a 16 mm diameter and length of 100 mm. These parameters are based on the characteristics of a conventional tracheal airway stent. The simulation was performed with the component system *Fluid Flow (with Fluent Meshing),* as recommended by Vandervelpen [23]. The parameters that are put in the model are all summarized in Table 2-1. The maximum skewness, minimal orthogonal quality, number of cells, and y+ value were used for the analysis of the mesh quality. The pressure drop, the absolute difference between the inlet and outlet static pressure, was evaluated to determine the influence of the mesh size on a parameter of interest.

Table 2-1 Overview of the parameters that are used within the simulation.

Boundary layers	10	
Mesh elements	Poly-hexcore	(see 2.1.1.1 Meshing)
Inlet velocity	0.5 L/s [6, 13] to m/s by input of Eq. 2.1	
Inlet flow direction	Normal to boundary	
Pressure outlet	0 Pa gauge pressure	(see 2.1.1.2.3 Inlet, outlet, and wall)
Wall	No-slip	(see 2.1.1.2.3 Inlet, outlet, and wall)
Air density	1.225 kg/m^3	
Air dynamic viscosity	1.79 x 10^{-5} kg/m·s	(see 3.4.1 Assumptions)
Solver	SST κ-ω model	(see 2.1.1.2.5 Solver)
Convergence	10^{-4}	(see 2.1.1.2.7 Convergence)
Number of iterations	300	
Computer specifications	Intel® Core™ i7-10850H CPU@2.70GHz, 6 cores and 12 logical processors	

2.3.1.1. Experiment 1

Experiment 1 was conducted to test the effect of different mesh sizes on the above-mentioned parameters. Number one had a minimum size of 0.05 and a maximum size of 0.5 mm, number two 0.5 and 1 mm, and number three 0.05 mm and 1 mm, respectively (see Table 2-2). Standard values for the Growth Rate (GR, 1.2) and Transition Ratio (TR, 0.272) were applied.

2.3.1.2.   Experiment 2

Experiment 2 was conducted to test the transition ratio (TR) and growth ratio (GR), that influence the inflation layers, and to evaluate their effects on the above-mentioned parameters. The mesh size was kept similar to in Experiment 1. First, standard values for the GR (1.2) and TR (0.272) were simulated. In the next simulation, the TR was decreased to 0.1. Lastly, a simulation was conducted with a GR of 1.5 and a TR of 0.1 (see Table 2-3).

2.3.2. Results

The first experiment considered the effect of the mesh size on the quality of the mesh and PD. which results are given in Table 2-2. The minimum orthogonal quality of all simulations lies within the range that is qualified as 'Good', skewness within 'Very good' (Figure 2-3). Test number 1 has the smallest mesh elements, the highest number of cells with the highest pressure drop, but relatively worst mesh quality. On contrary, it has a y+ below 1 hence suitable for near-wall modeling. Test number 2 has the biggest mesh elements and shows the best mesh quality. The highest range in mesh element size is evaluated in number 3 with similar results to test number 2.

Table 2-2 Results of the first experiment that investigated the effect of the mesh size on the quality of the mesh (orthogonal quality, skewness, y+) and the pressure drop. Test number 2 shows the best mesh quality.

| | Settings | | | | Results | | | | |
#	Min size	Max size	TR	GR	# cells	Min Orthogonal quality	Max Skewness	Y+	Pressure drop (Pa)
1	0.05	0.50	0.272	1.20	515738	0.37	0.41	0.89	2.60
2	0.50	1.00	0.272	1.20	127739	0.53	0.37	1.39	2.50
3	0.05	1.00	0.272	1.20	94438	0.51	0.37	1.39	2.51

TR = transition ratio, GR = growth rate

Secondly, the influence of the inflation layers on the mesh quality and pressure drop is described in Table 2-3. The minimum orthogonal quality of all simulations lies within the range that is qualified as 'Good', skewness within 'Very good' (Figure 2-3). Test number 4 is similar to number 1 but shows a different number of cells. A decrease in the TR for test number 5 shows an improved minimum orthogonal quality and y+ value together with an increase in pressure drop, relative to experiment number 4. An additional increase in GR shows a decrease in minimum orthogonal quality but an improved y+ value and an increase in pressure drop.

Table 2-3 Results of the second experiment that investigated the effect of the TR and GR of the inflation layers on the quality of the mesh (orthogonal quality, skewness, y+) and the pressure drop.

| | Settings | | | | Results | | | | |
#	Min size	Max size	TR	GR	# cells	Min Orthogonal quality	Max Skewness	Y+	Pressure drop (Pa)
4	0.05	0.50	0.272	1.2	431797	0.37	0.41	1.23	2.61
5	0.05	0.50	0.1	1.2	457062	0.52	0.41	0.48	2.77
6	0.05	0.50	0.1	1.5	462924	0.25	0.41	0.1	2.83

TR = transition ratio, GR = growth rate

2.3.3. Discussion

The objective was to assess the influence of the mesh size and inflation layers on the mesh quality, minimal orthogonal quality and skewness, and PD. Smaller mesh elements and a decrease in the TR improve the y+ value, related to enhanced near-wall modeling. An additional increase of the GR further improves the y+ value but affects the orthogonal quality. To conclude, small elements with a decreased TR (#5) are expected to give sufficient results within an acceptable computational time.

Smaller elements give the relatively worst orthogonal quality and skewness, also with the longest computational time, but can still be interpreted as good as indicated in figure 2-4. Therefore, all simulations have a sufficient mesh and computational time is the main consideration. However, this was not quantified but only qualitatively considered. It is required in further experiments to take this parameter as a quantitative value since it can currently not be discussed.

The geometry tested considered a straight pipe which is an uncomplicated geometry shape. Hence, the effect of setting different mesh element sizes, TR, and GR remain unknown to more complex geometries. Therefore, each simulation requires evaluation of the minimum orthogonal quality and maximum skewness with Figure 2-3 and ensuring a y+ value below 1 to ensure sufficient quality.

The fineness of the inflation layers was measured based on the y+ value and PD. The y+ value is an important measure for this experiment because it describes the capability of capturing near-wall fluid behavior. As a parameter, the PD was evaluated. However, wall shear stress (WSS) describes fluid interaction with the wall and is therefore expected to be a better evaluation of the inflation layers.

Results of test number 1 and 4 show an increased number of elements and y+ value for test 1 with similar mesh settings. One difference is a new mesh generation from similar geometry. Hence generating a mesh from a similar geometry can provide different results in the meshing due to other calculations of the mesh elements.

2.4. EFFECT OF INLET AND OUTLET CONDITIONS

A boundary condition for the inlet and outlet is required for a simulation. Since multiple airway geometries with different inlet and outlet areas will be simulated, comparable inlet values across different models are required. Since multiple assumptions can be made for both the inlet and outlet, combinations will be evaluated for the impact on the results and computational time. For the inlet, velocity and mass flow rate will be tested. It is hypothesized that results are similar since these parameters are related (see Eq. 2.1). At the outlet, an outflow and assumption of 0 Pa gauge pressure will be defined. Expected is also similar results but increased computational time for the outflow boundary condition, due to extrapolation.

2.4.1. Methods

Similar method and geometry as in Experiment 1 from Methods 2.3.1.1 Experiment 1 was performed. Parameters in this simulation are similar as mentioned in Table 2-1 unless mentioned differently below. A step-by-step guide is included in Appendix A: Manual for setting up airway simulations within ANSYS. Four different simulations were performed, with two options for both the inlet and outlet. For the results, the maximum skewness, minimal orthogonal quality, number of cells, y+ value, and pressure drop inlet and outlet planes were evaluated.

For the velocity inlet [m/s] the expression of Eq 2.1 was used as the input with an assumed flow rate of 0.5 L/s (see 2.3.1.3.). For the mass flow rate inlet [kg/s], the density of air was assumed to be 1.225 kg/m^3, hence the mass flow rate is $6.125 \cdot 10^{-4}$ kg/s. The outlet boundary condition is defined as outflow, or a pressure outlet with the assumption of 0 Pa gauge pressure. (see 2.1.1.2.3 Inlet, outlet, and wall).

2.4.2. Results

Table 2-4 shows the results of the different boundary conditions for the inlet and outlet. All inlet and outlet velocities were similar. A pressure outlet showed in both cases a higher static pressure at the inlet than the outflow outlet boundary condition. Additionally, the static pressure at the outlet was negative in both outflow outlets.

The maximum difference in the absolute static pressure difference is present between the velocity inlet with pressure outlet and both mass flow rate inlets, 0.03 Pa (1.1%). Both simulations with the outflow outlet had a relatively longer computational time than the simulations that considered the pressure outlet.

Table 2-4 Testing different boundary conditions in a straight tube with a length of 10 cm and cross-sectional area of 0.000201 m² (diameter 1.6 cm). The air flow rate in all models is 0.5 L/s with a density of 1.225 kg/m³.

Settings				*Results*			
Boundary condition inlet	**Inlet**	**Boundary condition outlet**	**Inlet velocity (m/s)**	**Outlet velocity (m/s)**	**Static pressure inlet (Pa)**	**Static pressure outlet (Pa)**	**| ΔPa |***
Velocity	2.49 m/s	Pressure	2.49	2.49	2.60	0 ˣ	2.60
		Outflow	2.49	2.49	0.39	-2.23	2.62
Mass flow rate	$6.125 \cdot 10^{-4}$ kg/s	Pressure	2.49	2.49	2.63	0 ˣ	2.63
		Outflow	2.49	2.49	0.41	-2.22	2.63

* The absolute difference in static pressure is measured between the inlet and outlet, also called pressure drop ΔPa
ˣ The static pressure at the outlet is also a setting

2.4.3. Discussion

Different boundary conditions for both the inlet and outlet planes were evaluated. The PD between all combinations differed by a maximum of 1.1%. Additionally, computational time with the outflow outlet boundary condition was relatively longer than the pressure outlet boundary condition. To conclude, since the velocity is more commonly used in the literature [7, 12, 13, 29, 41] and a pressure outlet takes less computational time, these are chosen to implement in further CFD analysis.

Results differed for a maximum of 1.1%. Therefore, the chosen boundary conditions are assumed to have a not significant impact on the results. Computation time is therefore the leading factor in choosing. This parameter was considered within this section but not quantified. If further research is required, this parameter must be quantified for clear results.

Using the outflow boundary condition at the outlet lacks the assumption of 0 Pa gauge pressure. As described in section 2.1.1.2.3 Inlet, outlet, and wall, outflow requires extrapolation of the interior that goes with increased computational time. Since results only varied 1.1% and 0 Pa gauge pressure is a common assumption in literature [8, 12, 13, 26], further simulations still have a pressure outlet.

2.5. DISCUSSION

Chapter 2 started with a theoretical overview of CFD analysis. Secondly, two CFD simulation experiments were conducted in ANSYS that support final airway simulations. This chapter showed the necessity of a mesh test before the simulation to evaluate mesh quality, especially in obstructed airways. Next, a velocity inlet and pressure outlet were chosen to implement in further simulations since these are also commonly used in literature, and the results only differ 1.1%. In short, this chapter helped in the understanding of CFD and contributed to the workflow of final airway simulations.

Section 2.2 described the parameters that are of interest during an airway simulation. The pressure drop (PD) describes the different in pressure between the inlet and outlet, hence the work of breathing is desired to be minimized. Second, wall shear stress (WSS) is the shear of the airflow against the wall of the geometry. It can be used as an indicator for stent migration, so it also needs to be reduced. Third, turbulence intensity (TI) describes the variation in velocity compared to the mean velocity. Within airways, it could provoke mucus plugging and is therefore undesired. Lastly, the mass flow rate (MFR) describes the amount of air across the inlet or outlet hence the ventilation of both lungs. Also, other parameters can be analyzed, such as the axial and tangent velocity, as mentioned in the literature. [12] It was chosen to not analyze these parameters for two reasons. First, the added value of these parameters to the currently chosen parameters could not be confirmed. Next, adding more parameters to the evaluation makes it more complex and a possible relation between the parameter and clinical evaluation becomes harder to mark.

Section 2.3 tested different mesh sizes. Towards airway and stent simulations, interaction with the wall is important. Hence, a y+ value below 1 is required. Smaller mesh elements and a decreased TR improve the y+ value. Following these results, small mesh elements with a TR of 0.1 will suffice. Before interpretation of results, the minimum orthogonal quality, maximum skewness, and y+ value must be evaluated (see Figure 2-3) to ensure the high enough quality of the mesh. The section proved the importance of these parameters, especially when interested in fluid-wall interactions.

Section 2.4 tested different boundary conditions for the inlet and outlet. Since the maximum difference between results only varied 1.1%, input parameters can be based on computational time. Since the mass flow rate and velocity are related to Eq. 2.1 which can be put into the model, almost no differences in outcome are analyzed. For the outlet, 0 Pa gauge pressure was assumed since computational time was the lowest and its frequent use in literature.

REFERENCES

[1]   Wikipedia.   "Computational   fluid   dynamics."
        https://en.wikipedia.org/wiki/Computational_fluid_dynamics (accessed 30-03, 2022).

[2]   J. D. Anderson, *Computational fluid dynamics : the basics with applications*. New York, NY:
        McGraw-Hill (in English), 2010.

[3]   Comsol. "Navier Stokes equations." https://www.comsol.com/multiphysics/navier-stokes-
        equations (accessed 30-03, 2022).

[4]   N.   Hall.   "Navier-Stokes   Equations."   Glenn   Research   Center.
        https://www.grc.nasa.gov/www/k-12/airplane/nseqs.html (accessed 26/06, 2022).

[5]   R. Agujetas, R. Barrio-Perotti, C. Ferrera, A. Pandal-Blanco, D. K. Walters, and A. Fernández-
        Tena, "Construction of a hybrid lung model by combining a real geometry of the upper
        airways and an idealized geometry of the lower airways," *Computer Methods and Programs
        in   Biomedicine,*   vol.   196,   pp.   105613-105613,   2020,   doi:
        https://doi.org/10.1016/j.cmpb.2020.105613.

[6]   F.-L. Chen, T.-L. Horng, and T.-C. Shih, "Simulation analysis of airflow alteration in the
        trachea following the vascular ring surgery based on CT images using the computational
        fluid dynamics method," *Journal of X-Ray Science and Technology,* vol. 22, no. 2, pp. 213-
        225, 2014, doi: 10.3233/XST-140420.

[7]   W. M. Faizal *et al.*, "Computational fluid dynamics modelling of human upper airway: A
        review," *Computer Methods and Programs in Biomedicine,* vol. 196, pp. 105627-105627,
        2020, doi: 10.1016/j.cmpb.2020.105627.

[8]   C.-Y. Ho *et al.*, "Numerical analysis of airflow alteration in central airways following
        tracheobronchial stent placement," *Experimental Hematology & Oncology,* vol. 1, no. 1, pp.
        23-23, 2012, doi: 10.1186/2162-3619-1-23.

[9]   A. Issakhov, Y. Zhandaulet, A. Abylkassymova, and A. Issakhov, "A numerical simulation of
        air flow in the human respiratory system for various environmental conditions," *Theoretical
        Biology and Medical Modelling,* vol. 18, no. 1, pp. 2-2, 2021, doi: 10.1186/s12976-020-
        00133-8.

[10]   Y. Shang, J. Dong, L. Tian, K. Inthavong, and J. Tu, "Detailed computational analysis of flow
        dynamics in an extended respiratory airway model," *Clinical Biomechanics,* vol. 61, pp. 105-
        111, 2019, doi: https://doi.org/10.1016/j.clinbiomech.2018.12.006.

[11]   B. Sul, A. Wallqvist, M. Morris, J. Reifman, and V. Rakesh, "A computational study of the
        respiratory airflow Characteristics in normal and obstructed Human airways," *Computers in
        Biology and Medicine,* vol. 52, 2014/9// 2014, doi: 10.1016/j.compbiomed.2014.06.008.

[12]   M. Tullio, L. Aliboni, F. Pennati, R. Carrinola, A. Palleschi, and A. Aliverti, "Computational
        fluid dynamics of the airways after left-upper pulmonary lobectomy: A case study,"
        International journal for numerical methods in biomedical engineering, vol. 37, no. 7, pp.
        e3462-e3462, 2021/7// 2021, doi: 10.1002/cnm.3462.

[13]   T. Zobaer and A. Sutradhar, "Modeling the effect of tumor compression on airflow dynamics
        in trachea using contact simulation and CFD analysis," *Computers in Biology and Medicine,*
        vol.   135,   pp.   104574-104574,   2021,   doi:
        https://doi.org/10.1016/j.compbiomed.2021.104574.

[14]   D. Apsley, "Pre- and Post-Processing," ed, 2022.

[15]   F. Codes. "Ansys Meshing Solutions." https://fluidcodes.com/software/ansys-meshing-
        solutions/ (accessed.

[16]   M. Spiegel *et al.*, "Tetrahedral vs. polyhedral mesh size evaluation on flow velocity and wall
        shear stress for cerebral hemodynamic simulation," *Computer Methods in Biomechanics*

and Biomedical Engineering, vol. 14, no. 1, pp. 9-22, 2011/02/01 2011, doi: 10.1080/10255842.2010.518565.

[17]   Ansys, "Turbulence Modeling Using Ansys CFD, Lecture 03," ed: Ansys, 2020, pp. 4-22.

[18]   H. Mendis, "What y+ should I run? Part 1 – The underlying physics," ed, 2019.

[19]   Ansys, "Introduction to ANSYS Meshing," ed: Ansys, 2015.

[20]   D. Rana. "Inflation Mesh And Transition Ratio." Cadsys25. https://www.cadsys25.com/2020/05/inflation-mesh-and-transition-ratio.html (accessed 29/06, 2022).

[21]   cfd.ninja. "Ansys Meshing - Sizing (SOFT/HARD)." CFD.ninja. https://cfd.ninja/ansys-meshing/ansys-meshing-sizing-soft-hard/#:~:text=The%20Growth%20Rate%20represents%20the,each%20succeeding%20layer%20of%20elements. (accessed 29/06, 2022).

[22]   T. Avraham. "Know Thy Mesh - Mesh Quality - Part 1." https://cfdisrael.blog/2019/02/01/know-thy-mesh-mesh-quality-part-i/ (accessed 25/07, 2022).

[23]   E. Vandervelpen, "Ansys (Computational Fluid Dynamics) Support," E-Mail & Meetings ed, 2022.

[24]   R. Hagmeijer, "Computational Fluid Dynamics Information," ed, 2022.

[25]   Ansys. "Boundary Conditions." Ansys Inc. https://www.afs.enea.it/project/neptunius/docs/fluent/html/ug/node247.htm (accessed.

[26]   C. van Ertbruggen, C. Hirsch, and M. Paiva, "Anatomically based three-dimensional model of airways to simulate flow and particle transport using computational fluid dynamics," *Journal of Applied Physiology,* vol. 98, no. 3, pp. 970-980, 2005/3// 2005, doi: 10.1152/japplphysiol.00795.2004.

[27]   I. Ansys, "Ansys Fluent: Turbulence," ed, 2009.

[28]   A. Fernández-Tena, A. C. Marcos, R. Agujetas, and C. Ferrera, "Simulation of the human airways using virtual topology tools and meshing optimization," *Biomechanics and Modeling in Mechanobiology,* vol. 17, no. 2, pp. 465-477, 2018/04/01 2018, doi: 10.1007/s10237-017-0972-9.

[29]   C.-L. Lin, M. H. Tawhai, G. McLennan, and E. A. Hoffman, "Characteristics of the turbulent laryngeal jet and its effect on airflow in the human intra-thoracic airways," *Respiratory Physiology & Neurobiology,* vol. 157, no. 2, pp. 295-309, 2007, doi: https://doi.org/10.1016/j.resp.2007.02.006.

[30]   W. Frei, "Which Turbulence Model Should I Choose for My CFD Application? | COMSOL Blog," ed, 2017.

[31]   S. Miyawaki, E. A. Hoffman, and C.-L. Lin, "Numerical simulations of aerosol delivery to the human lung with an idealized laryngeal model, image-based airway model, and automatic meshing algorithm," *Computers & fluids,* vol. 148, pp. 1-9, 2017/4// 2017, doi: 10.1016/j.compfluid.2017.02.008.

[32]   A. Davies and C. Moores, "Airflow in the Respiratory System," *The Respiratory System,* pp. 41-59, 2010, doi: 10.1016/b978-0-7020-3370-4.00004-9.

[33]   M. Kuron. "3 Criteria for Assessing CFD Convergence." Engineering. https://www.engineering.com/story/3-criteria-for-assessing-cfd-convergence (accessed.

[34]   R. Colombo *et al.*, "Effect of airway narrowing in asthma: active learning through a simple and didactic model," *Advances in Physiology Education,* vol. 42, no. 3, pp. 473-476, 2018/09/01 2018, doi: 10.1152/advan.00053.2018.

[35]   V. K. Holden and C. L. Channick, "Management of benign central airway obstruction," *AME Medical Journal,* vol. 3, pp. 76-76, 2018/7// 2018, doi: 10.21037/AMJ.2018.07.04.

[36]   Alicat Scientific. "What is pressure drop?" https://www.alicat.com/knowledge-base/what-is-pressure-drop/ (accessed.

[37]   J. Stéphano and B. Mauroy, "Wall shear stress distribution in a compliant airway tree," *Physics of Fluids,* vol. 33, no. 3, pp. 031907-031907, 2021/3// 2021, doi: 10.1063/5.0038706.

[38]   D. Katritsis, L. Kaiktsis, A. Chaniotis, J. Pantos, E. P. Efstathopoulos, and V. Marmarelis, "Wall Shear Stress: Theoretical Considerations and Methods of Measurement," *Progress in Cardiovascular Diseases,* vol. 49, no. 5, pp. 307-329, 2007/03/01/ 2007, doi: https://doi.org/10.1016/j.pcad.2006.11.001.

[39]   A. Rosell and G. Stratakos, "Therapeutic bronchoscopy for central airway diseases," (in eng), *Eur Respir Rev,* vol. 29, no. 158, Dec 31 2020, doi: 10.1183/16000617.0178-2019.

[40]   S. Qi, Z. Li, Y. Yue, H. J. van Triest, and Y. Kang, "Computational fluid dynamics simulation of airflow in the trachea and main bronchi for the subjects with left pulmonary artery sling," (in eng), *Biomed Eng Online,* vol. 13, p. 85, Jun 24 2014, doi: 10.1186/1475-925x-13-85.

[41]   Q. Gu *et al.*, "Structural and functional alterations of the tracheobronchial tree after left upper pulmonary lobectomy for lung cancer," *BioMedical Engineering OnLine,* vol. 18, no. 1, p. 105, 2019/10/25 2019, doi: 10.1186/s12938-019-0722-6.
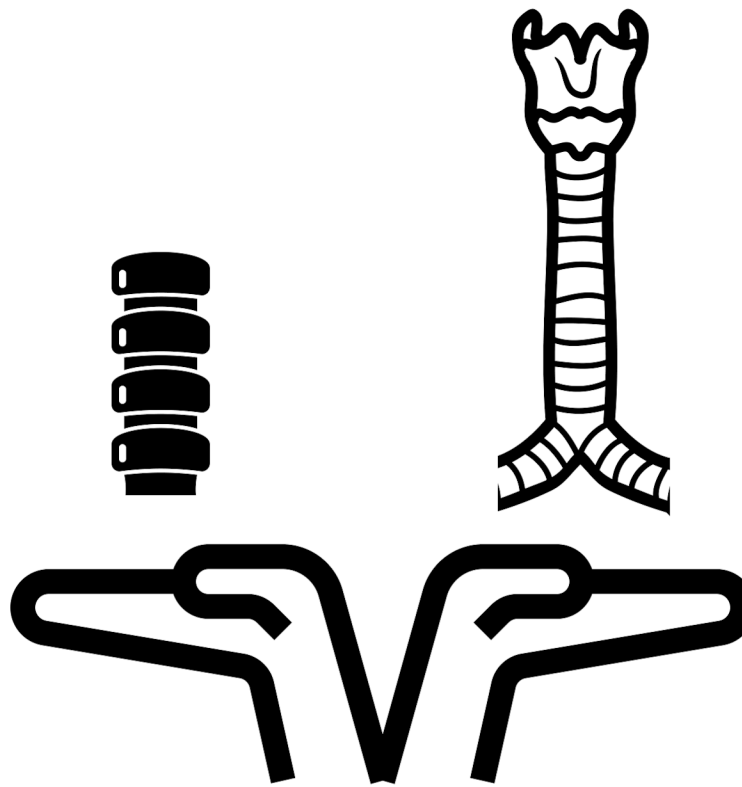
Chapter 3: Simulating and comparing stents and tracheas

"There's a way to do it better – find it."

THOMAS EDISON

Conventional airway stents vary in length, diameter, and shape. These characteristics determine the biomechanical properties relating directly to the postoperative outcomes. [1-7] Only during interventional bronchoscopy becomes clear which conventional stent length and diameter will fit best. Currently, the smallest length and greatest diameter possible are most likely chosen. A short length decreases the chance of mucus plugging, a great diameter will result in relief of symptoms because of a higher air flow (Eq. 1.1 and Eq. 1.2). If possible, dilation of the airway is performed for implantation of a bigger stent diameter, but this involves several risks, like bleeding and perforation of the airways. Hence, physicians currently rely on their personal experience in choosing stent dimensions, also since quantitative data about sizes and their clinical effect remains absent. [4]

Nevertheless, quantitative insight into airflow patterns and pressure might help in choosing the best possible airway stent and whether to perform additional procedures for implantation of another size. Additionally, an airway stent changes the geometry of the airway influencing breathing physiology. Towards designing a personalized airway stent, the influence of the tracheal geometry compared to stents will also be quantified. This comparison will show which shape pleads for increased congruence of an airway stent and least work of breathing.

To quantify the effect of different airway stents on the work of breathing and determine which characteristics a personalized airway stent must include in the design, this chapter will simulate different stent sizes and healthy tracheas. First, the chapter starts with assumptions made to perform CFD simulations. Next, simulating different stent sizes will give quantitative insight into whether to choose between a longer stent or a bigger one in diameter. Lastly, tracheas will be simulated and compared with stents to see the influence of geometry on the work of breathing. Parameters of interest (introduced in 2.2) for both studies are the pressure drop (PD), wall shear stress (WSS), and turbulence intensity (TI).

3.1. ASSUMPTIONS

Several assumptions were made concerning simulating the airflow with the CFD software ANSYS.

- The airway will be assumed to have a no-slip boundary (Chapter 2: 2.1.1.2.4 Wall) with rigid, stationary walls. This can be assumed due to the high percentage of cartilage present above the central airways. [8-11]
- Additionally, airway dynamics during breathing are neglected as well as gravity since another software package of ANSYS is required.
- Inhalation flow rates of exaggerated tidal breathing (0.5 L/s) and low-intensity exercise (1.0 L/s) were simulated since stents are the focus, and which critical range is at higher flow rates. Thus, higher flow rates than normal tidal breathing (around 0.1 L/s) were chosen to simulate. [12-14]
- At the inlet of the model, a steady-state uniform profile was simulated unlike the clinically present turbulent time-dependent flow.
- No entrance length was added.
- Lastly, air flowing through the geometry was assumed to be an incompressible gas with properties similar to comparable studies in the literature [9-11], assuming properties present at 15°C. [15]

3.2. QUANTITATIVE STENT GUIDE

Quantitative information about different stent sizes could help the physician during the decision-making of stent size and predict the clinical effect afterward. Therefore, this study simulates various stent dimensions using CFD and assesses the relative differences between stent dimensions in wall shear stress (WSS), pressure drop (PD), and turbulence intensity (TI). An increased TI is expected to give more shear, hence an increase in WSS. PD is expected to increase for a longer and decreased diameter of a stent for a similar flow rate (Eq. 1.2). Since the geometries are straight pipes, it is also expected that a doubled diameter decreases the resistance by a factor of 16, thus PD decreases with similar factor (Eq. 1.1 and Eq. 1.2).

3.2.1. Methods

ANSYS Academic Research CFD (Ansys Inc. v. 2021R2) Workbench was used to define the steps of the simulation. SpaceClaim was used to design stents with diameters of 10, 12, 14, 16, 18, and 20 mm and lengths of 20, 60, and 100 mm, based on conventional trachea airway stent characteristics.

The geometry was imported into *Fluid Flow (with Fluent Meshing)* in millimeters. All mesh sizes were set initially at a minimum size of 0.05 mm and a maximum size of 0.5 mm. Maximum skewness must be 0.95 and minimum orthogonal quality 0.2 (according to Figure 2-3). In case the y+ value was greater than 1, the mesh was refined by reducing the maximum surface mesh size by 0.1 and setting the transition ratio of the inflation layers to 0.1. Standard values ANSYS sets for the Growth Rate (GR, 1,2) and Transition Ratio (TR, 0,272) were used. Poly-hexcore elements were chosen with three peel layers. After, *Fluent* was converted to the solution mode. A step-by-step guide is included in Appendix A: Manual for setting up airway simulations within ANSYS.

3.2.2. Results

Figure 3-1 illustrates the results of the PD for all simulated stents. It indicates an exponential decay of the PD for increasing diameter for similar length and flow rate. The decreasing factor of the PD for the doubled flow rate is indicated in Table 3-1. Doubled flow rate for similar stent dimensions shows an increase in PD of 2.70 ± 0.07.

Table 3-1 Decrease factor of the PD for doubled diameter, calculated for each stent length and flow rate.

Stent length (mm)	20		60		100	
Flow rate (L/s)	0.5	1.0	0.5	1.0	0.5	1.0
Decreasing factor in PD from 10 to 20 mm	15.4	14.8	16.4	16.3	17.2	18.2

*PD = pressure drop

The Reynolds number can be calculated with Eq. 1.3 for each stent diameter with flow rate. Results are given in Table 3-2. Except for the stents of 12 mm and bigger with a flow rate of 0.5 L/s which have all transient flow, the rest is turbulent.

Table 3-2 Reynolds number for each stent diameter with a flow rate of 0.5 and 1.0 L/s.

Stent diameter (mm)	10	12	14	16	18	20
Re number for a flow rate of 0.5 L/s	4378	3637	3117	2729	2425	2182
Re number for a flow rate of 1.0 L/s	8731	7273	6232	5458	4850	4364

*Re number = Reynolds number

Extending the stent by three times for a flow rate of 0.5 L/s, the pressure drop increases by an average factor of 1.8 ± 0.07 (derived from Figure 3-1). Extending it five times, the average factor is 2.4 ± 0.1. For 1.0 L/s these average increasing factors for the pressure are 1.9 ± 0.1 and 2.5 ± 0.2, respectively.
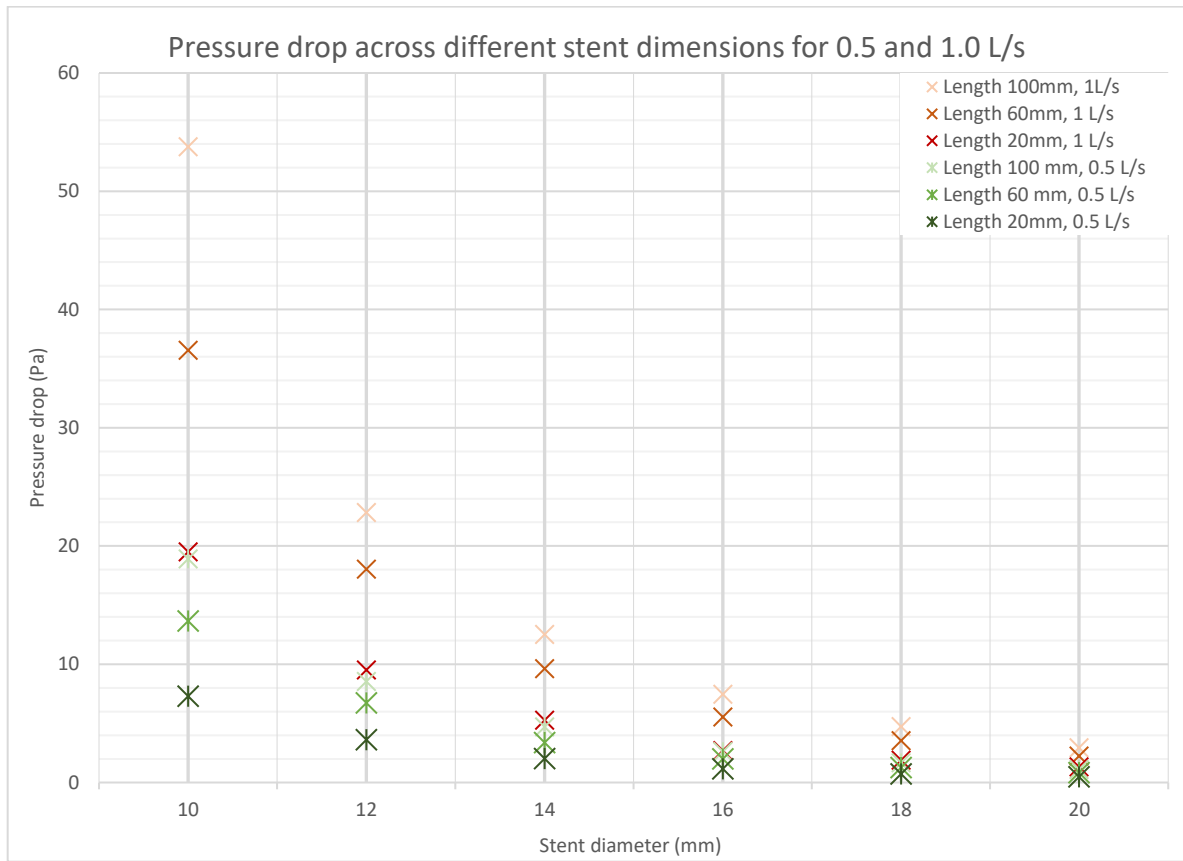
Figure 3-1 Results of the pressure drop of various stent dimensions for a flow rate of 0.5 and 1.0 L/s.

The WSS contour for 0.5 L/s is visualized for both the smallest and biggest stent dimensions in figure Figure 3-2. Due to the inlet boundary condition, the maximum value (red) is located at the inlet plane (left side) of both stents. A lower, constant value (blue) can be found along the length of the stent.
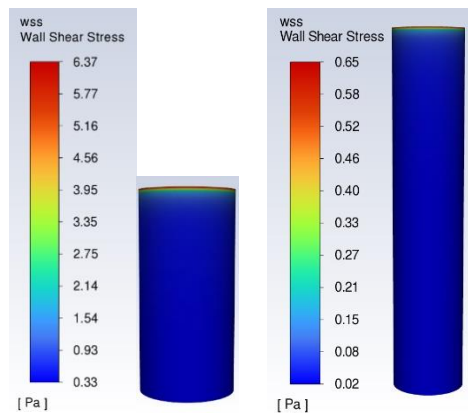
Figure 3-2 Relative WSS (red = high, blue = low) in the smallest (left, diameter 10mm, length 20 mm) and biggest stent (right, diameter 20 mm, length 100 mm).

Averaged TI of a flow rate of 0.5 L/s for a stent length of 100 mm are included in Table 3-3. As the diameter increases, the Reynolds number decreases (Eq. 1.3) indicating less turbulent flow.

Table 3-3 The average turbulence intensity for simulated stent diameters with a length of 100 mm and a flow rate of 0.5 L/s.

Diameter (mm)	10	12	14	16	18	20
Average TI (%)	21.1	14.5	11.0	9.42	7.40	6.00

3.2.3.   Discussion

This study investigated the effect of the diameter and length of simulated stents on the PD, WSS, and TI for two different flow rates. CFD analysis confirmed approximately 16 times less PD for doubled diameter for similar stent length and flow rate (Table 3-1, Figure 3-1). Decreased PD indicates less work of breathing. Moreover, the bigger stent diameter decreased the velocity, thus also the WSS and TI. Hence, physicians can refer to quantified data as substantiation for their stent choice toward the best predicted clinical outcome.

3.2.3.1.   Interpretation

Results of Table 3-1 confirm the decrease in PD by a factor of 16 for doubled diameter, based on Hagen-Poiseuille's law (Eq. 1.2). This relative difference verifies that CFD simulations mimic laws of nature indicating capabilities and accuracy of ANSYS CFD simulations, also clinically. Additionally, less pressure drop for a greater diameter requires less work of breathing for a similar flow rate. This pleads for implantation of the clinically possible greatest diameter of an airway stent.

Furthermore, an increase in stent length by a factor of 3 and 5 show an increase in the PD of approximately 1.8 and 2.4, respectively, for both flow rates (Figure 3-1). Hence, a longer airway stent increases the work of breathing. These results must be compared with simulated tracheas to see whether a longer stent provides less workload than the tracheal anatomy and is therefore preferred, only considering the work of breathing.

What also follows from Figure 3-1 is the decay of the pressure drop with increasing stent diameter for similar length and flow rate. It can be interpreted as an exponential decay which is also described by Hagen- Poiseuilles Law. However, this law is only applicable for laminar flow with a substantially longer length than diameter. As Table 3-2 describes, none of the geometries has laminar flow. Hence, the PD is higher than described by Hagen-Poiseuilles Law and is not applicable. In turbulent flow, the Darcy-Weisbach equation applies. Since this thesis does not focus on the verification of the simulation, it was chosen to not verify the simulations with calculated results from the Darcy-Weisbach equation. Hence, no line was inserted into Figure 3-1.

Next, an increase in velocity increases the WSS (see 2.2 Parameters of Interest). Since the flow in the airways mainly runs in a vertical direction, shear also does. It is therefore the determining factor for stent migration. WSS must be minimized to decrease the chance of stent migration. For a similar flow rate, an increased diameter decreases the velocity, thus the WSS. To conclude, the chance of stent migration can be minimized by inserting the greatest stent possible to ensure the lowest possible velocity thus consequently the WSS.

Following, TI decreases with a greater diameter of the stent since the Reynolds number decreases. Additionally, decreased TI also goes with a decrease in the pressure drop. Less turbulence ensures that mucus can be transported upwards for clearance of the airways. Hence, the greatest diameter possible will give less change of mucus plugging around the stent since it decreases turbulence.

Lastly, the lowest change of migration is with the lowest velocity, but a velocity > 1 m/s is required for easy mucus clearance. Therefore, simulations of stents in airways are required to see whether the stent meets both requirements, next to the congruence of the airway.

3.2.3.2.   Limitations

Above mentioned results plead for implantation of the greatest diameter of a stent that is possible to decrease the pressure drop as much as possible, lowest WSS, and ensure > 1m/s. However, clinical limitations have not yet been addressed. First of all, the stent must be introduced through the vocal cords, so folding the stent over its vertical axis is necessary. This already limits the maximum diameter. Next, the airway cannot be dilated endlessly. It still depends on the physician who estimates during the intervention whether dilation is possible and which stent will fit in the airway. Hence, dependent on measurements performed on a pre-intervention CT-scan the maximum diameter can be estimated.

Results show a relatively less decreasing factor of the PD for 20 mm long stents than for 100 mm (Table 3-1). No entrance length was added to the stents, thus the flow is less developed in shorter stents. The flow remains in the shorter stents fairly uniform instead of turbulent, resulting in a lower PD. In addition, a larger diameter gives a lower Reynolds number, so more laminar flow. These factors together, a short stent and a low Reynolds number at a larger diameter account for the smaller difference in the shorter tubes. Recommended is an extension of the model to guarantee a fully developed flow where measurements must be performed for reliable results.

Each stent finds its maximum WSS value at the inlet plane and has a constant value further along the stent, two examples are shown in Figure 3-2. The increased WSS at the inlet plane is a result of the boundary condition that is set at the inlet plane. For internal fluid flow, this is insurmountable and does not affect the final results. [16]

Results verify the relative effect of the fourth power radius on the pressure drop. However, whether values themselves are correct to experimental ones has not been established. Towards a clinically representable simulation, such translation is required. Hence, measuring the pressure drop experimentally with similar geometries and parameters is required to verify whether simulated results are in a similar order of magnitude.

3.2.3.3.   Clinical interpretation and future work

CFD analysis of various stent dimensions created a quantitative guide regarding the PD to choose between various sizes of stents, visualized in Figure 3-2. Provided results could help the physician during placement of an airway stent or better predict the clinical outcome; prefer a stent dependent on the decrease in pressure drop. Consequently, help in the decision-making of whether to perform airway dilation to insert a bigger stent, because dilation entails risks such as airway perforation. Results plead for implantation of the greatest diameter possible to decrease the change of stent migration and mucus plugging, with providing the least work of breathing. A future perspective could be an app or easy overview for the physician, to check the pressure drop differences between stent dimensions. With a simple action, it is clear for the physician whether dilation before stent insertion could give a significant clinical improvement or only stenting is expected to be sufficient.

3.3. STENT VERSUS TRACHEA

A straight smooth round stent differs in shape from the C-shaped cartilage rings that make up the trachea. The shape of the lumen of the geometry influences the fluid flow. [17] Implantation of such airway stents into the airway will influence the PD, WSS, and TI. This section will compare results from section 3.2 and tracheas to see the effect of the geometry on the work of breathing. Secondly, the comparison will show whether to design a straight stent or one that is congruent to the anatomy.

Since tracheas are approximately 110 mm long [18], tracheas of 100 mm long will be simulated to compare with similar length stents from section 3.2. Hypothesized is a higher PD, WSS, and TI in tracheal geometries compared to stents due to the increased complexity of the geometry. Similar measurements as performed with stents in section 3.2 will be conducted to evaluate the influence of the geometry.

3.3.1. Methods

An application was developed and submitted to the Institutional Review Board in the NKI-AVL, for permission to collect patients who have received an airway stent. After approval, 131 unique patients were identified. Patients were manually selected on the presence of a CT neck and/or thorax and/or abdomen at least 6 months before the diagnosis of the stenosis. For reconstruction of a 3D model was chosen for a maximum slice thickness of 1.5 mm. Data selection resulted in 4 straight tracheas of 100 mm without obstruction, based on the radiologic report.

3.3.1.1.   Airway segmentation

DICOM files of each patient were imported into ITK-snap (version 3.8.0) to segment the airway. [19] The function Active Contour Segmentation Mode (Snake) was used for the segmentation of the airway. The region of interest (ROI) was set in all directions that included airway generation 0 to 3. Click on Segment 3D and select the images with blue contrast.

- Threshold mode 'upper and lower' is used with the lower threshold as low as possible and the upper one initially at -300.
- Next, bubbles are placed into the airway at multiple locations in various slices and growth can be initiated. Update the 3D model during the growth to monitor the result.
- Stop the growth if airway generations 0 to 2 are completely segmented. Go back and add more bubbles if necessary.
  - If bubbles grow into regions other than the airway, minimize the number of iterations.
  - If adding more bubbles is not sufficient, increase the upper threshold in step 1.

When airway generations 0 to 2 are fully segmented, export the segment as a surface mesh in a Standard Triangle Language (.STL) format.

3.3.1.2.   Simulation

ANSYS Academic Research CFD (Ansys Inc. v. 2021R2) Workbench was used to define the steps of the simulation. A step-by-step guide is included in Appendix A: Manual for setting up airway simulations within ANSYS. The component system *Fluid Flow (with Fluent Meshing)* is subsequently used to define the parameters and perform the simulation. The minimum size of the surface mesh was set to 0.05 and the maximum size to 0.5 mm. Three different non-obstructed straight tracheas were simulated with 0.5 and 1 L/s.

3.3.2. Results

Out of the database of 131 patients that have received an airway stent, 4 were eligible for simulation of a healthy trachea with a length of 100 mm. The method is summarized in Figure 3-3.
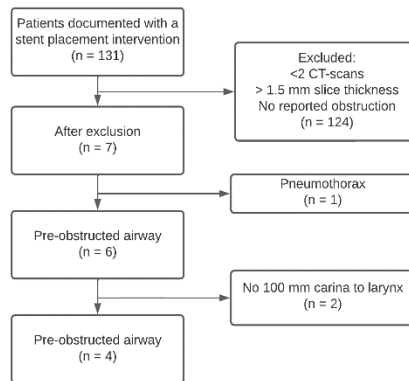
Figure 3-3 Overview of the patient selection for the simulation of straight tracheas without an obstruction.

The segmented tracheas are shown in the last row of Table 3-4, with an orthogonal distance of 100 mm. All tracheas show a higher pressure drop for a flow rate of 1.0 L/s than 0.5 L/s. The first two show a higher factor than stents (2.70 ± 0.07) but the latter two have a lower difference.

Table 3-4 Characteristics and pressure drop of the four simulated tracheas with a visualization of the geometries.

	1	2	3	4
Inlet diameter (mm)	16.4	15.2	16.8	11.7
Outlet diameter (mm)	14.4	15.5	19.4	10.7
Relative difference between inlet and outlet area	-12.0%	+1.84%	+15.6%	-1.09%
Pressure drop 0.5 L/s (Pa)	7.03	6.17	1.22	1.46
Pressure drop 1 L/s (Pa)	23.6	20.1	2.70	2.82
Ratio of pressure drop 0.5 vs 1 L/s	3.35	3.26	2.2	1.93
Geometry				

The PD of stents 100 mm long from section 3.2 are visualized again in Figure 3-4, together with the PD of the simulated tracheas. For similar inlet diameter and flow rate, trachea 1 and 2 show a higher pressure drop than stent dimensions, trachea 3 is in line and number 4 shows a lower PD.
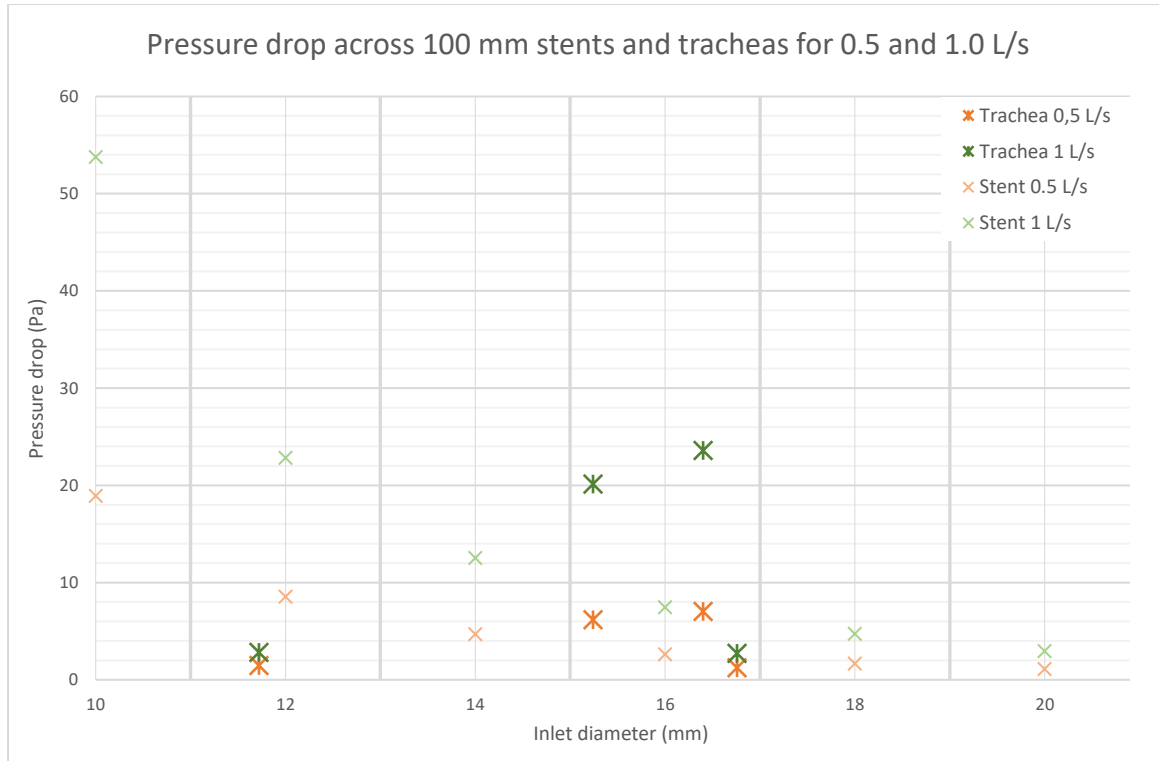
Figure 3-4 Pressure drop across stents of 100 mm long for different inlet diameters and a flow rate of 0.5 L/s (orange crosses) and 1.0 L/s (green crosses), similar results as in Figure 3-1. Bold stars indicate the pressure drop in the four simulated tracheas for 0.5 L/s (orange stars) and 1.0 L/s (green stars).

WSS contours of the tracheas for a flow rate of 0.5 L/s are visualized in Table 3-5 with the average TI. All visualizations of the WSS show an increased value at the annular ligaments. The maximum value of the WSS can be found at the inlet plane of the geometry due to the inlet boundary condition (see 3.2.3 Discussion).

Table 3-5 Visualization of the relative WSS in each trachea, with the average turbulence intensity and average wall shear stress (WSS) in tracheas with a length of 100 mm at a flow rate of 0.5 L/s.

Trachea	1	2	3	4
Average TI (%)	9.41	12.6	8.69	4.50
Maximum TI (%)	14.4	37.3	20.5	6.97
Contours of the WSS				

TI = Turbulence intensity, WSS = Wall shear stress

3.3.3. Discussion

This study investigated the effect of the tracheal shape on the PD, WSS, and TI for two different flow rates. The PD of trachea 1 and 2 are in line with the literature and confirmed the hypothesis of an increased PD relative to similar stent dimensions. On contrary, trachea 3 and 4 showed a lower pressure drop compared to similar-sized stents. Both WSS and TI are in tracheas higher than in similar-sized stents. In short, half of the simulations verify the increased PD and WSS compared to stents, which are mainly influenced by the shape of the geometry. The already present anatomic variation between these four tracheas pleads for more personalized care. Moreover, the lumen of an airway stent is recommended to be smooth for decreases the chance of stent migration and mucus plugging and decreases dyspnea significantly.

3.3.3.1.   Interpretation

Shih, et al. [20] investigated the effect of stent implantation in the trachea on the PD using CFD. A PD during inspiration of 7.05 Pa for a flow rate of 0.5 L/s and 23.86 Pa for 1 L/s were found. It is assumed that inspiration post-stent results of the pressure drop can be compared with the geometries used in this study. With this assumption, literature is in line with the results of trachea 1 and 2 of this study. Additionally, trachea 1 and 2 show more turbulent flow than trachea 3 and 4 based on the increase in pressure drop for doubled flow rate (Table 3-4). This can also be confirmed with the TI in Table 3-5. To conclude, the results of trachea 1 and 2 verify the hypothesis of an increased PD compared to similar-sized stents due to the increased complexity of the geometry.

Since the results of trachea 1 and 2 are in line with literature and confirm the hypothesis of an increased pressure drop compared to stents, it is assumed that these geometries reflect anatomy best. Additionally, the increasing factor for the PD for the doubled flow rate is increased for these geometries concerning stents (Table 3-4). This indicates more turbulence, as also expected. A relatively lower PD in trachea 3 and 4 could result from a bad segmentation of all cartilage rings causing a less complex shape.

TI was also investigated using CFD in the literature. Razi, et al. [21] modeled the trachea pre- and post-stent implantation. They found a post-stenting TI of $13\pm2\%$. Lin, et al. [22] found a value of the TI in the healthy trachea of 5-20%. Assuming the post-stenting tracheas as healthy and consequently comparable to results from this thesis, the results are in line with literature.

Both the WSS and TI are higher in all tracheas than in similar inlet-sized stents, as hypothesized. Compared to stents, the geometry of the tracheas is therefore more prone to stent migration and mucus plugging. Based on these results, a smooth lumen of geometry is preferred over an airway considering clinical consequences.

3.3.3.2.   Limitations

Finishing up the geometries in ANSYS SpaceClaim towards a simulation considered manually setting planes. They were set at the inlet and outlet to determine the length of the geometry and cut a flat inlet and outlet. First of all, manual placement of the faces did not allow to place them exactly orthogonal to the geometry which increases the intersection area. This lowers the inlet velocity for a similar flow rate and consequently affects the PD, WSS, and TI. Therefore, an automated workflow for setting the planes orthogonally would increase reliability.

Furthermore, planes were set parallel at the inlet and outlet with a 100 mm orthogonal distance. Since tracheas are approximately 110 mm long [18], it was hardly possible to cut a straight trachea without diverging parts towards the larynx or main carina (see Appendix B:). This is an additional error to the

inlet and outlet areas, on top of the manual placement of planes. Therefore, further studies must cut a shorter part of the trachea and extrude it to a clinically relevant length of 100 mm to overcome the error of the diverging ends.

Lastly, 100 mm was measured orthogonally between the parallel planes at the inlet and outlet. In a straight geometry, this implies a similar traveling distance. Regarding results from 3.2, increased traveling distance increases the PD. Trachea 2 shows a curve in the geometry which increases the traveling distance. Thus, the measured PD in trachea 2 is higher than it would be for a traveling distance of 100 mm which is present in most tracheas. For better comparison of results, it is therefore recommended to measure the path through the geometry and not the orthogonal distance in further studies.

Since conventional airway stents are consistent in diameter, a simulation toward one direction suffices. Tracheas, on contrary, are not consistent in diameter so the inlet and outlet areas vary. Hence, full analysis of the pressure drop in an airway requires simulations in two directions. Especially looking towards stent migration which is influenced by the direction of WSS. This study only simulated inhalation since the research focused on the effect of the geometry on the PD, WSS, and TI. Especially with the differences in the inlet, outlet and shape the PD is expected differently during reversed air flow. Unfortunately, exhalation is not yet quantified but is recommended in further research.

Contradictory to the verifying results of trachea 1 and 2, trachea 3 and 4 show a decrease in the PD. Trachea 4 is most similar to stents in terms of geometric characteristics: equal inlet and outlet diameter with a traveling distance of air of 100 mm. Additionally, a comparison of the PD between tracheas and the influence of velocity, and the difference between inlet and outlet surface does not result in any relation. To conclude, simulating only four tracheas is too little to see any relation. On the other hand, it also concludes that airway data must always be compared within an individual since 'unhealthy' values can be experienced as normal by patients due to familiarization.

3.3.3.3.   Clinical interpretation and future work

Simulations of different tracheas partially confirmed the increase in PD compared to similar-sized stents. Results of four tracheas are already differing advocating for more patient-specific treatment. On contrary, all tracheas show an increase in the WSS and TI compared to similar-sized stents. Hence, the increased complexity of a geometry relieves dyspnea less and is more prone to migration and mucus plugging. Towards the design of an airway stent, these results plead for a smooth lumen. Additionally, a stent congruent to the airway minimizes the transition from the airway into the stent. [4] The complexity of the geometry is subsequently minimized. In short, an airway stent must follow the anatomy of the airway but has a smooth lumen on the inside to decrease the complexity of the interacting surface with air.

3.4. DISCUSSION

This chapter aimed to simulate stents and tracheas with CFD for quantitative data on the effect of airway stents and their expected clinical effect. As a part of the thesis, this chapter contributes to the quantitative insight into the effect of stent dimensions and differences with tracheal geometries.

Section 3.1 describes the assumptions that were made for the simulation to run. Consequently, simulations do not mimic the actual situation. The assumptions did not mimic the actual simulation but aimed to reach this as close as possible within the possibilities.

Section 3.2 resulted in a stent choosing guide for the physician to see the PD decrease with increasing diameter of an airway stent (Figure 3-1). Consequently, the expected work of breathing also decreases. It could help as a guideline on whether to perform airway dilation to insert a bigger stent. WSS and TI are parameters that influence stent migration and mucus plugging, respectively. Hence, both parameters need to be minimized which is with increasing diameter. In short, the diameter of an airway stent must be chosen as big as clinically possible to minimize complications and improve dyspnea.

Section 3.3 described the simulation of tracheas and compared these results to stents of similar size. Results of two tracheas were in line with the literature and also confirmed the increased PD compared to stents. WSS and TI were increased in all tracheas, compared to stents, pleading for the less complex geometry of an airway stent for less chance of stent migration and mucus plugging. To conclude, these results advocate for a smooth lumen of an airway stent. Additionally, the varying results of the tracheas advocate for more patient-specific treatment.

3.4.1. Assumptions

The first assumption in the model is rigid, stationary tracheal walls and a steady-state inflow of air that simplify the breathing mechanism. Assuming rigid walls in the simulations can lead to better correlation with experiments that can verify the results. Due to the increased computational time and better conversion to real-life experiments was chosen to implement a fixed geometry. Clinically, the diameter of the airway fluctuates over time dependent on the phase in the breathing cycle. Implementation of such into the simulation would require multiple CT-images of the airway during the respiratory cycle or a numerical description of the airway expansion during a breathing cycle. [23] The first would require a 4D CT-scan with, as can be assumed, unnecessary radiation exposure and requires approval. Hence, a numerical description of the breathing cycle with a corresponding movement of the airway would be better achievable concerning time but requires an engineer.

Another factor eliminated from physiologically breathing is the time-dependent air flow, which is assumed to be a steady state. Clinically, pressure builds up during the respiratory cycle instead of reaching its maximum flow directly. Building up the airflow means a rise in the velocity over time, thus a decrease in pressure (based on Bernoulli). Hence, time-dependent simulation is recommended in further studies.

As also noted in section 2.1.1.2.6 Entrance length, an entrance length enables fully developed flow within the geometry. The glottal region in the upper airway is the main cause of the development of the turbulent laryngeal jet. [24] Lin, et al. [22] stated that a velocity parabola and negligible turbulence result from the absence of the oropharynx and larynx. CT-data does not always include the extra-thoracic area due to increased exposure to radiation. [24] It can therefore be considered to add a geometrical model of the airway onto the trachea as proposed by Miyawaki et al. (2017). [24] No entrance length was added to the simulations to simplify post-processing and increase the capability of translating the simulation to experiments. However, preferably a laryngeal model is added to the geometry of interest.

Normal tidal breathing considers an airflow of 0.1 L/s, but stent complications are expected to present at higher airflows. A peak flow is the greatest work of breathing an individual can generate,

approximately 6-8 L/s. [25] Patients with a CAO are not expected to reach these values. Hence, increased tidal breathing (0.5 L/s) and low-intensity exercise (1 L/s) were simulated to show the difference in breathing workload by the caused pressure drop. Additionally, exhalation was not simulated but is required for a complete evaluation of the breathing cycle. Therefore, it is recommended in further studies to simulate exhalation after inhalation. The mass flow rate of each outlet during inhalation needs to be noted and can be used as the input parameter of each outlet during the exhalation.

Properties of air are set similar to comparable studies in the literature. Assumed properties are present at 15°C [15] but the air in the trachea varies between 31°C and 36°C, dependent on location, inhalation or exhalation, and environmental temperature. [26] Increased air temperature goes with decreased density. [15] A less dense substance means less pressure hence the pressure found in vivo will be lower than simulated. However, Tullio, et al. [10] state that the effects of temperature and humidity on the simulations are negligible concerning other environmental conditions. Therefore, literature comparison was chosen over the clinical situation. Nevertheless, in a further stage of airway simulation is recommended to add more clinically translatable properties.

REFERENCES

[1]   C. Aravena *et al.*, "Idiopathic subglottic stenosis: a review," *Journal of thoracic disease,* vol. 12, no. 3, pp. 1100-1111, 2020/3 2020, doi: 10.21037/jtd.2019.11.43.

[2]   E. Folch and C. Keyes, "Airway stents," *Annals of Cardiothoracic Surgery; Vol 7, No 2 (March 2018): Tracheal Surgery,* 2018. [Online]. Available: https://www.annalscts.com/article/view/16462.

[3]   N. Guibert *et al.*, "Treatment of complex airway stenoses using patient-specific 3D-engineered stents: a proof-of-concept study," *Thorax,* vol. 74, no. 8, pp. 810-813, 2019/8// 2019, doi: 10.1136/thoraxjnl-2018-212732.

[4]   N. Guibert, H. Saka, and H. Dutau, "Airway stenting: Technological advancements and its role in interventional pulmonology," *Respirology,* vol. 25, no. 9, pp. 953-962, 2020/9// 2020, doi: https://doi.org/10.1111/resp.13801.

[5]   S. D. Murgu and B. Laxmanan, "Biomechanical Properties of Airway Stents," *Journal of Bronchology & Interventional Pulmonology,* vol. 23, no. 2, pp. 89-91, 2016/4// 2016, doi: 10.1097/LBR.0000000000000267.

[6]   J. Xu, H. X. Ong, D. Traini, M. Byrom, J. Williamson, and P. M. Young, "The utility of 3D-printed airway stents to improve treatment strategies for central airway obstructions," *Drug Development and Industrial Pharmacy,* vol. 45, no. 1, pp. 1-10, 2019/1// 2019, doi: 10.1080/03639045.2018.1522325.

[7]   J. Xu *et al.*, "Using individualized three-dimensional printed airway models to guide airway stent implantation," *Interactive CardioVascular and Thoracic Surgery,* vol. 31, no. 6, pp. 900-903, 2020/12// 2020, doi: 10.1093/icvts/ivaa206.

[8]   L. Chen and X. Zhao, "Characterization of air flow and lung function in the pulmonary acinus by fluid-structure interaction in idiopathic interstitial pneumonias," *PloS one,* vol. 14, no. 3, pp. e0214441-e0214441, 2019/3// 2019, doi: 10.1371/journal.pone.0214441.

[9]   C.-Y. Ho *et al.*, "Numerical analysis of airflow alteration in central airways following tracheobronchial stent placement," *Experimental Hematology & Oncology,* vol. 1, no. 1, pp. 23-23, 2012, doi: 10.1186/2162-3619-1-23.

[10]   M. Tullio, L. Aliboni, F. Pennati, R. Carrinola, A. Palleschi, and A. Aliverti, "Computational fluid dynamics of the airways after left-upper pulmonary lobectomy: A case study," *International journal for numerical methods in biomedical engineering,* vol. 37, no. 7, pp. e3462-e3462, 2021/7// 2021, doi: 10.1002/cnm.3462.

[11]   T. Zobaer and A. Sutradhar, "Modeling the effect of tumor compression on airflow dynamics in trachea using contact simulation and CFD analysis," *Computers in Biology and Medicine,* vol. 135, pp. 104574-104574, 2021, doi: https://doi.org/10.1016/j.compbiomed.2021.104574.

[12]   W. F. Boron and E. L. Boulpaep, "Medical Physiology: A cellular and molecular approach," 2nd ed. Philadelphia: Saunders/Elsevier, 2012.

[13]   F.-L. Chen, T.-L. Horng, and T.-C. Shih, "Simulation analysis of airflow alteration in the trachea following the vascular ring surgery based on CT images using the computational fluid dynamics method," *Journal of X-Ray Science and Technology,* vol. 22, no. 2, pp. 213-225, 2014, doi: 10.3233/XST-140420.

[14]   C. van Ertbruggen, C. Hirsch, and M. Paiva, "Anatomically based three-dimensional model of airways to simulate flow and particle transport using computational fluid dynamics," *Journal of Applied Physiology,* vol. 98, no. 3, pp. 970-980, 2005/3// 2005, doi: 10.1152/japplphysiol.00795.2004.

[15]   Engineering Toolbox. "Air - Density, Specific Weight and Thermal Expansion Coefficient vs. Temperature and Pressure." https://www.engineeringtoolbox.com/air-density-specific-weight-d_600.html?vA=37&units=C (accessed 25-05, 2022).

[16]   E. Vandervelpen, "Ansys (Computational Fluid Dynamics) Support," E-Mail & Meetings ed, 2022.

[17]   N. Lohith, H. B. Bhaskar, and S. Manu, "Influence of various parameters on pressure drop during flow condensation in pipe Using Taguchi Approach," *IOP Conference Series: Materials Science and Engineering,* vol. 376, p. 012010, 2018/06 2018, doi: 10.1088/1757-899x/376/1/012010.

[18]   Y. Premakumar, M. F. Griffin, and M. Szarko, "Morphometric characterisation of human tracheas: focus on cartilaginous ring variation," (in eng), *BMC Res Notes,* vol. 11, no. 1, pp. 32-32, 2018, doi: 10.1186/s13104-018-3123-1.

[19]   P. A. Yushkevich *et al.*, "User-guided 3D active contour segmentation of anatomical structures: Significantly improved efficiency and reliability," *NeuroImage,* vol. 31, no. 3, pp. 1116-1128, 2006, doi: https://doi.org/10.1016/j.neuroimage.2006.01.015.

[20]   T.-C. Shih, H.-D. Hsiao, P. Y. Chen, C.-Y. Tu, T.-i. Tseng, and Y.-J. Ho, "Study of Pre- and Post-Stent Implantation in the Trachea Using Computational Fluid Dynamics," *Journal of Medical and Biological Engineering,* vol. 34, pp. 150-156, 2014.

[21]   S. S. Razi *et al.*, "Pre- and post-stent modeling of airflow dynamics in patients with malignant tracheal obstruction," *Journal of the American College of Surgeons,* vol. 211, no. 3, pp. S39-S39, 2010/9// 2010, doi: 10.1016/j.jamcollsurg.2010.06.096.

[22]   C.-L. Lin, M. H. Tawhai, G. McLennan, and E. A. Hoffman, "Characteristics of the turbulent laryngeal jet and its effect on airflow in the human intra-thoracic airways," *Respiratory Physiology & Neurobiology,* vol. 157, no. 2, pp. 295-309, 2007, doi: https://doi.org/10.1016/j.resp.2007.02.006.

[23]   R. Agujetas, R. Barrio-Perotti, C. Ferrera, A. Pandal-Blanco, D. K. Walters, and A. Fernández-Tena, "Construction of a hybrid lung model by combining a real geometry of the upper airways and an idealized geometry of the lower airways," *Computer Methods and Programs in Biomedicine,* vol. 196, pp. 105613-105613, 2020, doi: https://doi.org/10.1016/j.cmpb.2020.105613.

[24]   S. Miyawaki, E. A. Hoffman, and C.-L. Lin, "Numerical simulations of aerosol delivery to the human lung with an idealized laryngeal model, image-based airway model, and automatic meshing algorithm," *Computers & fluids,* vol. 148, pp. 1-9, 2017/4// 2017, doi: 10.1016/j.compfluid.2017.02.008.

[25]   British Lung Foundation. "Breathing and lung function tests." https://www.blf.org.uk/sites/default/files/Section%202%20-%20tests%20to%20measure%20your%20breathing.pdf (accessed 25-05, 2022).

[26]   K. Liener, J. Durr, R. Leiacker, A. Rozsasi, and T. Keck, "Measurement of tracheal humidity and temperature," (in eng), *Respiration,* vol. 73, no. 3, pp. 324-8, 2006, doi: 10.1159/000088659.
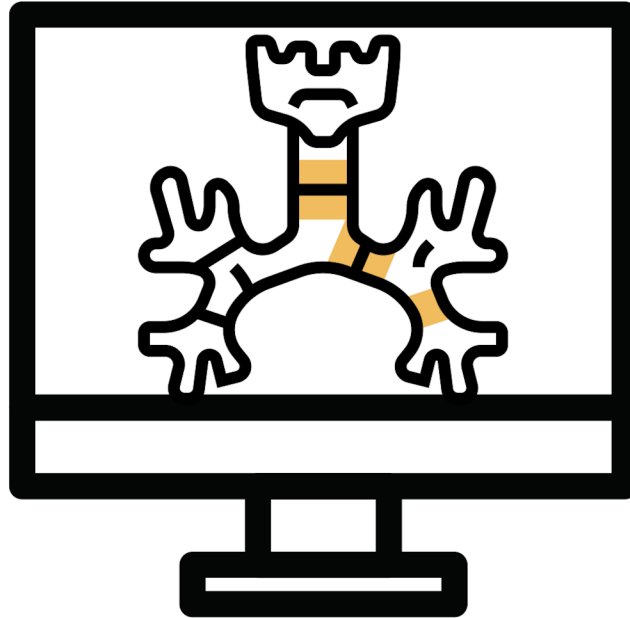
Chapter 4: Airway simulations

"The doctor of the future will be oneself."

ALBERT SCHWEITZER

Patients with central airway obstruction (CAO) often present complex anatomy of the airway. Conventional airway stents do therefore not always fit properly in these airways. As Chapter 3:Simulating and comparing stents and tracheal geometries also concluded, shape influences air flow behavior. The changing anatomy from stent implantation hence influences the airflow and thereby may increase the chance of complications and minor relieve of symptoms. Poor congruence of an airway stent to the airway is designated as the main cause. Personalized airway stents can offer increased congruence to the airway which is expected to improve the outcome: fewer complications and increased relieve of symptoms. [1] Since the problem with conventional stents has not been numerically investigated, the substantiation for the design of a personalized airway stent lacks. Currently, personalized airway stents are designed based on trial-and-error. This may result in a wrong fit or not a fit at all, which can result in an unnecessary intervention.

However, the current problem must be addressed since personalized airway stents can otherwise not be improved relatively to conventional stents. Therefore, this chapter aims to simulate pre-obstructed and obstructed airways and post-obstruction with conventional airway stents with computational fluid dynamics (CFD) and evaluate the parameters described in 2.2 Parameters of Interest. Hence, the analysis will investigate the pressure drop (PD), wall shear stress (WSS), static pressure to the wall, velocity path lines, mass flow rate (MFR) and turbulence intensity (TI) that with clinical relevance. A comparison of these parameters between different pre-obstructed airways will give insight into the influence of the anatomical variation. Next, the obstruction is expected to affect all parameters relative to the pre-obstructed airway and will plead for different designs. Additionally, an airway with a stent will give numerical insight into the current problem with conventional stents which has to be addressed with personalization.

4.1. ASSUMPTIONS

Similar assumptions as in 3.1 Assumptions have been made within this chapter. The only difference concerns the flow rate, which is only 0.5 L/s for this chapter because an increased flow rate requires a finer mesh to ensure y+ < 1 (see 2.1.1.1.1 Near wall modeling). Consequently, this requires more computational time. Since only differences between different airways want to be proved, it is not necessary to simulate increased flow rate and have a longer computational time.

4.2. METHODS

An application for approval was made to the Institutional Review Board in the NCI-AVL to collect patients who have received an airway stent. Criteria were an interventional bronchoscopy with stent placement between 01-01-2015 and 01-11-2021, including a CT-scan within 6 months before and after the intervention. This databased showed 131 unique patients. First, patients were manually selected from the database on the presence of a CT neck and/or thorax and/or abdomen and >2 scans in the database. Exclusion criteria were >1.5 mm CT slice thickness, no reported obstruction, or no pre- or post- intervention CT-scan. For the pre-obstructed airway, the CT-scan a year before the intervention the scan was chosen. Next, obstructed CT-scans were chosen as close to the intervention as possible. Lastly, post-intervention CT-scans were checked for al five patients, of which two had no stent placement and were excluded. Hence, three patients remained for the segmentation of the obstructed airway.

4.2.1. Segmentation

DICOM files of the CT-scan of each patient were imported into ITK-snap [2] for segmentation of the airway. Approximately airway generations 0 to 2 were segmented using Active Contour Segmentation Mode (Snake). After obtaining the whole airway the segment must be exported into a surface mesh Standard Triangle Language (STL) to work with. For the whole method of airway segmentation, see 3.3.1.1 Airway segmentation.

4.2.2. Meshing

ANSYS Academic Research CFD (Ansys Inc. v. 2021R2) Workbench was used to define the steps of the simulation. A step-by-step guide is included in Appendix A: Manual for setting up airway simulations within ANSYS. The trachea is cut with three planes perpendicular to the model to generate the airway model that will be used for simulation.

Patient 5 had a totally obstructed RMB. In the simulation was assumed that no air went through this bronchus, so this simulation only had an outlet at the LMB. The RMB was considered as the wall.

4.2.3. Simulation

In the component system *Fluid Flow (with Fluent Meshing)* all parameters were defined, see Table 2-1 for the overview. Additionally, the mesh sizes were set to a minimum and maximum value of 0.5 and 1 mm, respectively. The GR was set to 1.2, the TR to 0.1. If the y+-value was greater than 1, the mesh was refined by reducing the maximum surface mesh size by 0.1 until the y+ value was below 1. A full step-by-step manual for airway simulations is included in Appendix A: Manual for setting up airway simulations within ANSYS. Results from the pre-obstructed and obstructed airways are put into IBM SPSS Statistics (IBM Corp. Released 2021. IBM SPSS Statistics for Windows, Version 28.0. Armonk, NY: IBM Corp). A Wilcoxon-Mann-Whitney U test was performed to test the pressure drop between the pre-obstructed and obstructed airways to see the significance of an obstruction.

4.3. RESULTS

Figure 4-1 shows the flowchart for the patient selection for airway segmentation. In total 131 unique patients were documented with stent placement. After exclusion, 7 patients remained. One patient had a pneumothorax which was expected to influence the airway segmentation. Hence, 6 patients were eligible for segmentation of the airway pre-obstruction. Patient characteristics are in Appendix C: Patient Characteristics. Case number 6 (Table 4-1) had tracheal stenosis which was excluded for simulation of an obstructed airway. Subsequently, 5 patients remained of which numbers 1, 3, and 5 had a CT scan with a conventional airway stent that was eligible for segmentation.
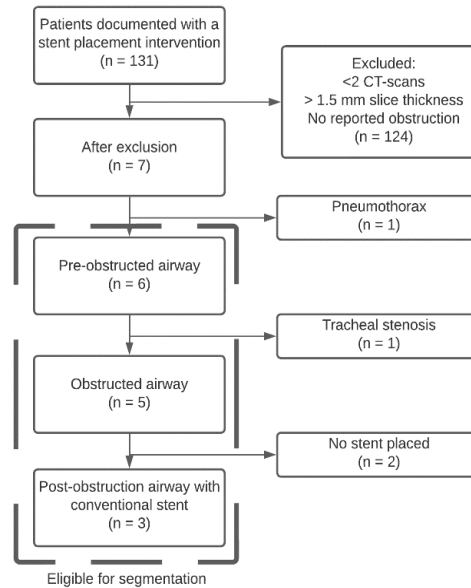
Figure 4-1 Flowchart of the patient selection from the database that were eligible for segmentation of the airway. From the total 131 unique patients, 6 were eligible for pre-obstructed airway segmentation, 5 for obstructed and 3 for post-obstruction.
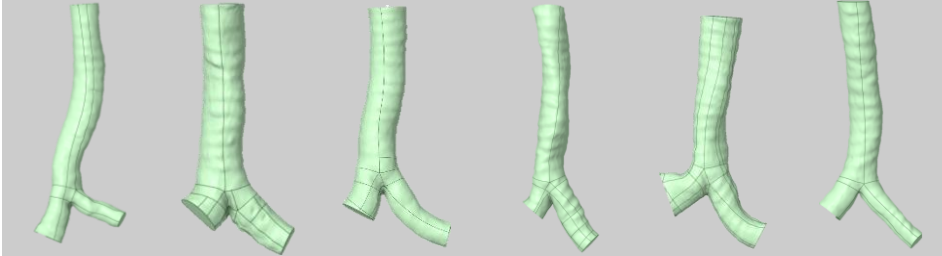
For the simulations, only the segmentation of the airway with a conventional airway stent of case number 1 was not eligible for simulation because the mesh contained too many irregularities. Results of only patient 3 are included below, all other visualizations are included in Appendix A:, Appendix E: Results of obstructed airways, and Appendix F: Results of post-obstruction with stent airway.

4.3.1. Pre-Obstruction

Table 4-1 shows the geometries of the pre-obstructed airways for 6 cases. The mean PD was 2.93 Pa $\pm$ 2.12 following descriptive statistics in SPSS. The mean MFR ratio between the LMB and RMB was 35.7% $\pm$ 7.01 and 65.4% $\pm$ 7.34, respectively.

Table 4-1 Pre-obstructed airways from 6 cases with the inlet velocity (m/s) and pressure drop (Pa).

Case	1	2	3	4	5	6
Velocity in (m/s)	2.72	1.19	1.23	1.65	1.00	2.34
Pressure drop (Pa)	7.12	2.28	1.57	2.80	2.46	10.36
Geometry						

4.3.2. Obstruction

Table 4-2 shows the geometries of the obstructed airways from cases 1 to 5. Descriptive statistics in SPSS showed a mean PD of 33.9 Pa ± 34.1.
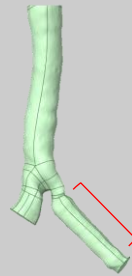
Table 4-2 Obstructed airways following the geometries of cases 1 to 5. The obstructed side is given, as well as the inlet velocity (m/s) and pressure drop (Pa).

Case	1	2	3	4	5
Obstruction	LMB	RMB	LMB	MC	RMB
Velocity in (m/s)	2.82	1.42	1.58	1.68	0.910
Pressure drop (Pa)	48.7	7.27	20.7	86.6	6.35
Symptoms	Lot of coughing; hemoptysis	Inspiratory stridor; changing tough sputum	Dyspnea; lot of coughing; hemoptysis;	Dyspnea; inspiratory stridor; tough sputum	Dyspnea; stridor; coughing with sputum

4.3.3. Post-obstruction with stent

Table 4-3 shows the post-obstruction airway with implanted airway stent for cases 1, 3, and 5. Case 1 was not simulated because the mesh contained too many irregularities at the proximal side of the stent. Case 3 shows an increased and case 5 a decreased PD compared to the obstructed situation.

Table 4-3 Three obstructed airways with an inserted stent for cases 1, 3, and 5 with the inlet velocity (m/s) and pressure drop (Pa). Case 1 was not simulated, only the airway was segmented. The symptoms patients experienced from stent insertion are also mentioned. Case 1 has a Y-stent, case 3 has a stent in the LMB, and case 5 in the RMB, indicated with red lines and brackets.

Case	1	3	5
Velocity in (m/s)	x	1.76	0.904
Pressure drop (Pa)	x	14.6	5.00
Geometry			
Symptoms	Increased coughing	Mucus plugging in the stent	Less dyspnoeic; more coughing with sputum

4.3.4.   Comparison

All tracheas show an increase in the PD and its standard deviation for the obstructed airway compared to the pre-obstructed airway. The Wilcoxon-Mann-Whitney U test was performed to test the difference in PD between these groups. It showed a significant difference in the pressure drop between both groups ($p=0.011$) with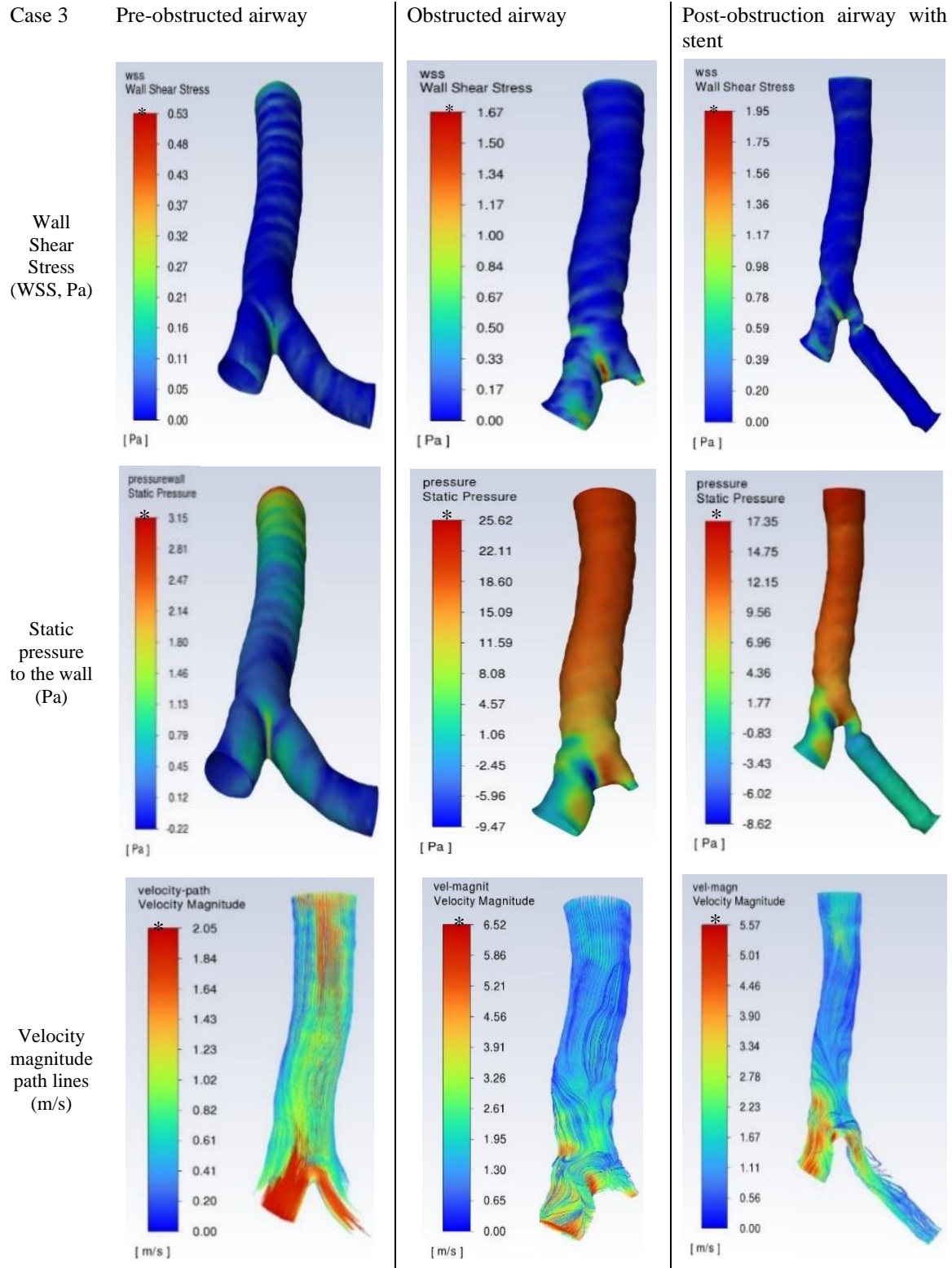 the obstructed group having a higher sum of ranks. Furthermore, the effect size of the test was 0.65, implying that 65% of the variability in the sum of ranks can be explained by the presence of an obstruction.

The first row in Figure 4-2 describes the WSS in case 3 for three situations. All show a consistent value along the trachea and a maximum area on the main carina. The maximum WSS in the obstructed airway is higher compared to the pre-obstructed airway. Next, the WSS in the obstructed and post-obstructed airway is more inconsistent after the bifurcation. After stent placement, two things are remarkable. First, the WSS is even more increased at the main carina than with airway obstruction, but the area is smaller. Secondly, proximal to the airway stent an increase in the WSS is present.

Next, the static pressure to the wall increases from the main carina towards the proximal end in all geometries. The increase is the biggest in the obstructed airway, the airway with stent follows. Stent placement decreases the maximum static pressure, but it does not return to its initial value. Lastly, a comparison of the static pressure and WSS show a contradictory color, which conforms to Bernoulli's law.

The last row shows the velocity magnitude path lines. Relatively more turbulence is present in the obstruction and post-obstruction with a stent airway. The obstruction airway shows increased turbulence mainly above the main carina. The stented airway shows at this location relatively less turbulence but increased in the stent. Additionally, the proximal superior part of the stent does not contain any velocity path lines.

Case 3	Pre-obstructed airway	Obstructed airway	Post-obstruction airway with stent
Wall Shear Stress (WSS, Pa)			
Static pressure to the wall (Pa)			
Velocity magnitude path lines (m/s)			

* Note the different scales of the color bar

Figure 4-2 Results of the wall shear stress (WSS, Pa), static pressure to the wall (Pa), and velocity path lines (m/s) of case 3 from top to bottom. The first column is the pre-obstructed airway, the second the obstructed airway, and the third includes the post-obstructed airway with a stent.

TI is measured in all cases and averaged, with a separate row for case 3 in Table 4-4. For case 3, the TI is increased for the obstructed airway, and even more increased when an airway stent is inserted. On average, the TI increases when an obstruction is developed but decreases on average towards the initial, pre-obstructed value.

Table 4-4 Turbulence intensity of the pre-obstructed, obstructed, and post-obstructed with stent airway. For each situation, the average and maximum TI are given. For case 3, the values are indicated separately. The mean includes the number of all cases (including case 3) indicated in the first row.

	Turbulence Intensity (%)					
	Pre-obstruction (n=6)		*Obstruction (n=5)*		*Stent (n=2)*	
	Average	*Max*	*Average*	*Max*	*Avg*	*Max*
3	4.72	11.2	6.74	60.7	10.4	100
Mean	7.76	25.6	9.89	102	7.27	64.4

MFR ratios of the left and right lung for the pre-obstructed and obstructed airway are visualized in Figure 4-3. Orange notates the ipsilateral side of the obstruction, green the contralateral side. The MFR at the ipsilateral side decreases if an obstruction is present, and the contralateral MFR increases.
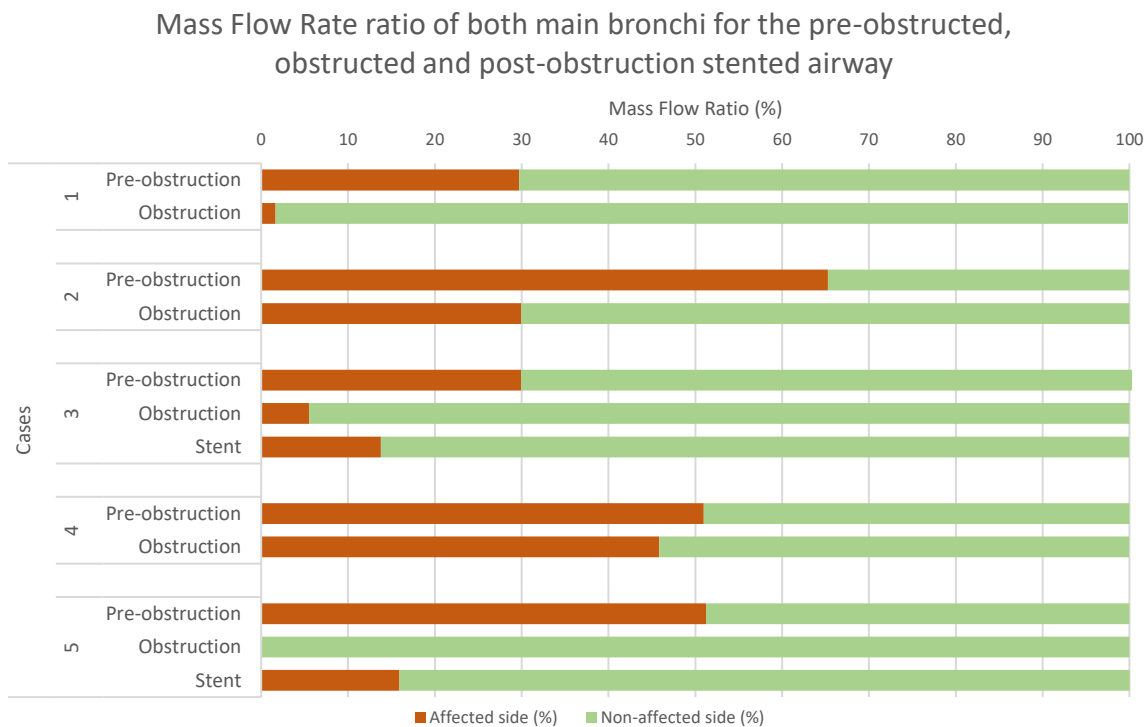
Figure 4-3 Mass Flow Rate ratios of both main bronchi, the affected and non-affected side, for each simulated airway.

The difference in MFR ratios for the affected and non-affected side is given in Table 4-5 for case 3. Due to the obstruction, the MFR of the affected side decreases by 24.4% of the total mass flow. After stent implantation, this MFR increases by 8.25%. As indicated in the last column, 16.2% of the total mass flow has returned to the affected side.

Table 4-5 Numerical data of the differences in the MFR for the affected and non-affected side of case 3.

	Mass Flow Rate ratios of case 3		
	Obstruction – Pre-obstruction	Stent – Obstruction	Stent – Pre-obstruction
Affected side (%)	-24.4	8.25	-16.2
Non-affected (%)	23.4	-8.28	15.1

4.4. DISCUSSION

This study investigated the PD, WSS, static pressure on the wall, velocity path lines, TI, and MFR of the LMB and RMB in pre-obstructed, obstructed, and a post-obstructed stent implanted airways. It showed an increase in all parameters for the obstructed airway compared to the pre-obstructed airway. Moreover, the MFR decreases in the affected bronchi for each case. Additionally, stent placement in case 3 showed the possible effect of the PD on the work of breathing, increased WSS to stent migration, velocity path lines, and turbulence to mucus plugging. Lastly, it showed suboptimal use of the stent with the visualization of the velocity path lines. In short, CFD analysis demonstrated differences in variation in airways and the available space for airway stent improvement, hence the personalization of an airway stent.

4.4.1. Interpretation

The post-obstruction airway of case 1 with Y-stent was segmented and is visualized in Table 4-3. It was excluded from a simulation since it was not eligible for meshing. It contains too many irregularities at the proximal transition from the trachea to the stent. Additionally, a blind volume of air is on the anatomical left side. This cannot be segmented since only contours follow from the segmentation. But it is expected that this blind volume influences the air flow and thus the behavior of the stent.

The pre-obstructed scan of case 1 shows the curved anatomy of the trachea. As seen in the segmentation post-obstruction with a stent, the conventional airway stent remodels the tracheal anatomy to its shape. At the proximal right side, the stent rubs into the trachea. A combination of this poor fit and a dynamic trachea will irritate the airway. Relying on the physicians' experience this causes coughing, which also increased after stent placement. Such segmentation is a visual example of the required improved congruence of a stent to the airway by personalization for improved outcomes.

PD does not increase with increasing inlet velocity or the difference between the inlet and outlet area or any other parameter for the pre-obstructed airways (as also proven in 3.3 Stent versus Trachea). As PD also varied between different tracheas of similar length (3.3 Stent versus Trachea), the difference in PD is a result of the shape of the geometry. Anatomic variation between cases showed different numerical results for all evaluated parameters (PD, WSS, static pressure, velocity magnitude, TI, MFR). Hence, no range of healthy, pre-obstructed results exists. Consequently, obstructed airways must be therefore be compared with a simulation of the patient's airway before the disease. This will conclude whether the numerical difference is significant and to what extent corresponds with the clinical presentation.

Literature shows MFR ratios for left and right of 46.83%:53.28% in 1 healthy case [3] and 43.43%:56.57% in 7 healthy adults [4], respectively. Results of the simulated pre-obstructed airways

show a mean value of 35.7% and 65.4% for left and right, respectively. Hence, results are in a similar order of magnitude as found in the literature.

In the obstructed airways, the standard deviation is almost similar to the mean indicating widespread results. As proven, the PD in an airway geometry is due to its shape. Hence, the widespread in data is due to the obstructions that are present in different severities and locations influencing the geometries differently. No standardized range can be derived from the results, but it can be concluded that PD increases in an obstructed airway. In short, the PD of an obstructed airway must always be compared with a pre-obstructed airway model to evaluate the severity of the obstruction.

Case 5 had a total obstruction of the RMB. Therefore, it was chosen in the simulation to assume this side as the wall. Hence, only one outlet at the LMB was set. This would explain the decrease in PD in the obstructed situation compared to the pre-obstructed one. It shows that a full obstruction of the airway causes less PD compared to a partial obstruction. These simulations hence indicate that patients would experience less work of breathing with a full obstruction. Based on the physicians' experience this is the case. Hence, this implies a correct assumption within the model and consequently the possible clinical translation of CFD analysis.

4.4.2.   Comparison

The Wilcoxon-Mann Whitney U test was performed on the pressure drop of the pre-obstruction and obstruction airways. It showed a significantly higher pressure drop in the obstructed airways. However, the number of cases in both groups was very low thus this significant difference is not a reliable outcome. Power analysis with the Mann-Whitney U test must be performed for the minimum group size to have a significant difference that is reliable.

The WSS shows an increased value at the inlet plane and for case 3 the obstructed and stented airways have an area of maximum WSS on the main carina and varying values more distally. The increased value at the inlet plane is due to the set boundary condition as also explained in Chapter 3: 3.2.3 Discussion. Variation in the WSS around the main carina and more distally is due to the obstruction that changes the shape of the geometry. Increased stress at and around the obstruction comes with an increased chance of airway wall damage. This chance is decreased in the stented airway since WSS showed less variance distally to the main carina and a smaller maximum area on the main carina. On contrary, proximal to the stent in the LMB an increased area is still located. This location and increased WSS may increase the chance of stent migration (as explained in 2.2 Parameters of Interest). Additionally, the most proximal part of the LMB still shows a smaller diameter (Table 4-3). Unless the decreased WSS after placement of the conventional airway stent in case 3, the increased WSS and small diameter proximal to the conventional airway stent imply a wrong fit of the airway stent which increases the chance of complications.

Next, the stenosis increases the static pressure to the wall from the main carina towards the inlet at the proximal side due to increased resistance of the airway by narrowing. Hence, the pressure before the stenosis increases due to the consistent inflow of air. By inserting the stent, the diameter increases and decreases the pressure, also seen in the visualization in Figure 4-2. The pressure has not returned to the initial situation as also confirmed by the PD. Hence, the still increased wall pressure could provoke airway damage. Also, the still increased PD does not give a similar amount of work after conventional stent placement as before the obstruction. Hence, inserting a better fit of an airway stent, hence personalized, that fits from the main carina on and does not migrate would decrease the static pressure and PD more, hence airway wall damage and work of breathing.

Velocity path lines of the pre-obstructed and obstructed airways show a value of around 1 m/s in the trachea. As earlier discussed, easy mucus transportation is present with a minimum velocity of 1 m/s. Complaints noted about the tough sputum at the time of the obstructed airway cannot be explained by lower velocity. Therefore, turbulence seems the leading cause of the tough sputum. TI is increased in the obstructed and stented airway. Since the total cross-sectional area of the airway increases when reaching more distally, more laminar flow is expected in the LMB and RMB. Velocity path lines indicate the location of the turbulence above the main carina, and also in the stent for the post-obstruction airway. Additionally, the superior proximal part of the stent does not contain any velocity path lines. Results show that the implanted stent does not decrease the TI and air does not take full use of it, pleading for disturbed airflow by the inserted stent. An airway stent that opens up the LMB will decrease the turbulence and thereby streamline the mucus transportation.

Figure 4-3 shows the MFR ratio for the affected and non-affected sides of the LMB and RMB for all simulated airways. Each MFR of the affected side decreases concerning the pre-obstructed situation. Case 4 shows the least difference between the airflow ratios in the pre-obstruction and obstruction airways. As its geometry in Table 4-2 shows, the obstruction is located at the main carina which affects both main bronchi. Hence, this explains the small difference between both situations.

Numerical data of the MFR of the affected and non-affected side of case 3 is given in Table 4-5. The initial airflow of the affected side was 29.9% of the total airflow but decreases to 5.52% when affected. Hence, 24.4% of the airflow has been lost but stent placement returns 8.25% of the total mass flow. However, this subsequently means that 16% of the initial MFR is not restored with an airway stent. Hence, the majority of the airflow can still be restored. As the geometry of the post-obstruction airway with stent also implies. proximal to the airway stent is still a narrowing located. A personalized airway stent is expected to recover more of the initial MFR by improved congruence.

4.4.3.   Limitations

Only airway generations 0 and 1 (Figure 1-2) were simulated within this study since a CAO is present within this region and it simplifies the geometry, compared to the whole airway tree. Cutting the geometry after generation 1 means that a relatively short length of the geometry is present after the main carina. Since the main carina influences the fluid flow due to the bifurcation, this short length between the main carina and outlet may result in reversed flow or erroneous measurements. Hence, more length is required to let the fluid flow develop (2.1.1.2.6 Entrance length). This additional length can be calculated, or determined by looking at the path lines of the visualization after the simulation. Further studies require similar lengths of geometries and their outlets and extended bifurcations towards more reliable results. This could be done by a standardized measure of the outlet lengths during segmentation, or by manually extruding the outlets to similar lengths after segmentation.

Symptoms patients experienced were noted in all tables for the obstructed situations and stented airways. Whether these symptoms were a result of the underlying disease, or the obstruction is unclear but can also not be proved. It is therefore assumed that these symptoms are related to the obstruction or stent placement and not the disease.

The MFR of the non-affected side shown in Figure 4-3 fully compensates for the loss of the obstructed side. The clinical limitation of the lung volume of approximately three liters has not been considered. This enables the non-affected side to compensate, which is not the case *in vivo*. As also stated by Tullio, et al. [5] the lobar rate maximizes the flow rate of one lung and improves clinical translation. Nevertheless, it does not impact the simulations since only the difference in MFR for the affected side is of interest.

Cartilage rings have an average thickness of 1 mm. [6] CT scans with a slice thickness of 1.5 mm, therefore, lose details by which the trachea is smoothened. As proven, this decreases the PD, WSS, and TI. Appendix C: Patient Characteristics includes slice thicknesses of each CT scan. Since 1 or 1.5 mm is included in the standard procedure in the NCI these scans were used. For a detailed reconstruction of the airway, a CT scan with a maximal slice thickness of 1 mm is recommended.

4.4.3.1.   *Assumptions*

Similar assumptions were made as in Chapter 3: Simulating and comparing stents and tracheal geometries. Discussion of these assumptions is therefore similar within this chapter. See 3.4.1 Assumptions, for the effect of the assumptions on the simulation.

One difference is the simulation of only an airflow of 0.5 L/s. As described in 2.1.1.1.1 Near wall modeling, an increased airflow for the similar geometry required a finer mesh to ensure a y+ <1. Simulations would reach an exceptionally long computational time. It was considered to be not worth it since only a difference wants to be proven, higher airflows are not required. Future research should include extreme airflows as occurs whilst coughing since this generates the highest forces within the airway that give the greatest chance of complications.

4.4.4.   Clinical interpretation and future work

The literature describes one study that focuses on tumor growth in the trachea and investigates the impact on airflow dynamics as a predictor for medical intervention. [7] Other literature focuses on the translation of CFD to pulmonary function test results [4, 8], evaluation of the surgery [3, 5, 9, 10], exploration of airflow in the airway [11], also in obstructed airways [4, 12-14], and improvement of the airway mesh and/or simulation [15-17]. Taking these studies together, CFD is a patient-specific approach that provides additional information, and understanding of alterations after surgery helps in follow-up and correlates with pulmonary function tests. However, no clinical translation of these simulations has been described, other than the numerical outcomes of the pulmonary function test.

Since the patient population within this thesis suffers from a CAO with a malignant cause and is so severe that it was treated with an airway stent, a pulmonary function test is not always possible. This is the only test that can quantify the dyspnea, also important during the follow-up. As also confirmed by previous studies, CFD is a tool to quantify dyspnea. Since a CT scan is performed during the follow-up, the data is available and quantification of the disease that considers airflow is possible.

Despite the impact of the assumptions in this simulation of the *in vivo* situation, as described in Chapter 3: 3.4.1 Assumptions, it is the first model that simulates a pre-obstructed, obstructed, and post-obstruction with airway stent situation in one case. It showed variation in the PD, WSS, static pressure, velocity path lines, and TI in between all cases due to the anatomic variation. This implies that a comparison of an obstruction airway within one case is required and generalization of results cannot be applied. Next, stent placement did not return the work of breathing to the pre-obstructed situation. More work on breathing is still required for similar airflow. The WSS in the stented airway is increased proximal to the stent, pleading for an increased chance of stent migration. Next, the velocity path lines show together with the numerical increase of the TI the increased change of mucus plugging in and around the stent. Additionally, no flow is present in the proximal superior part of the stent indicating suboptimal use, thus the placement of the stent. Lastly, the MFR also confirms the space for improvement of the conventional stent, since it does not restore the initial airflow. In short, this case proves the suboptimal design and consequently placement of a conventional airway stent. It shows the increased chance of complications and the minor relief of symptoms, quantitatively.

Clinical translation of CFD analysis was, next to case 3, also confirmed by case 5. Total obstruction of the RMB resulted in simulating this end as a wall instead of an outlet. In contrast to all other simulations, this resulted in a decrease in the PD in the obstructed airway compared to pre-obstructed. Compared to other obstructed airways, this patient experiences relatively less work of breathing which is in line with clinical experience. Hence, the results of the CFD imply the possible clinical translation.

Future work must consider more of the assumptions described in the previous chapter. Incorporating more clinically relevant parameters, such as airway dynamics or time-dependent flow, would increase the clinical translation of such CFD analysis. If set, more cases have to be simulated to see different kinds of obstructions and the inserted conventional airway stents. This additionally shows how to select patients that are not eligible for a conventional airway stent.

REFERENCES

[1]   N. Guibert, H. Saka, and H. Dutau, "Airway stenting: Technological advancements and its role in interventional pulmonology," *Respirology,* vol. 25, no. 9, pp. 953-962, 2020/9// 2020, doi: https://doi.org/10.1111/resp.13801.

[2]   P. A. Yushkevich *et al.*, "User-guided 3D active contour segmentation of anatomical structures: Significantly improved efficiency and reliability," *NeuroImage,* vol. 31, no. 3, pp. 1116-1128, 2006, doi: https://doi.org/10.1016/j.neuroimage.2006.01.015.

[3]   S. Qi, Z. Li, Y. Yue, H. J. van Triest, and Y. Kang, "Computational fluid dynamics simulation of airflow in the trachea and main bronchi for the subjects with left pulmonary artery sling," (in eng), *Biomed Eng Online,* vol. 13, p. 85, Jun 24 2014, doi: 10.1186/1475-925x-13-85.

[4]   C.-Y. Ho *et al.*, "Numerical analysis of airflow alteration in central airways following tracheobronchial stent placement," *Experimental Hematology & Oncology,* vol. 1, no. 1, pp. 23-23, 2012, doi: 10.1186/2162-3619-1-23.

[5]   M. Tullio, L. Aliboni, F. Pennati, R. Carrinola, A. Palleschi, and A. Aliverti, "Computational fluid dynamics of the airways after left-upper pulmonary lobectomy: A case study," *International journal for numerical methods in biomedical engineering,* vol. 37, no. 7, pp. e3462-e3462, 2021/7// 2021, doi: 10.1002/cnm.3462.

[6]   Y. Premakumar, M. F. Griffin, and M. Szarko, "Morphometric characterisation of human tracheas: focus on cartilaginous ring variation," (in eng), *BMC Res Notes,* vol. 11, no. 1, pp. 32-32, 2018, doi: 10.1186/s13104-018-3123-1.

[7]   T. Zobaer and A. Sutradhar, "Modeling the effect of tumor compression on airflow dynamics in trachea using contact simulation and CFD analysis," *Computers in Biology and Medicine,* vol.   135,   pp.   104574-104574,   2021,   doi: https://doi.org/10.1016/j.compbiomed.2021.104574.

[8]   T.-C. Shih, H.-D. Hsiao, P. Y. Chen, C.-Y. Tu, T.-i. Tseng, and Y.-J. Ho, "Study of Pre- and Post-Stent Implantation in the Trachea Using Computational Fluid Dynamics," *Journal of Medical and Biological Engineering,* vol. 34, pp. 150-156, 2014.

[9]   F.-L. Chen, T.-L. Horng, and T.-C. Shih, "Simulation analysis of airflow alteration in the trachea following the vascular ring surgery based on CT images using the computational fluid dynamics method," *Journal of X-Ray Science and Technology,* vol. 22, no. 2, pp. 213-225, 2014, doi: 10.3233/XST-140420.

[10]   Q. Gu *et al.*, "Structural and functional alterations of the tracheobronchial tree after left upper pulmonary lobectomy for lung cancer," *BioMedical Engineering OnLine,* vol. 18, no. 1, p. 105, 2019/10/25 2019, doi: 10.1186/s12938-019-0722-6.

[11]   Y. Shang, J. Dong, L. Tian, K. Inthavong, and J. Tu, "Detailed computational analysis of flow dynamics in an extended respiratory airway model," *Clinical Biomechanics,* vol. 61, pp. 105-111, 2019, doi: https://doi.org/10.1016/j.clinbiomech.2018.12.006.

[12]   M. Malvè, S. Chandra, J. López-Villalobos, E. Finol, A. Ginel, and M. doblaré, "CFD analysis of the human airways under impedance-based boundary conditions: Application to healthy, diseased and stented trachea," *Computer methods in biomechanics and biomedical engineering,* vol. 16, 01/06 2012, doi: 10.1080/10255842.2011.615743.

[13]   S. S. Razi *et al.*, "Pre- and post-stent modeling of airflow dynamics in patients with malignant tracheal obstruction," *Journal of the American College of Surgeons,* vol. 211, no. 3, pp. S39-S39, 2010/9// 2010, doi: 10.1016/j.jamcollsurg.2010.06.096.

[14]   B. Sul, A. Wallqvist, M. Morris, J. Reifman, and V. Rakesh, "A computational study of the respiratory airflow Characteristics in normal and obstructed Human airways," *Computers in Biology and Medicine,* vol. 52, 2014/9// 2014, doi: 10.1016/j.compbiomed.2014.06.008.

[15]   R. Agujetas, R. Barrio-Perotti, C. Ferrera, A. Pandal-Blanco, D. K. Walters, and A. Fernández-Tena, "Construction of a hybrid lung model by combining a real geometry of the upper airways and an idealized geometry of the lower airways," *Computer Methods and Programs in Biomedicine,* vol. 196, pp. 105613-105613, 2020, doi: https://doi.org/10.1016/j.cmpb.2020.105613.

[16]   A. Fernández-Tena, A. C. Marcos, R. Agujetas, and C. Ferrera, "Simulation of the human airways using virtual topology tools and meshing optimization," *Biomechanics and Modeling in Mechanobiology,* vol. 17, no. 2, pp. 465-477, 2018/04/01 2018, doi: 10.1007/s10237-017-0972-9.

[17]   S. Miyawaki, E. A. Hoffman, and C.-L. Lin, "Numerical simulations of aerosol delivery to the human lung with an idealized laryngeal model, image-based airway model, and automatic meshing algorithm," *Computers & fluids,* vol. 148, pp. 1-9, 2017/4// 2017, doi: 10.1016/j.compfluid.2017.02.008.
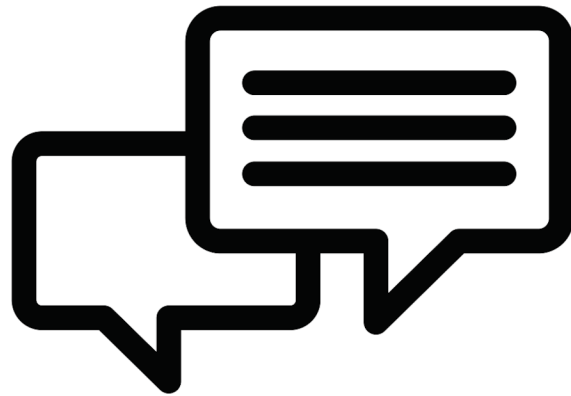
Chapter 5: General discussion

"Man has always to be busy with his thoughts if anything is to be accomplished."

This thesis aimed to obtain quantitative evidence for the design of personalized airway stents using computational fluid dynamics (CFD) analysis of airways, stents, and a combination. Results showed that the increased diameter of the stent results in the least pressure drop (PD), wall shear stress (WSS), and turbulence intensity (TI). Minimizing these parameters decreases the work of breathing, the chance of stent migration, and mucus plugging, respectively. Similar simulation performed on a trachea, hence an increased complexity of the geometry, increases these parameters. Additionally, all tracheas show different results of the PD, WSS, and TI, advocating for more patient-specific treatment. In short, a smooth lumen of an airway stent is desired for implantation since this decreases the chance of stent-related complications and increases the relief of symptoms.

Furthermore, a pre-obstructed, obstructed and post-obstruction airway with a conventional airway stent was simulated to obtain numerical insight into airflow within a more *in vivo* situation. It evaluated the PD, WSS, TI, static pressure to the wall, velocity path lines, and mass flow rate (MFR) ratio. These parameters are predictors for the work of breathing, stent migration, mucus plugging, airway wall damage, the location of mucus plugging, and lung ventilation, respectively. The PD, WSS, TI, and static pressure to the wall all increase for the obstructed airway. The velocity path lines locate the increased TI, mainly around the obstruction. Lastly, the MFR decreases in the affected side compared to the pre-obstructed airway.

For evaluated case 3, the conventional airway stent helped in relieving dyspnea by decreasing the PD. However, it showed increased WSS proximal to the stent and increased TI which suggests stent migration and mucus plugging, respectively. Velocity path lines indicate the suboptimal use of the inserted airway stent. Additionally, visualization of the geometry also proves the bad congruence of the stent since a narrowed airway is still present proximal to the airway stent. Visualization of the stented airway of case 1 also shows bad congruence and corresponding complaints of increased coughing.

To conclude, this model is the first that simulates the pre-obstructed, obstructed, and post-obstruction airway with a stent using CFD. It demonstrated increased PD, WSS, TI, and static pressure to the wall, pleading for increased work of breathing and chance, airway wall damage, and mucus plugging. Implantation of a conventional airway stent in case 3 showed a decrease in PD and static pressure to the wall. Despite the improved dyspnea, the static pressure, WSS, and TI are still increased compared to the pre-obstructed results. Additionally, suboptimal use of the airway stent is shown by the velocity path lines and the visualization of case 3 in Table 4-3 demonstrates the poor fit of the conventional airway stent. The visualization of case 1 in Table 4-3 also shows a poor fit of the conventional airway stent. These results plead for more personalized airway stents with the greatest diameter clinically possible with a smooth lumen but congruent to the airway, to decrease the chance of complications and improve symptoms and the work of breathing.

5.1. FUTURE PERSPECTIVES

As described in section 3.1, multiple assumptions were required to let the CFD model run as close as possible to an *in vivo* airflow within the time frame. As mentioned in the discussion of Chapter 3: these assumptions need to be adjusted towards a more clinically representable model. The least time-consuming improvements that must be implemented in an improved model are setting a time-dependent flow, simulating exhalation and different flow rates, and adjusting air properties to 37°C. Next up, airway dynamics and adding an entrance length require more experience but are the most important parameters. Airway dynamics play a crucial role in breathing physiology and are therefore

also expected as the main element in stent fitting, and related complications. However, simulating such is very computationally expensive and must be performed by an experienced CFD engineer. Additionally, another ANSYS software package is required to implement these dynamics. Secondly, adding the upper airways as an entrance length will simulate the *in vivo* airflow better. Unfortunately, most the CT-scans lack this part of the anatomy. Hence, a geometrical model that mimics the upper airways as proposed by Miyawaki, et al. [1] is an alternative to include in further research.

Towards the virtual design of an airway stent, ANSYS is capable of automatic mesh adaption. This means that ANSYS can deform a part of the mesh to the target input parameters. For example, the stenosis in an obstructed airway can be marked as the area of interest. Next, the outflow of the outlets must be set (almost) similar to the outflow that is measured during the simulation of the pre-obstructed airway. During simulation, ANSYS deforms the mesh until the input outflow values are reached. CFD analysis is in this context used towards a prediction of the optimal design of a personalized airway stent.

Next to the design of an airway stent, ANSYS can help in the mechanical interaction between the stent and the airway. This thesis only considered the fluid behavior of a combined geometry of airways with inserted airway stent. But mechanical forces also play a role in stent behavior mainly due to airway dynamics. Therefore, the shear and forces that are caused by the interaction of an airway stent and the airway cannot be considered. However, this will determine the strength of a stent and the predicted migration. Simulation of mechanical properties of the interaction between the stent and airway is possible within another ANSYS software package. Hence, determine the shear and (radial) forces of the stent onto the airway. Increased shear compared to radial forces will likely cause the stent to migrate, which has to be overcome in a stent design. Simulation of such properties will go a step towards personalized stents, which are not conventional in shape.

After setting up a simulation of the mechanical interaction between the stent and airway, virtually testing of airway stents can be performed. Segmentation of the obstructed airway is required to virtually place an airway stent. Next, virtual models of airway stents, or the airway stent as predicted by ANSYS as described above, must also be finished. These stent geometries can be virtually placed within an airway and both the mechanical and fluid simulations can be performed. Effectivity of the stent, thus expected migration, mucus plugging, and work of breathing can be predicted.

Lastly, another mechanical property that could be included in the model is the pressure of other thoracic structures. Stent migration is one of the main stent-related complications. It results from the balance of radial forces of the stent on one side, and the external pressure from the trachea and other thoracic structures on the other side. Modeling these external pressures onto the trachea help in setting up this balance and determining the chance of stent migration.

Clinical translation of the simulation has been proved within this thesis based on flow behavior. This has also been investigated by Ho, et al. [2], who performed pulmonary function tests to correlate simulations to the clinical function. They also concluded that the CFD solutions corresponded with the performed clinical tests. Also, Razi, et al. [3] concluded the reliability of the non-invasive CFD simulations of an airflow across lesions. Both studies also based their clinical translation on fluid behavior, but as mentioned above, the mechanical interaction is also of interest in predicting the outcome. With a correct clinical translation, based on both fluids and mechanics, CFD is expected to be used for the prediction of an interventional outcome. [4]

In the end, CFD could be used as a clinical predictive model, due to its verified clinical translation and non-invasive nature. Pulmonary function tests can be hard to perform, especially for lung cancer

patients who are in general not in good condition. In addition, simulations can collect data that cannot be measured ex vivo, such as pressure drop. prediction of the design of a personalized stent, the clinical outcome after placement, but also the follow-up of these patients using CFD analysis will be the future.

REFERENCES

[1]   S. Miyawaki, E. A. Hoffman, and C.-L. Lin, "Numerical simulations of aerosol delivery to the human lung with an idealized laryngeal model, image-based airway model, and automatic meshing algorithm," *Computers & fluids,* vol. 148, pp. 1-9, 2017/4// 2017, doi: 10.1016/j.compfluid.2017.02.008.

[2]   C.-Y. Ho *et al.*, "Numerical analysis of airflow alteration in central airways following tracheobronchial stent placement," *Experimental Hematology & Oncology,* vol. 1, no. 1, pp. 23-23, 2012, doi: 10.1186/2162-3619-1-23.

[3]   S. S. Razi *et al.*, "Pre- and post-stent modeling of airflow dynamics in patients with malignant tracheal obstruction," *Journal of the American College of Surgeons,* vol. 211, no. 3, pp. S39-S39, 2010/9// 2010, doi: 10.1016/j.jamcollsurg.2010.06.096.

[4]   R. Agujetas, R. Barrio-Perotti, C. Ferrera, A. Pandal-Blanco, D. K. Walters, and A. Fernández-Tena, "Construction of a hybrid lung model by combining a real geometry of the upper airways and an idealized geometry of the lower airways," *Computer Methods and Programs in Biomedicine,* vol. 196, pp. 105613-105613, 2020, doi: https://doi.org/10.1016/j.cmpb.2020.105613.

Chapter 6: Appendix

APPENDIX A: MANUAL FOR SETTING UP AIRWAY SIMULATIONS WITHIN ANSYS

This Appendix includes a step-by-step guide of setting up a simulation for both a stent and airway in ANSYS.

Workbench

The 'Ansys Workbench' is the starting point of all simulations, depicted in Figure 6-1. On the left side the toolbox shows Analysis or Component systems that can be dragged into the project. Dependent on the licenses available, a different number of systems is shown. Two systems are used for the simulations in this thesis. The first component is 'Geometry' where the specific geometry is made ready for simulations. The component system 'Fluent (with Fluent Meshing)' is used for the whole simulation part: pre-processing, processing and post-processing.
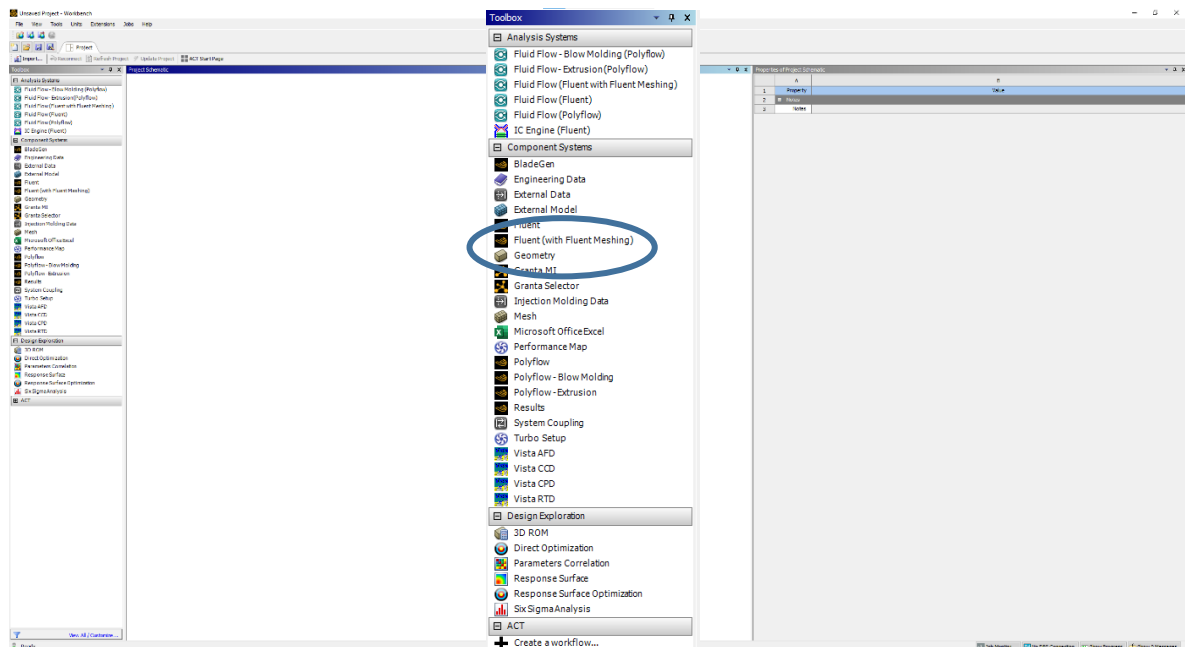
Figure 6-1 Screenshot of the ANSYS workbench. On the left, the toolbar is visualized, which is also depicted larger in the middle of the image. The two components that will be used during simulation are circled.

Both component systems are dragged into the Workbench next to each other, as visualized below. The Geometry component must be connected with *Mesh* from the Fluent component system. Therefore, the geometry section must be dragged towards the mesh section of the Fluent component. This generates a connection between the systems (Figure 1-2). In this way, the geometry is loaded to generate a mesh.

Next up is specifying the geometry of interest. Within this thesis, this considered an airway stent or airway. A right click on the geometry part gives a sub-menu (Figure 1-2). If the workflow for a simulation of a stent will be followed, *New SpaceClaim Geometry* must be selected. If it considers a segmented airway, choose *Import Geometry* and browse to the specific .STL file to import.
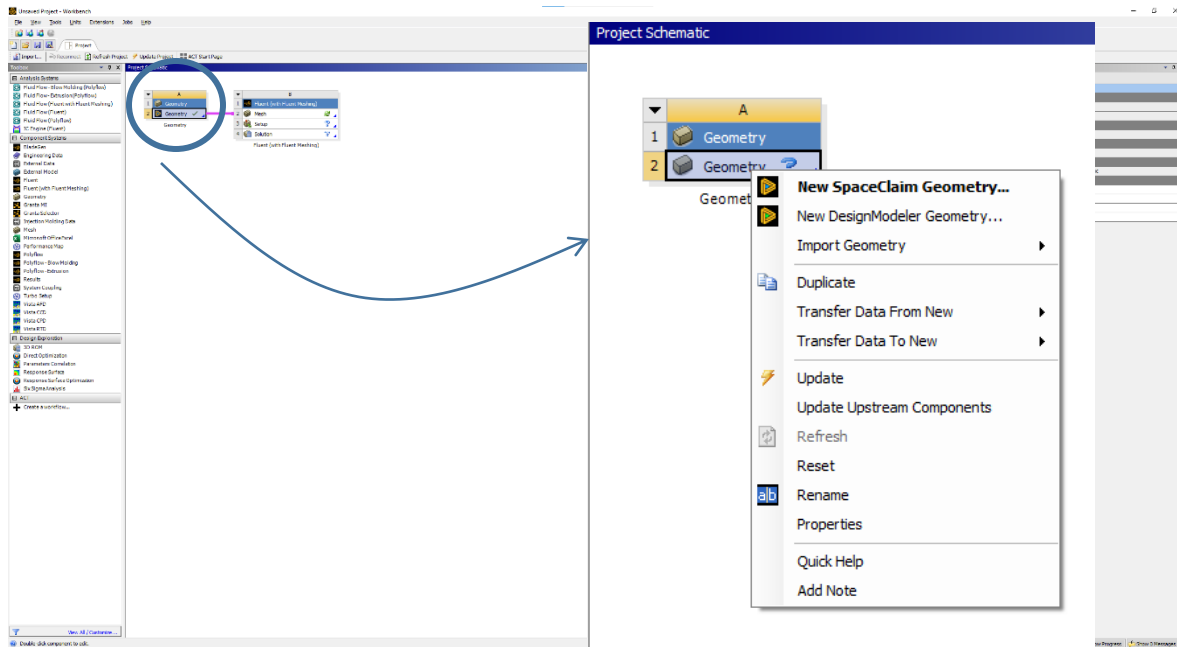
Figure 1-2 Screenshot of the workbench with the Geometry and Fluent (with fluent meshing) components dragged into the workbench. The pink line between the geometry and mesh indicates their connection. Right, the sub-menu that opens after right-clicking the geometry component is visualized.

The workflow for a stent will go on below, the section that follows describes the workflow for a segmented airway.

SpaceClaim: Stent

If a stent is desired to simulate, a new geometry must be designed within Spaceclaim. Hence, with a right click onto the Geometry part, 'New SpaceClaim Geometry' must be chosen. SpaceClaim opens with the following screen in Figure 1-3:
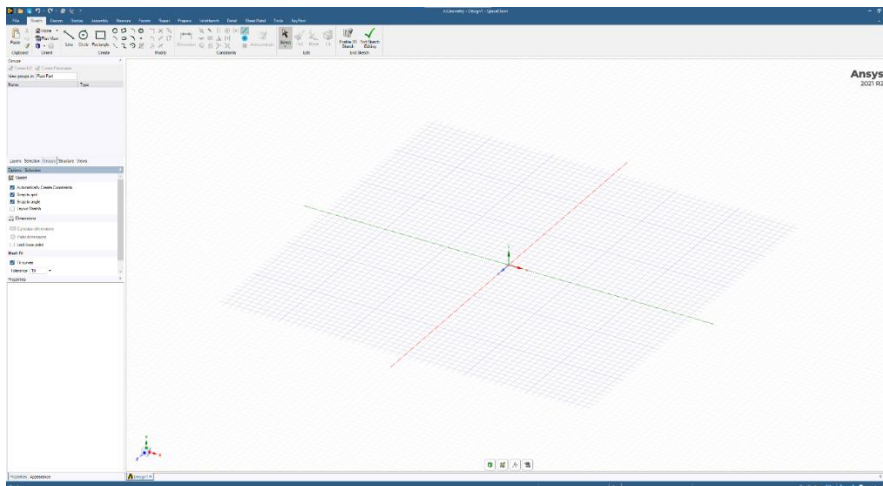
Figure 1-3 Screenshot of SpaceClaim when defining a new design.

In the *Home* toolbar, select the *circle* tool and define a circle with specified diameter on the showing sketch plane (Figure 1-4):
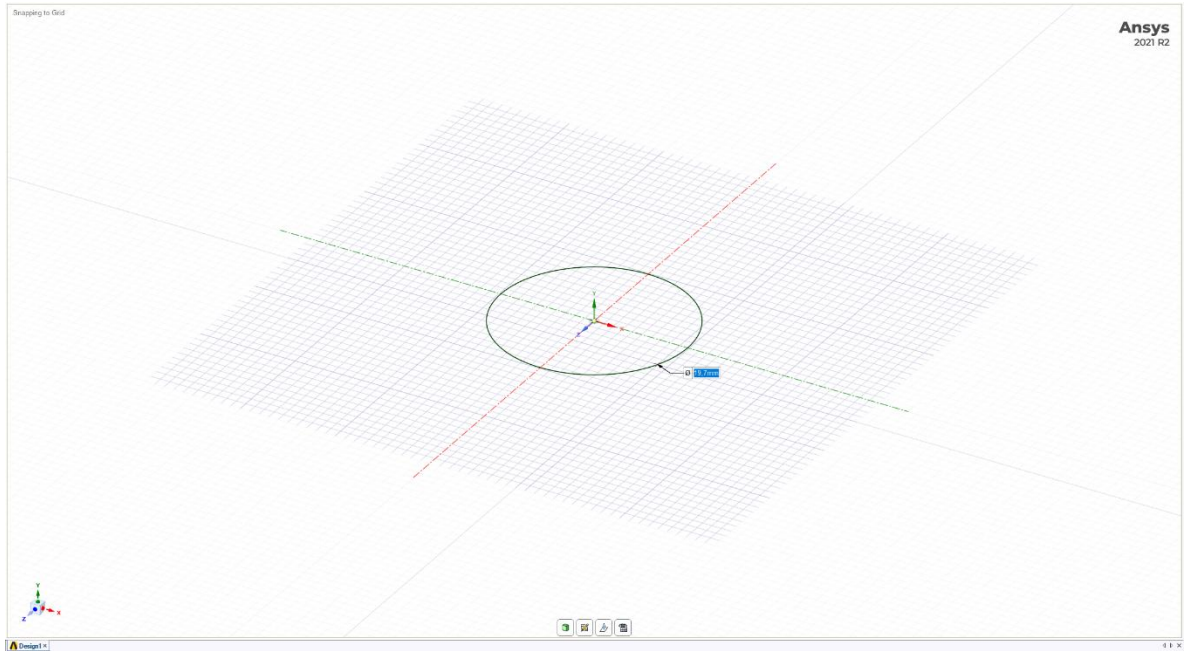
Figure 1-4 Screenshot of SpaceClaim with a circle designed on the sketch plane.

A 2D shape of the stent has now been designed. To make it a 3D geometry, click on *Extrude* in the *Design* toolbar. Extrude the geometry for a specified length as in Figure 1-5.
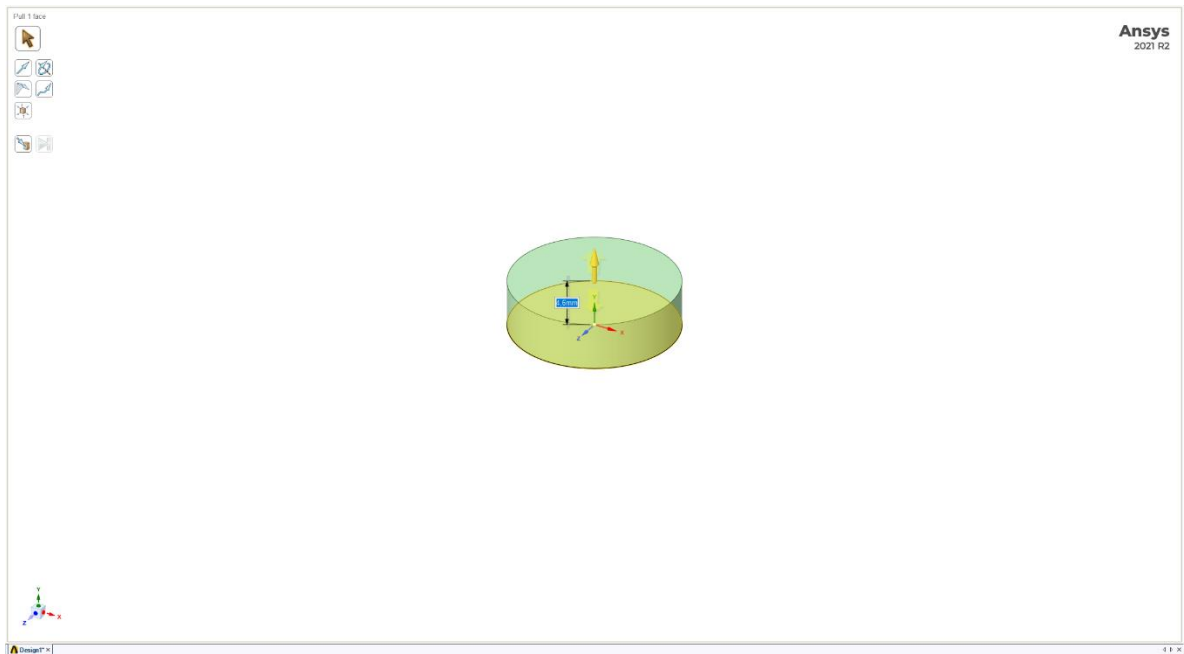
Figure 1-5 A screenshot of SpaceClaim. The circle that is defined in the previous step is now extruded with the yellow arrow. The measurement can be given into the white box.

Now, the stent has been designed as a 3D geometry. For the inlet, outlet and wall a named selection must be made. In the toolbar on the left side, click on *Groups*. Select a plane, for example the inlet, and give this selection a name (Figure 1-6). Do this for all planes.
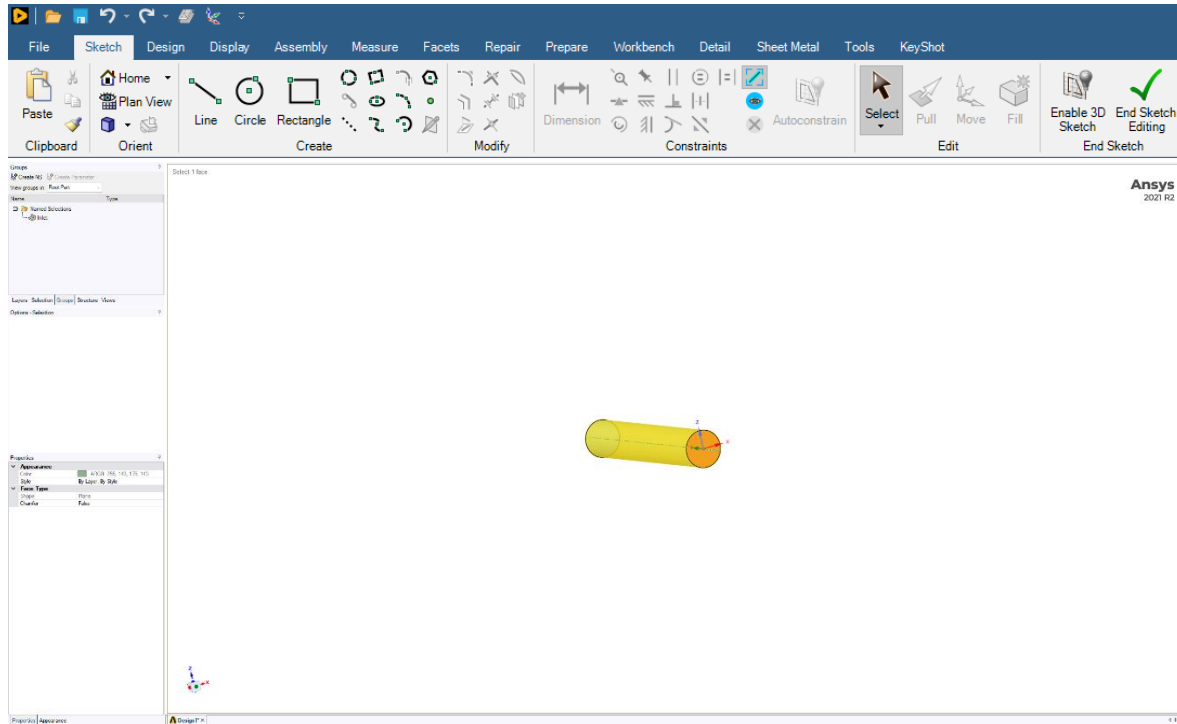
Figure 1-6 Screenshot of the designed stent within SpaceClaim. All planes must be defined as a named selection. This is done at the toolbox at the right side, in the Groups section. in the picture, the orange selection is defined as the inlet.

The geometry of the stent is now finished for simulation. SpaceClaim can be closed, and the setup section is the next step, described below in the section Fluent.

SpaceClaim: Airway

In the sub-menu that appears after right-clicking the geometry component, *Import Geometry* must be selected. The specific .STL file must be opened and will appear in SpaceClaim as below (Figure 1-7).
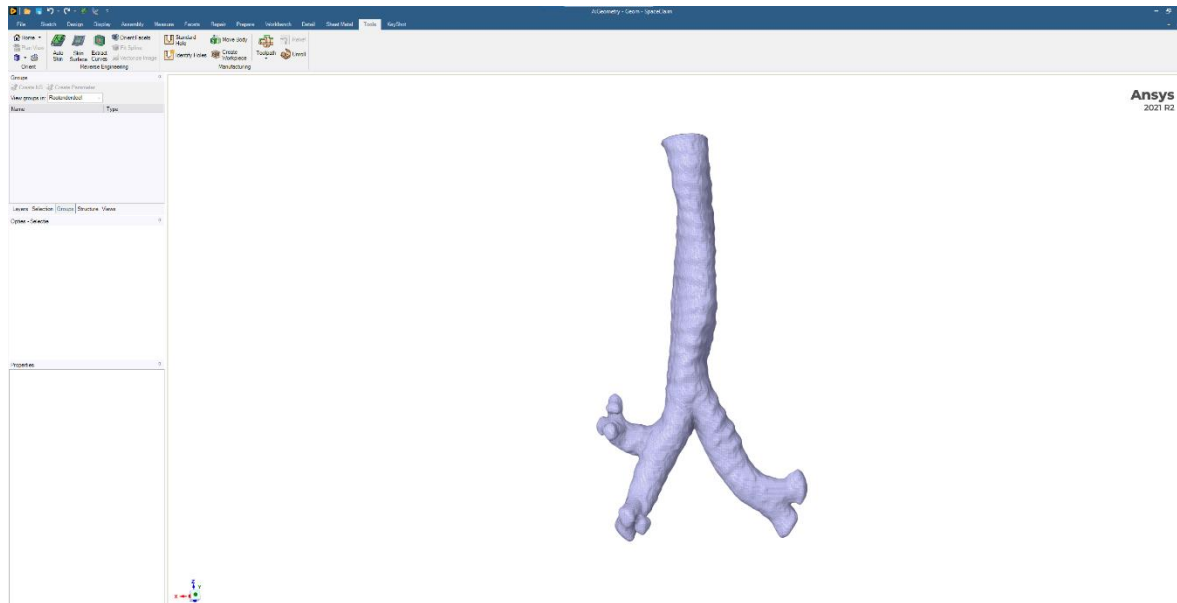
Figure 1-7 Screenshot of SpaceClaim with the imported airway as an .STL file.

The easiest way towards a complete geometry is the use of *Tools – Auto Skin*. This function generates relatively big surfaces that describe the geometry with greater planes. This uses less computational time when converted to the simulation software part. Another pro is that it checks the mesh prior to converting it into a CAD-body. If any faults are detected, they will pop-up and they can be repaired with functions in the Repair tab. Such error is depicted in Figure 1-8.
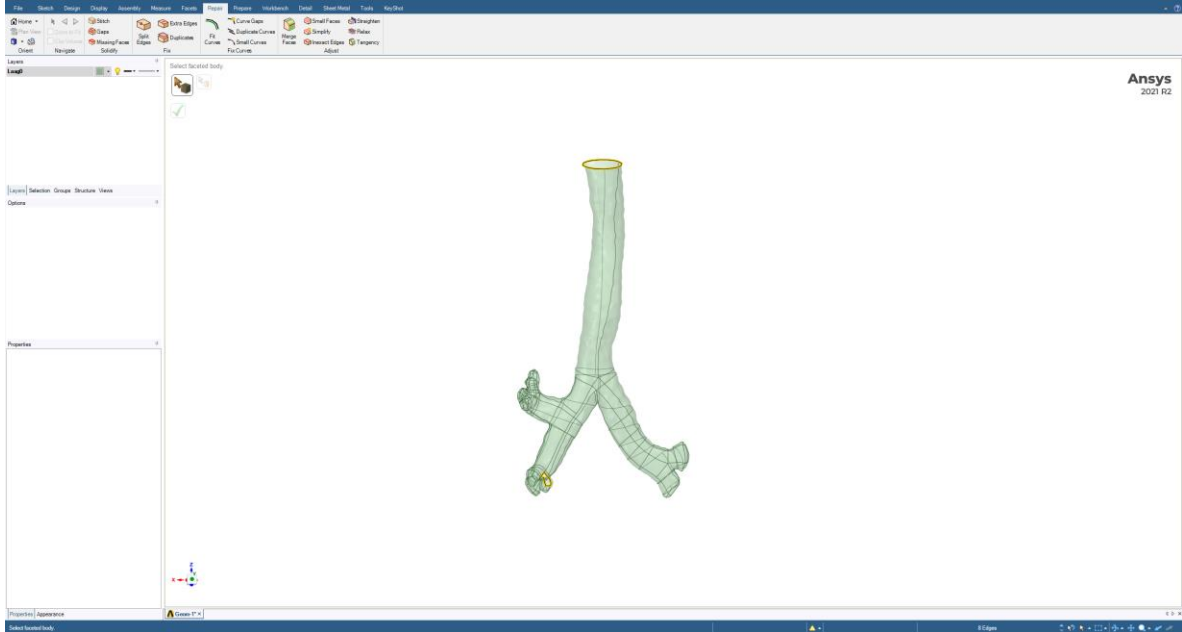

Figure 1-8 Screenshot of the conversion with Auto Skin towards a CAD-body. Two errors are present, one at the inlet and one at the distal right side. Using Repair -> Missing faces, these faces can be generated, and the CAD-body is complete.

If faces cannot be generated with the Missing Faces function, faces of the mesh needs to be reduced. Hence, the conversion with Auto Skin needs to be canceled. Next, the areas that gave an error, such as the distal end of the right side in Figure 1-8 need to be selected. Within the Facets section, reduce must be clicked on. The selected area, example given in Figure 1-9. After mesh reduction, try the Auto Skin function again. If the error is still present, repeat the reduction and try again.
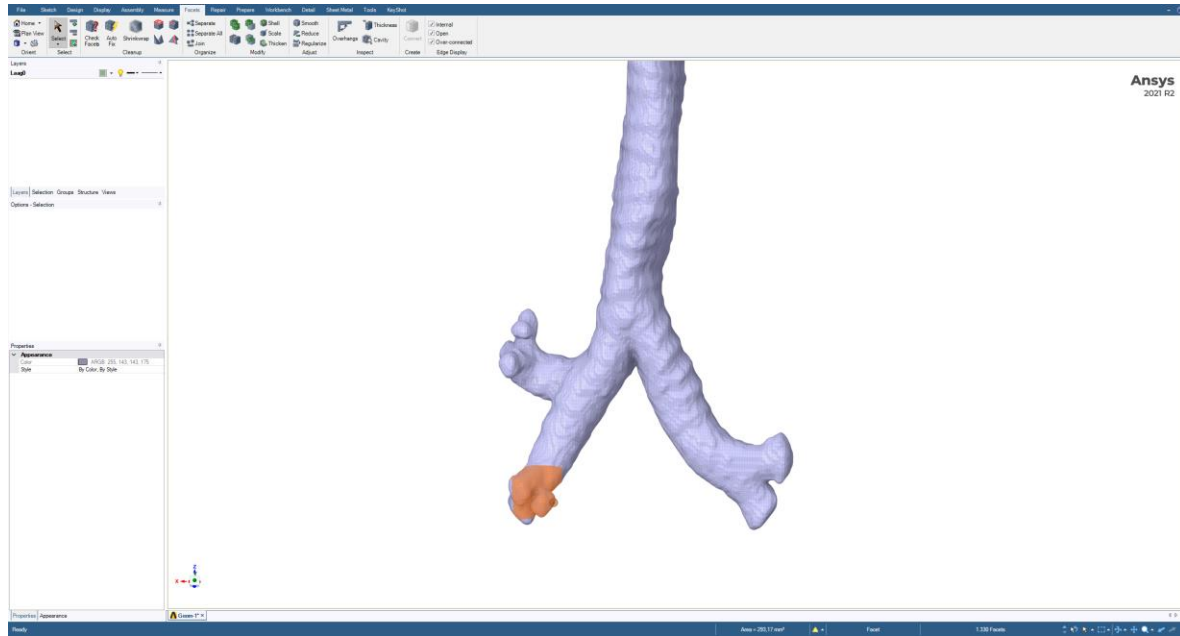
Figure 1-9 Screenshot of the airway mesh (grey) with the selected area that gave an error during conversion into a CAD-body (orange).

If conversion into a CAD-body has finished, the geometry turns green as in Figure 1-10. Next, planes are designed to measure the length of the trachea and define the outlets. A plane must be defined orthogonal to the length of the airway that crosses the main carina. In the Design tab, click plane and define a plane as in Figure 1-10.
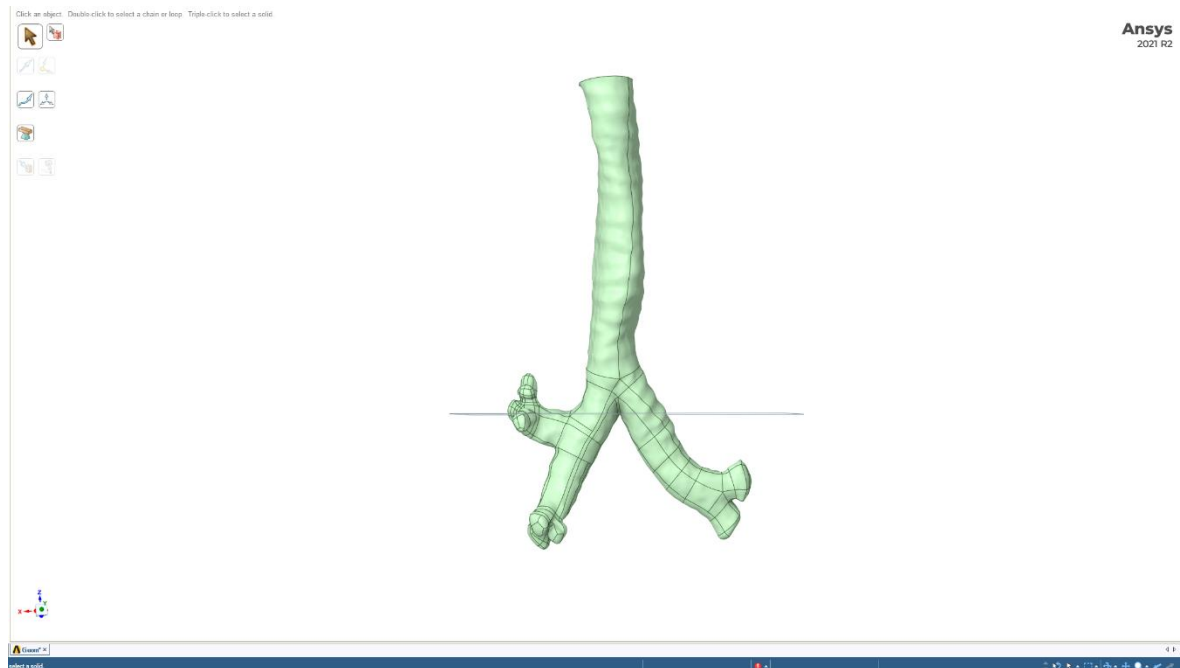

Figure 1-10 Screenshot of the CAD-body of the airway geometry. The plane in the middle is orthogonal to the airway and lies horizontally on the main carina.

The plane of Figure 1-10 must be copied and translated 100 mm superiorly as in Figure 1-11. This is performed to ensure similar lengths of the trachea across different airway models.
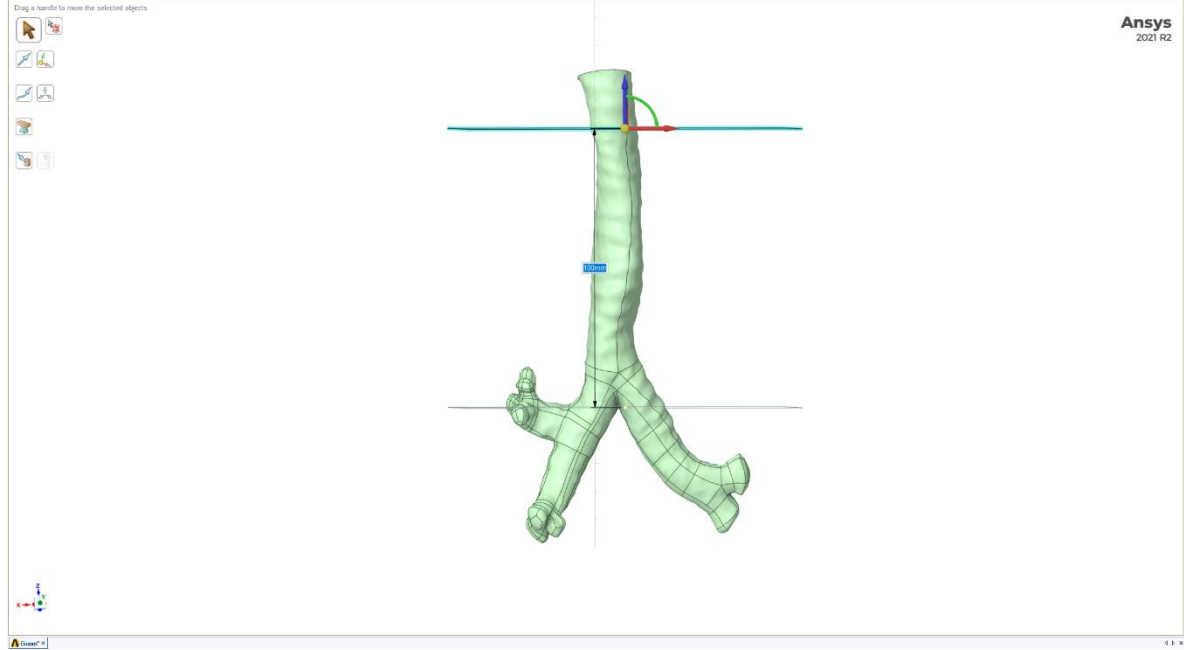

Figure 1-11 Screenshot of the geometry with the plane orthogonal to the airway and one translated 100 mm superiorly.

Lastly, two planes must be defined: one at each outlet. Again, design two new planes and set them orthogonally to the airway. An example of such placement is given in Figure 1-12.
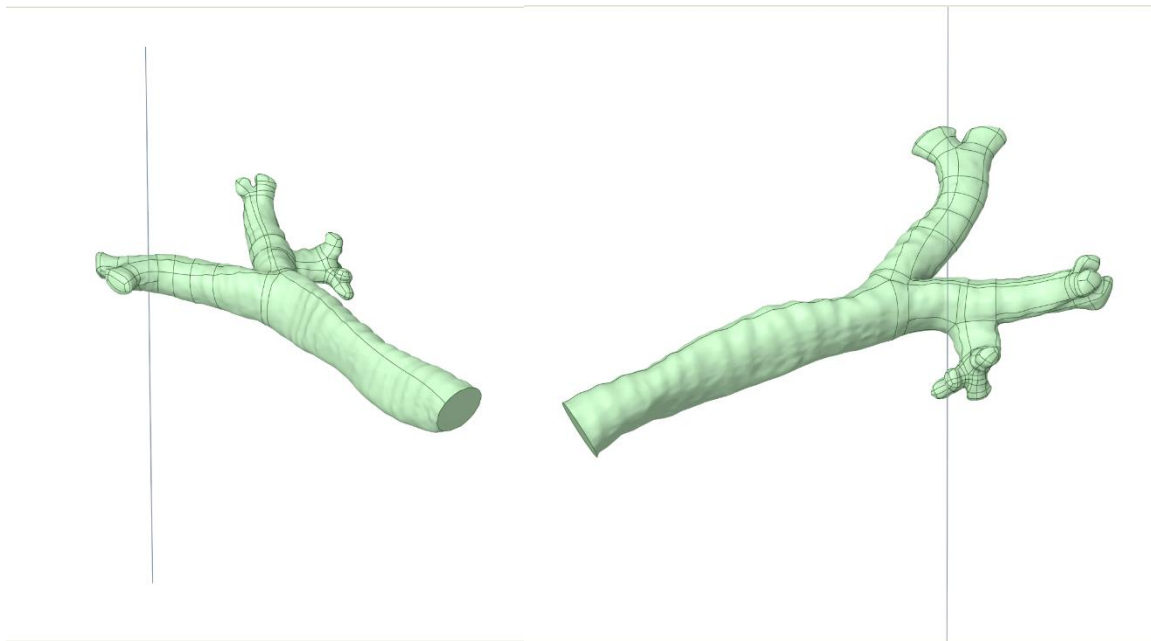

Figure 1-12 Screenshot of setting both outlets planes for the airway. The left picture depicts the plane for the left outlet, right for the right outlet.

All planes are now defined to cut an inlet and two outlets. This is performed using the function Split Body (see Figure 1-13). It enables cutting the geometry with the designed plane. The plane on the main carina is not cut with but only defined for a standardized measure of the trachea. After each cut, click in the saw icon. It is not recommended to remove the parts that have been cut off, since they can be reused/stitched to the body again when copying the geometry.

After cutting the geometry with all three planes, the parts that will not be used during the simulation must be turned off to be sure that it will not be simulated. Figure 1-14 shows the menu that opens at the right side after a right-click on the specific component. The figure also already shows absence of the more distal parts of the airway.
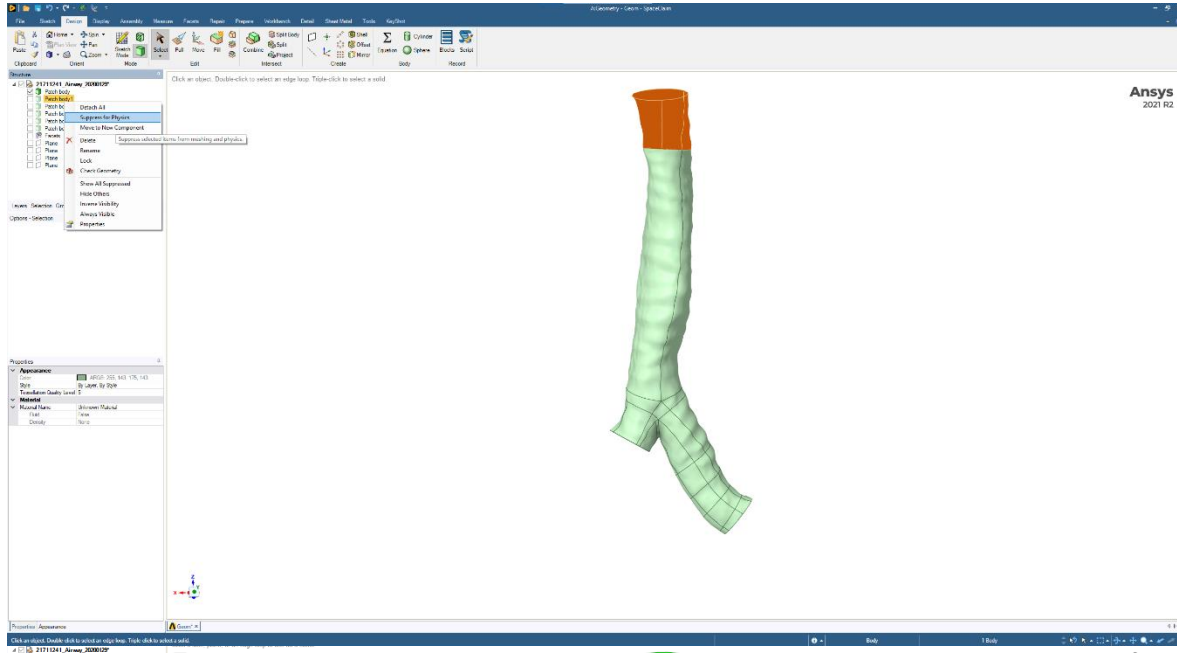

Figure 1-14 Screenshot of the airway (green) with the selected cut part (orange). At the left side, a right click on the part that has been cut opens the menu. By clicking 'Suppress for Physics', the part is suppressed and will not be imported for simulation. This must be performed for every part that is not of interest.
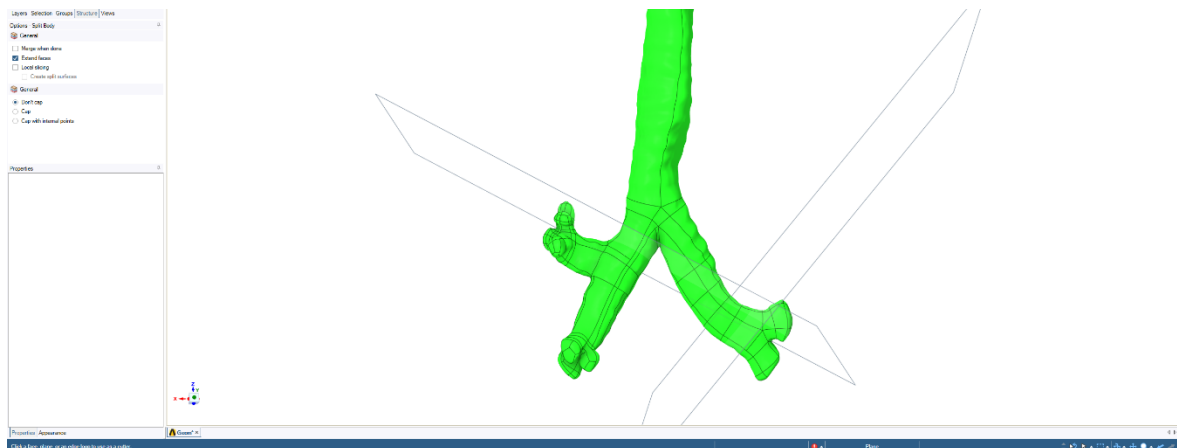

Figure 1-13 Screenshot of the geometry with the planes that will be used to cut the geometry with. The inlet plane is highlighted blue since it is selected to cut with.

The last step that has to be performed in SpaceClaim is definition of the named selections. At the left side in the toolbox, the tab Group must be opened. Every plane has to have a name. In Figure 1-16 is an example depicted. The left outlet is here selected and with *Create NS,* a name will be given such as 'OutletL'. This is performed for the outlet on the right side ('OutletR'), inlet ('inlet') and whole airway wall ('wall'). For the latter, the whole airway must be selected (ctrl + a). By holding *ctrl*, the inlet and both outlets must be selected and will be removed from the selection. If all named selections are done, SpaceClaim can be closed.
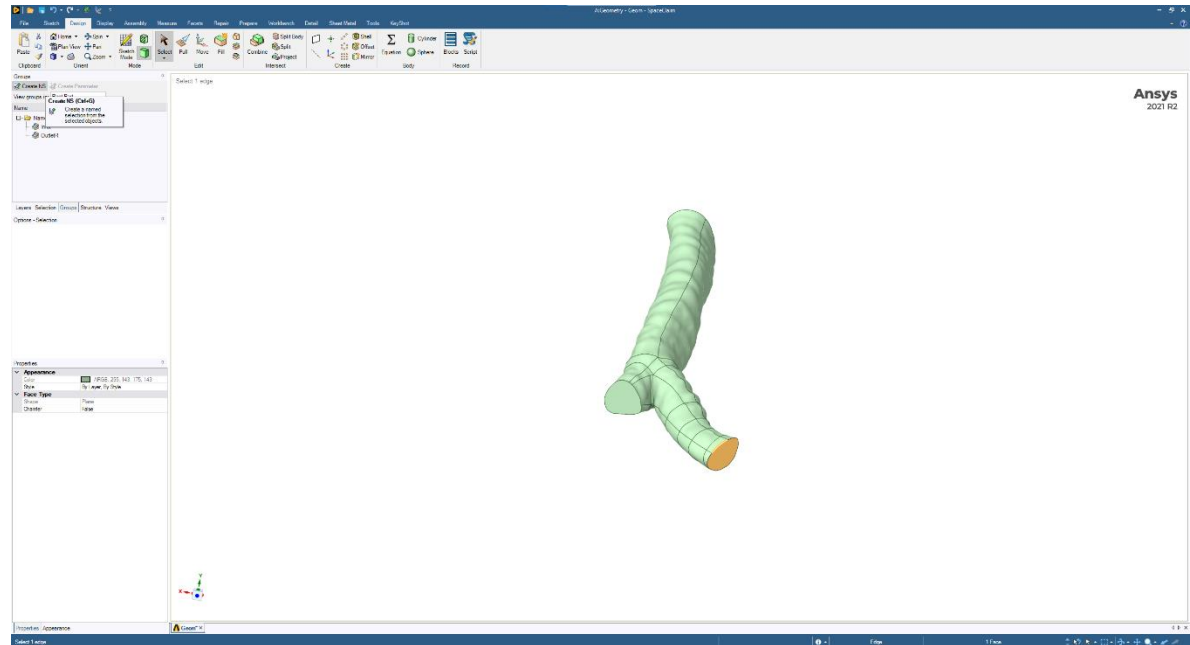

Figure 1-16 Screenshot of the airway geometry with the selected left outlet (orange) that is defined as a named selection.
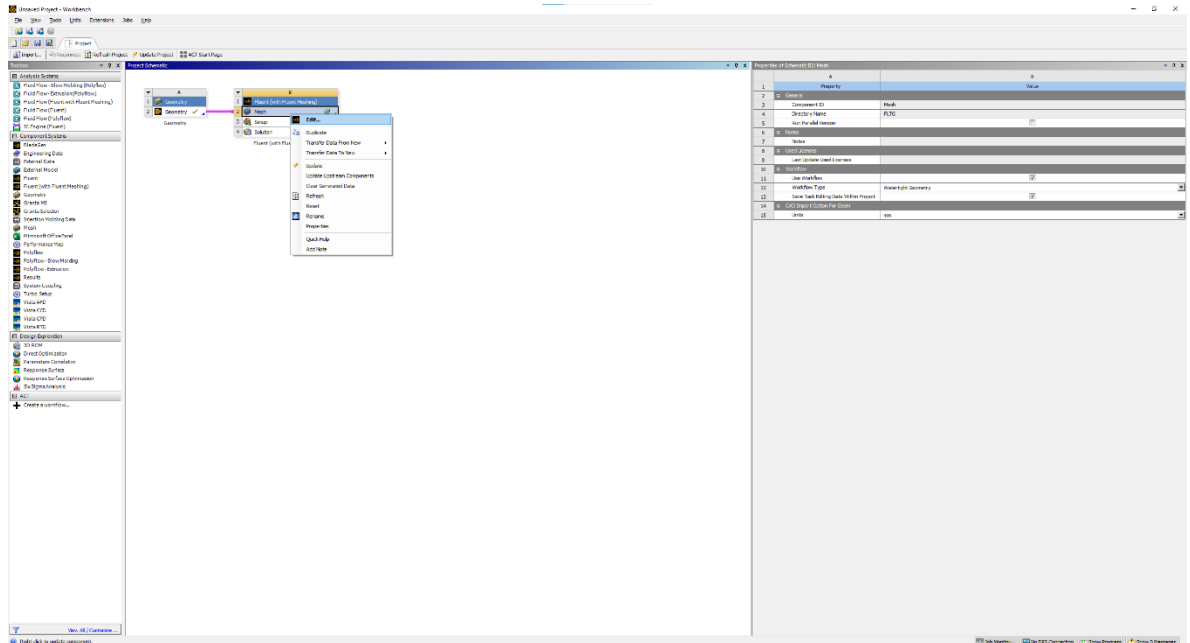

Figure 1-15 Screenshot of ANSYS Workbench with the two-component systems Geometry and Fluent. The sub-menu that opens after right-clicking the mesh section is visualized.

Fluent

After closing SpaceClaim, the Workbench is showing again. The next step is generating the surface and interior mesh of the geometry. First, on the right side, the units must be set to 'mm' since the geometries of stents and airways are relatively small. All units will now be set to millimeters. Next, a right-click on the mesh section gives the sub-menu as seen in Figure 1-15. Click on edit.

Now, the program ANSYS Fluent will open. This software consists of two parts, first the meshing and secondly the simulation part. First, the mesh will be created. The following screen as in Figure 1-17 opens. At the left side, the whole workflow is visualized. Each step is followed by another which must be run through in the specified order.
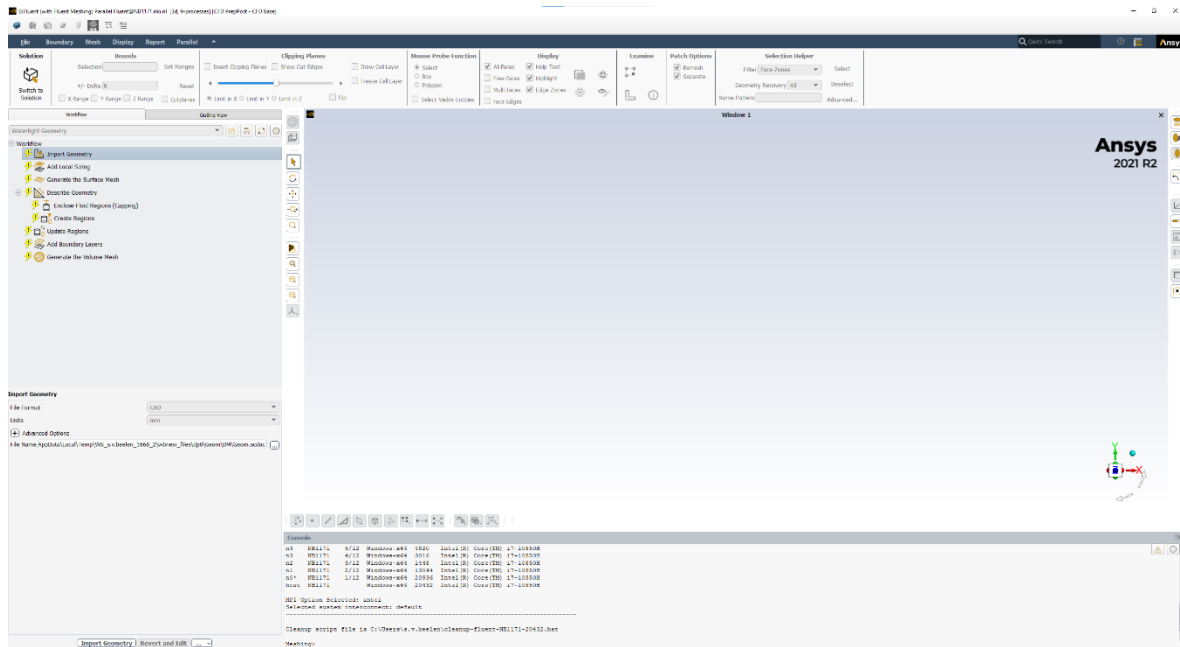

Figure 1-17 Screenshot of ANSYS Fluent that opens. At the left side, all steps that are required for a mesh are visualized. It is required to run through them all.

All steps in similar order are described below for the simulations.

- *Import Geometry*
  - o click at the bottom on Import Geometry.
- *Add Local Sizing*
  - o No local sizing is added (local sizing can be added if a certain part of the geometry must be meshed differently than the rest).
- *Generate surface mesh*
  - o Includes the minimum and maximum size of the mesh elements. This is in each simulation set to a minimum of 0.5 and maximum of 1.0 mm. The GR is kept at the standard value of 1.2. The size function used is curvature. Click on *Generate surface mesh* at the bottom. After meshing, ANSYS gives a maximum skewness. This value must be checked whether it is good enough (Figure 2-3). Otherwise, refine.
- *Describe geometry*
  - o The setting 'The geometry consists of only fluid regions with no voids' is selected.
- *Update boundaries*

- The boundary conditions for all Named selections are defined here. For these simulations, the inlet is defined as velocity, the outlets as pressure and the wall as wall.
- *Boundary Layers*
  - Near wall modeling is included within boundary layers. The number of layers is set to 8, transition ratio to 0.1 and growth rate is kept at 1.2.
- *Generate volume mesh*
  - Lastly, the mesh is generated. Poly-hexcore elements are used with eight buffer layers and three peel layers. All other settings are kept similar. Generate the mesh.
  - After, ANSYS comes with the minimal orthogonal quality. Check in Figure 2-3 whether the quality is good enough.

Setup the simulation

If the quality of the mesh is sufficient and no errors are present, the simulation can be set up. At the left upper side of the screen, the button 'Convert to simulation' must be selected. The Fluent software opens. Here, boundary conditions and input parameters can be set. The following screen (Figure 1-18) opens:
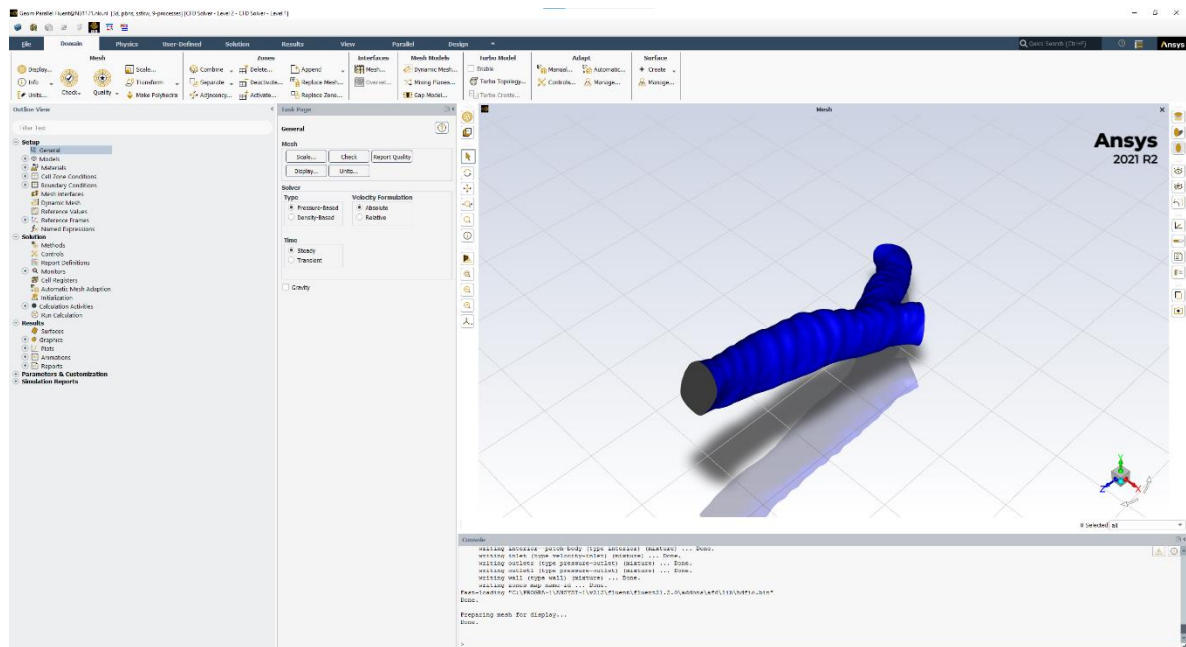

Figure 1-18 Screenshot of the Fluent software of ANSYS. In blue, the imported and meshed geometry is visualized.

At the left side, all input options are visualized that can be used to define the simulation with. Only a couple of the settings are used.

- Models: check if the κ-ω SST model is selected
- Materials: Standard properties of air are used, present at 15°C. This means a density of 1.225 [kg/m^3] and viscosity of $1.78 \cdot 10^{-5}$ [kg/(m·s)].
- Cell zone conditions: must be fluid and defined as air
- Boundary conditions: check if all areas are defined with the right boundary condition

- Inlet: sub-menu – expression. Assume 0.5 L/s, hence 0.0005 m³/s. Define the equation as stated in Eq. 2.1 and described in Figure 1-19. Inserting the inlet area is done by selecting Functions – Reduction – Area, and set the area to inlet (as in Figure 1-19).
- Outlet: check if gauge pressure = 0 Pa
- Turbulence intensity = 5%, turbulent viscosity ratio = 10
- Verification = magnitude, normal to boundary
- Monitors: in Residuals – Absolute criteria, set the convergence level to 0.0001

All settings are now set for the simulation. Click on Initialization, Hybrid initialization to initialize the simulation. Next, go to Run Calculation. Set the maximum number of iterations to 300 and let the simulation run. It will run until the convergence has reached. If it does not converge, it will stop at 300 iterations.
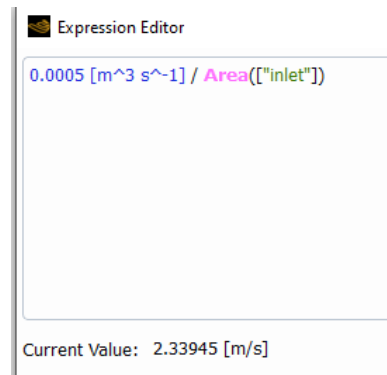

Figure 1-19 Screenshot of the inlet expression of a simulation. Assuming a flow rate of 0.5 L/s and dividing by the inlet area generates the velocity used for the simulation.

If the simulation has run, the maximum y+ value must be checked first. Go to Graphics, Contours, Turbulence, Y-plus. This will give the contours of the y+ value on the geometry and shows the maximum value. If the maximum value is below 1, near wall modelling the fluid near the wall is captured sufficient. If not, go back to the meshing section and refine the mesh by smaller elements and increased inflation layers.

Otherwise, define the parameters that are of interest. Go to Report Definitions to report the pressure drop, mass flow rate and turbulence intensity. Click on New – Surface – Area Weighted Average. For the pressure drop, choose Static Pressure at Inlet plane and calculate. For the mass flow rate, choose New – Flux Report – Mass flow rate. Choose the inlet, both outlets and check the box 'Per zone'. The mass flow rate of each surface is calculated in kilograms per second. The ratio of each outlet can be calculated compared to the inlet. For the Turbulence intensity, both Volume Average and Max are chosen in the upper box, in the lower is turbulence intensity chosen.

The wall shear stress, velocity path lines, and static pressure to the wall are all visualized in graphics. For both the wall shear stress and static pressure to the wall, go to Graphics, Contours. For the wall shear stress, choose Wall Fluxes, Wall shear stress and choose the wall. After clicking save, the contours will show. For the static pressure, go to Pressure, Static pressure, and choose wall. Velocity magnitude is visualized with path lines. Hence, go to Graphics, Path lines, Velocity, Velocity magnitude. Path lines of the velocity magnitude are now visualized in the model.

APPENDIX B: DIVERGING ENDS OF THE TRACHEA

This Appendix include examples of the mentioned limitation about the diverging ends of the trachea in the Limitations of 3.3 Stent versus Trachea. A length of 100 mm of the trachea wants to be cut for comparison with stents. Additionally, the cross-sectional area of the inlet and outlet must therefore as similar as possible. However, the increasing diameters of the ends towards the larynx or bifurcation make the latter not possible in every airway.

As depicted in the figure below, a length of 100 mm of the trachea is measured. However, the inferior plane is located just above the main carina. Since a bifurcation follows, the area is enlarged. A similar problem is present at the superior plane, due to the upper airways that follow superiorly. This increases the cross-sectional area due to the bifurcation and influences the velocity of the air, hence the pressure drop, wall shear stress and turbulence intensity.
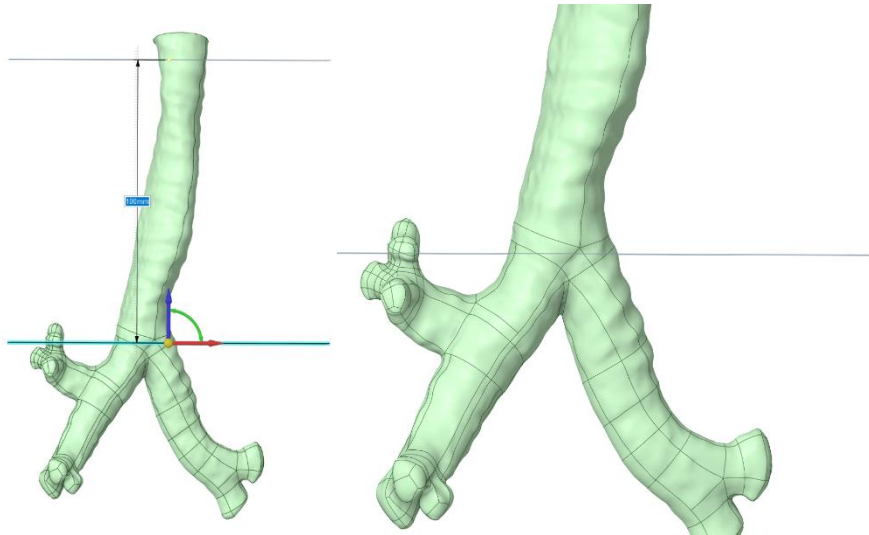
Figure 1-20 Two segmentations of the airways (green). Left, the airway with a measured orthogonal distance of 100 mm is depicted. As seen, both planes cut the trachea at a relatively bigger cross-sectional area than the trachea has. Right, a zoomed in figure of the plane that is cut at the lower end of the trachea.

APPENDIX C: PATIENT CHARACTERISTICS

This Appendix includes extra data of each case. The sex, length, days of the CT-scans with respect to the intervention date, slice thickness of the CT-scans and the type of intervention are included.

| Case	1	2	3	4	5	6
M/F	F	M	F	M	M	F
Length (cm)	171	181	180	180	193	160
Pre-obstructed CT-scan (days before intervention)	-1154	-433	-385	-786	-349	-652
Slice thickness (mm)	1	1	1	1	1	1
Obstructed CT-scan (days before intervention)	-10	160	0	-2	-16	-2
Slice thickness (mm)	1.5	1.5	1	1.5	1	x
Post-obstruction CT-scan with stent (days after intervention)	x	x	52	x	6	x
Intervention	Y-stent	Stent RHB	Stent LHB	Debulking	Stent RHB	Stent trachea
After intervention	More coughing; tough sputum; less dyspnea	Less dyspnea		Coughing sometimes; less dyspnea		x

APPENDIX D: RESULTS OF PRE-OBSTRUCTED AIRWAYS

This Appendix includes the results of all cases that were eligible for simulation of the pre-obstructed airways.

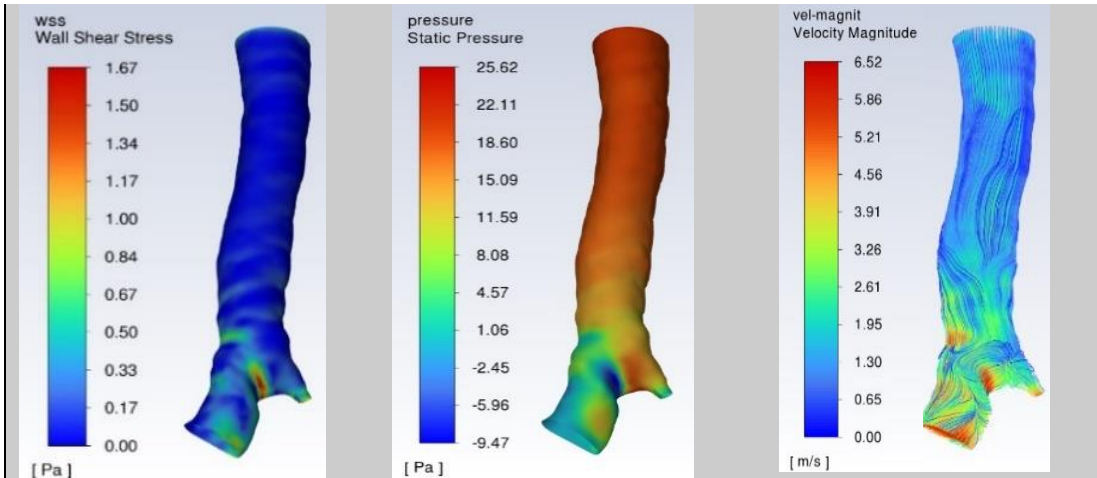| Case	Wall Shear Stress (Pa)	Static pressure to the wall (Pa)	Velocity magnitude (m/s)
1			
2			
3			
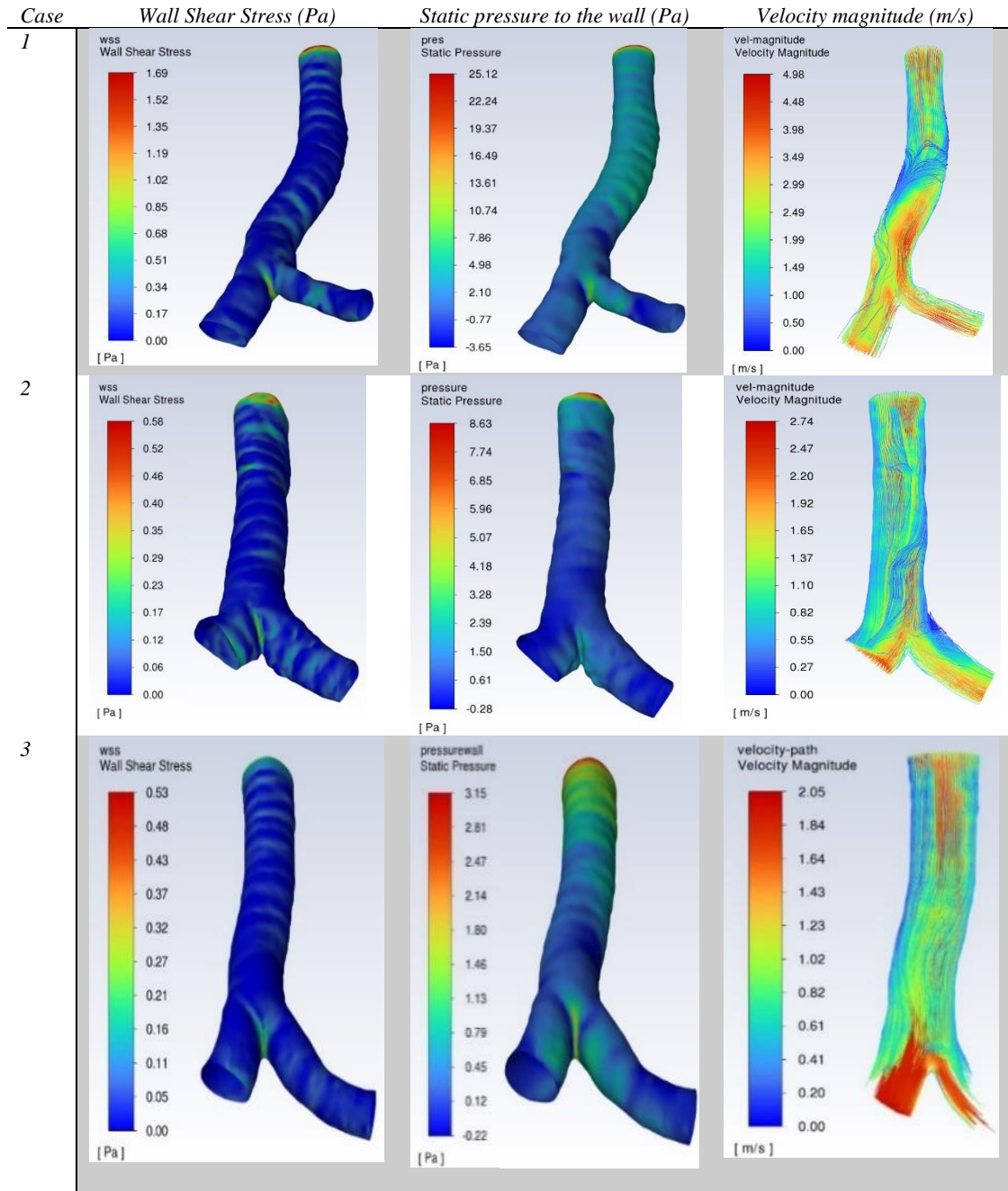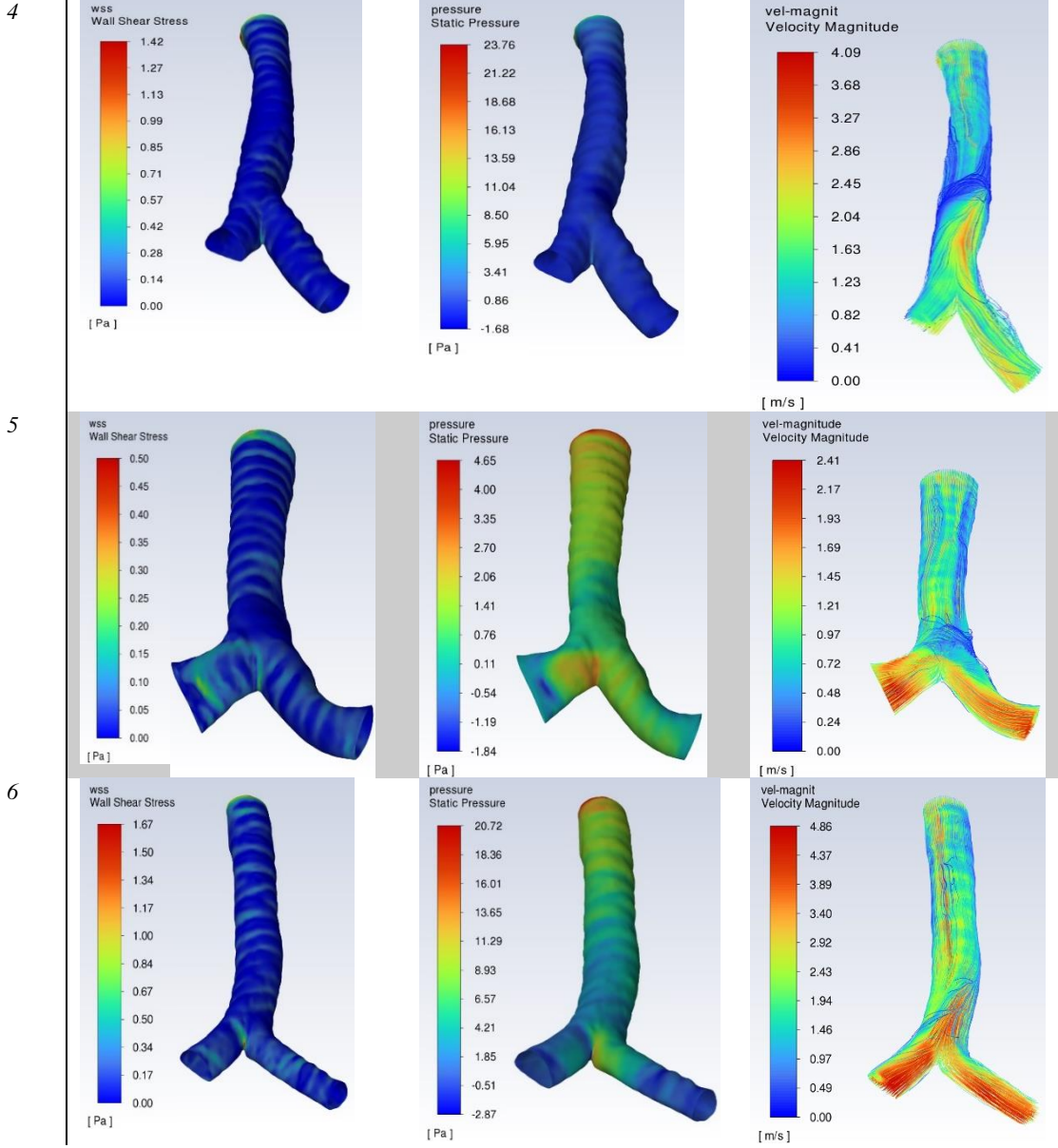
APPENDIX E: RESULTS OF OBSTRUCTED AIRWAYS

This Appendix includes the results of all 5 cases that were eligible for simulation of the pre-obstructed airways.
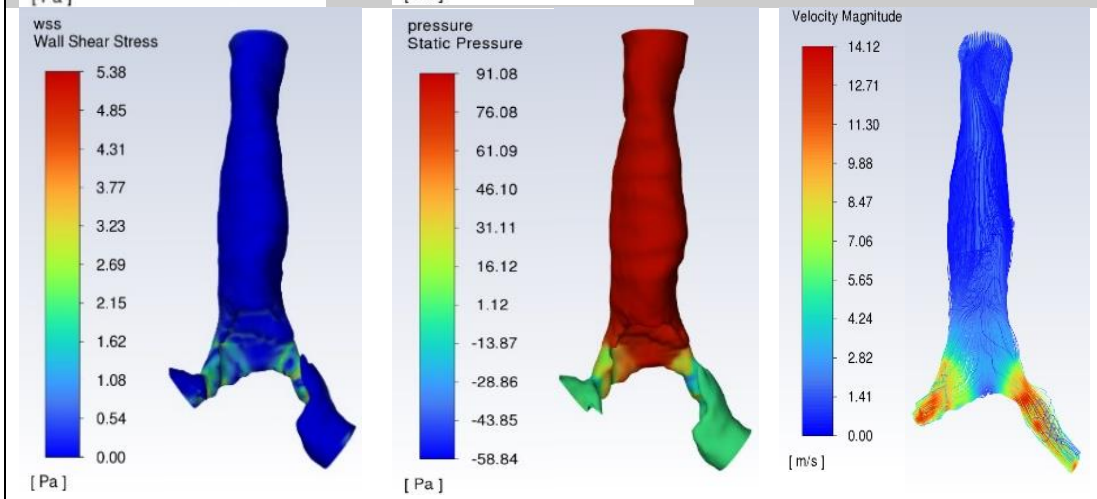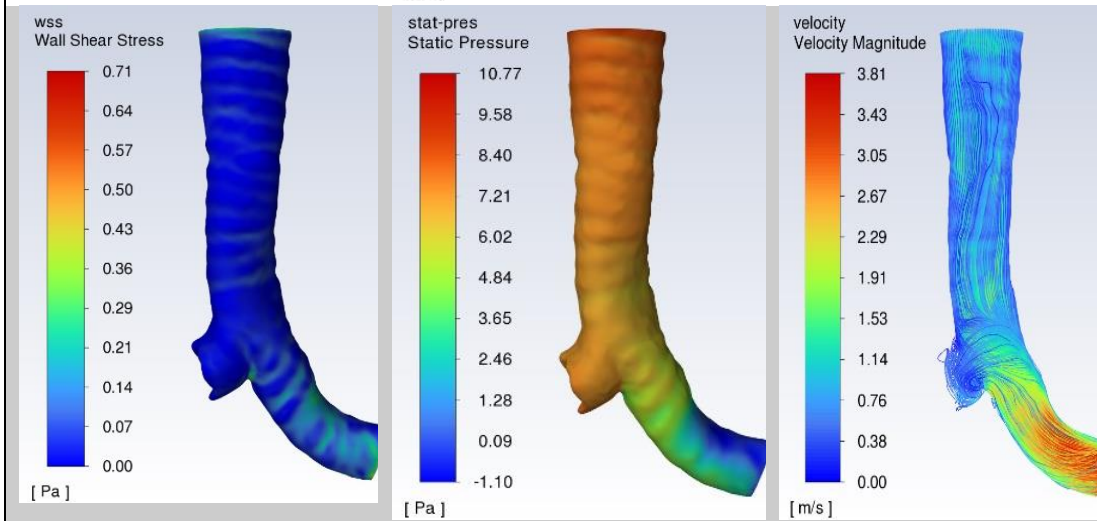
Case	Wall Shear Stress (Pa)	Static pressure to the wall (Pa)	Velocity magnitude (m/s)
1			
2			
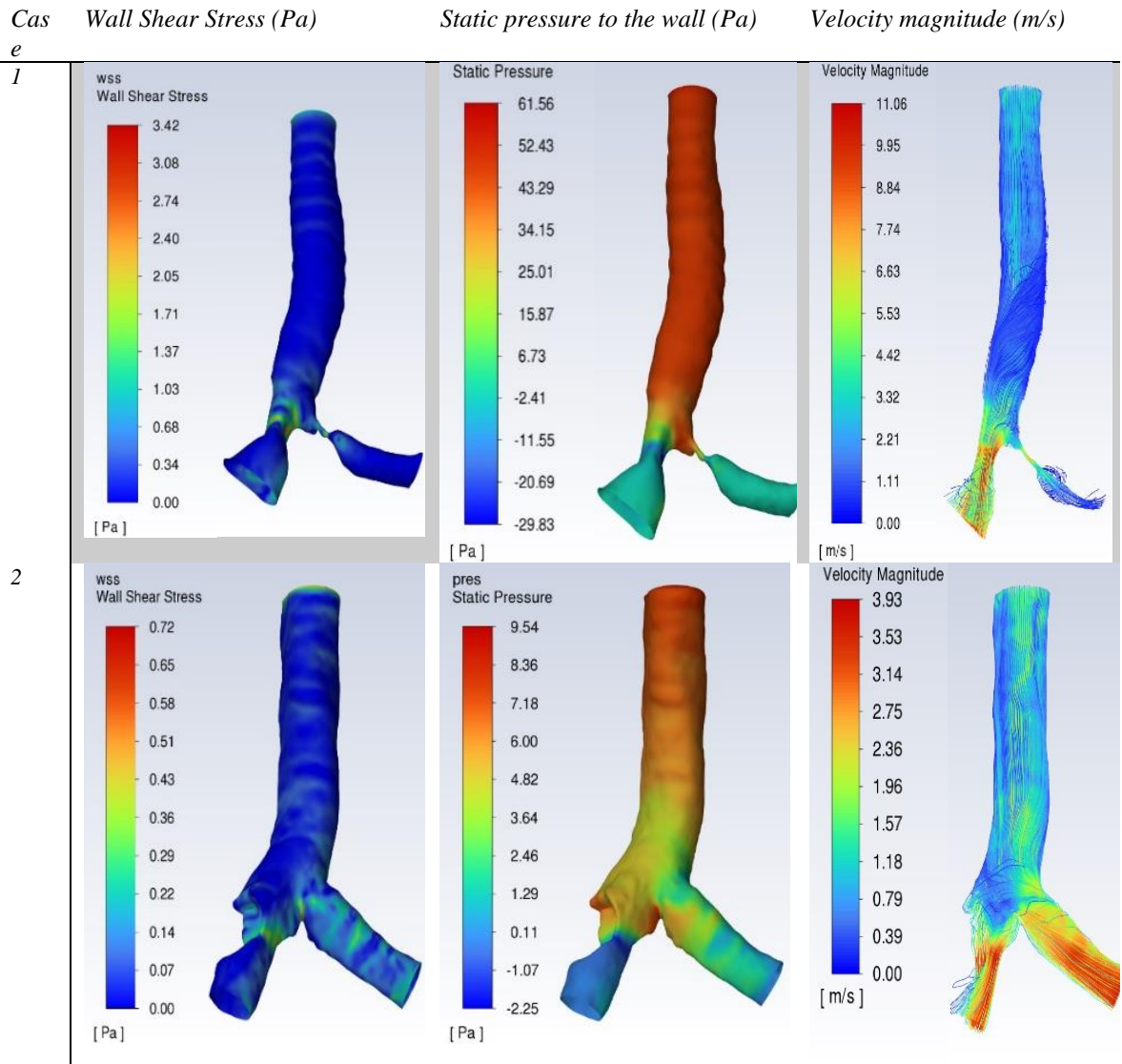
3

4

5

APPENDIX F:　RESULTS OF POST-OBSTRUCTION WITH STENT AIRWAY

This Appendix includes the results of all 2 cases that were eligible for simulation of the pre-obstructed airways.

Case	Wall shear stress (Pa)	Static pressure to the wall (Pa)	Velocity magnitude (m/s)
3			
5			